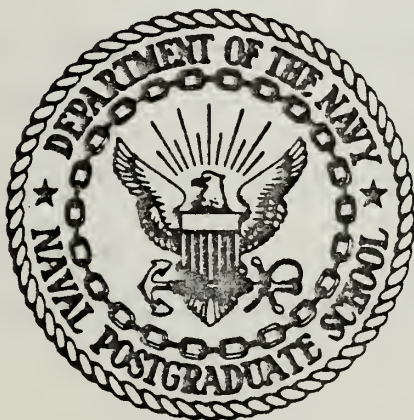


DUDLEY KNOX LIBRARY
NAVAL POSTGRADUATE SCHOOL
MONTEREY CALIF 93940

NAVAL POSTGRADUATE SCHOOL

Monterey, California



THESIS

Concept Evaluation: Field Feedback
Computation of Electromagnetic Scattering

by

Bryant Welch

June 1980

Thesis Advisor:

M. A. Morgan

Approved for public release; distribution
unlimited

T196296

REPORT DOCUMENTATION PAGE		READ INSTRUCTIONS BEFORE COMPLETING FORM
1. REPORT NUMBER	2. GOVT ACCESSION NO.	3. RECIPIENT'S CATALOG NUMBER
4. TITLE (and Subtitle) Concept Evaluation; Field Feedback Computation of Electromagnetic Scattering		5. TYPE OF REPORT & PERIOD COVERED Master's Thesis; June 1980
7. AUTHOR(s) Bryant Welch		6. PERFORMING ORG. REPORT NUMBER
9. PERFORMING ORGANIZATION NAME AND ADDRESS Naval Postgraduate School Monterey, California 93940		8. CONTRACT OR GRANT NUMBER(s)
11. CONTROLLING OFFICE NAME AND ADDRESS Naval Postgraduate School Monterey, California 9394b		10. PROGRAM ELEMENT, PROJECT, TASK AREA & WORK UNIT NUMBERS
14. MONITORING AGENCY NAME & ADDRESS (if different from Controlling Office)		12. REPORT DATE June 1980
		13. NUMBER OF PAGES 136
		15. SECURITY CLASS. (of this report) UNCLASSIFIED
		15a. DECLASSIFICATION/DOWNGRADING SCHEDULE
16. DISTRIBUTION STATEMENT (of this Report) Approved for public release; distribution unlimited		
17. DISTRIBUTION STATEMENT (of the abstract entered in Block 20, if different from Report)		
18. SUPPLEMENTARY NOTES		
19. KEY WORDS (Continue on reverse side if necessary and identify by block number) Electromagnetic Scattering, Thin-Wire Scattering, Finite-Element Numerical Method, Integral Equation, Variational Calculus, Coupled Azimuthal Potentials		
20. ABSTRACT (Continue on reverse side if necessary and identify by block number) A new method of numerical solution for time-harmonic field scattering problems involving inhomogeneous bodies of revolution is presented. A simple single-loop multiport feedback system is driven by the incident field. The forward path transfer matrix, found by use of the finite-element method, translates the total near-field into the body-surface field. The feedback path matrix is established by the magnetic vector potential formulation; it		

translates the body-surface currents into the scattered near-field. The thin-wire scattering problem is formulated in terms of this field-feedback method. Results of this computation are compared in graphical form to those found by Hallen's integral equation solution of the scattering problem for several cases of interest.

Approved for public release; distribution unlimited

Concept Evaluation: Field Feedback Computation
of Electromagnetic Scattering

Bryant Welch
Lieutenant, United States Navy
B.S., University of Illinois, 1972

Submitted in partial fulfillment of the
requirements for the degree of

MASTER OF SCIENCE IN ELECTRICAL ENGINEERING

from the

NAVAL POSTGRADUATE SCHOOL
June 1980

ABSTRACT

A new method of numerical solution for time-harmonic field scattering problems involving inhomogeneous bodies of revolution is presented. A simple single-loop multiport feedback system is driven by the incident field. The forward path transfer matrix, found by use of the finite-element method, translates the total near-field into the body-surface field. The feedback path matrix is established by the magnetic vector potential formulation; it translates the body-surface currents into the scattered near-field. The thin-wire scattering problem is formulated in terms of this field feedback method. Results of this computation are compared in graphical form to those found by Hallen's integral equation solution of the scattering problem for several cases of interest.

TABLE OF CONTENTS

I.	INTRODUCTION-	6
II.	THE PROBLEM AND METHOD OF SOLUTION-	8
	A. THE FIELD FEEDBACK FORMULATION-	9
	B. THE WIRE SCATTERING PROBLEM -	10
	C. COUPLED AZIMUTHAL POTENTIALS-	12
III.	COMPUTATIONAL PROCEDURES-	16
	A. THE FINITE ELEMENT METHOD -	16
	1. Basis Function Expansions -	18
	2. The Euler-Lagrange Variational Technique -	22
	3. Application of the Thin-Wire Problem-	24
	B. THE SCATTERED FIELD INTEGRAL-	27
	1. The Vector Potential Formulation-	27
	2. The Scattered Field Matrix Equation -	29
	C. PROBLEM IMPLEMENTATION-	33
IV.	RESULTS AND ANALYSIS-	38
	A. INTEGRAL EQUATION COMPARISON-	39
	B. ERROR ANALYSIS-	43
V.	CONCLUSIONS -	47
APPENDIX A-		49
APPENDIX B-		87
APPENDIX C-		105
APPENDIX D-		119
LIST OF REFERENCES-		135
INITIAL DISTRIBUTION LIST -		136

I. INTRODUCTION

The objective of this endeavor is to investigate the performance of a new, and potentially quite powerful, technique for the computation of electromagnetic scattering problems. For reasons that will later become apparent, this new technique will be denoted the "field feedback formulation" (FFF or F^3). The work reported here is a first application of F^3 , where the calculation of scattering from straight thin-wires has been performed. This is an almost classical electromagnetic field problem that has been routinely solved by use of integral equations for many years. Such a cononical problem was chosen as a testing vehicle for the newly conceived F^3 analysis method since alternate integral equation solutions are readily available for comparisons.

The formulation developed here employs a combination of the finite element numerical method and the classical magnetic vector potential. The finite element method (FEM) is an application of variational techniques which implements a weighted residual approximation. The high accuracy of the finite element method is used to advantage in reducing the amount of computing required, as compared to other numerical methods. Use is also made of coupled azimuthal potentials (CAP). The CAP formulation restricts the class of approachable

problems to those which are axially symmetric, but does allow the treatment of material inhomogeneities and multiwavelength dimensions.

Thin-wire assumptions are made which greatly simplify the current-scattering problem. These assumptions, however, are by no means critical to the solution method. The formulation should be readily extendable to a large class of important interior, radiation, and scattering problems.

II. THE PROBLEM AND METHOD OF SOLUTION

Electromagnetic scattering problems usually involve a known incident field, such as a uniform plane wave. The scattered field can be found from the current induced by the presence of the incident field, but the induced current can be found only after the total field is known. Since the total field is just the sum of the incident and scattered fields, a definite difficulty has been encountered. Knowledge of the induced current is needed to find the scattered field, while at the same time, the scattered field must be known to determine the induced current.

This is clearly seen in the form of Maxwell's equations for the scattering problem. Assume that a scatterer with properties $Y_1 = \sigma_1 + j\omega\epsilon_1$, $Z_1 = j\omega\mu$, is in free space where $Y_0 = j\omega\mu_0$, $Z_0 = j\omega\mu_0$, and in the presence of sources \bar{J}_0 , \bar{M}_0 . Then the curl equations have the form

$$\nabla \times \bar{H} = \bar{J}_0 + Y_1 \bar{E} \quad (1a)$$

$$\nabla \times \bar{E} = -\bar{M}_0 - Z_1 \bar{H} \quad (1b)$$

where the induced electric and magnetic currents are

$$\bar{J}_1 = (Y_1 - Y_0) \bar{E} \quad (2a)$$

$$\bar{M}_1 = (Z_1 - Z_0) \bar{H}$$

and the scattered magnetic field is

$$\bar{H}_{\text{scat}} = \bar{H} - \bar{H}_{\text{incident}} \quad (3)$$

The electric field relationship is, of course, similar.

The simple and compact nature of the simultaneous equations (1) and (2) is highly appealing, but of little practical use in obtaining numerical answers to a problem because of the excessive computing required. Yet, while the requirement to have two unknowns cannot be escaped, the equations relating these unknowns can at least be rendered more tractable.

A. THE FIELD FEEDBACK FORMULATION

As will be shown later, two simple matrix equations can be derived which relate the magnetic and electric fields at a number of points along the surface of the scatterer to the fields at points along a boundary some distance away. These equations are independent and work in opposite directions. That is, from the first equation, given the total boundary field values, \underline{e}_t and \underline{h}_t , the scatterer surface total field values, \underline{e}_w and \underline{h}_w , can be found:

$$[\underline{e}_w | \underline{h}_w]^T = \underline{V} [\underline{e}_t | \underline{h}_t]^T \quad (4a)$$

The column vectors, $[\underline{e}_i | \underline{h}_i]^T$, contain the field values at the computation points. The second equation takes $[\underline{e}_w | \underline{h}_w]^T$ and yields the scattered field values $[\underline{e}_s | \underline{h}_s]^T$ along the boundary:

$$[e_s | h_s]^T = \tilde{T} [e_w | h_w]^T \quad (4b)$$

Equations (4a), (4b), and (3) comprise a simple feedback system, as in Figure 1.

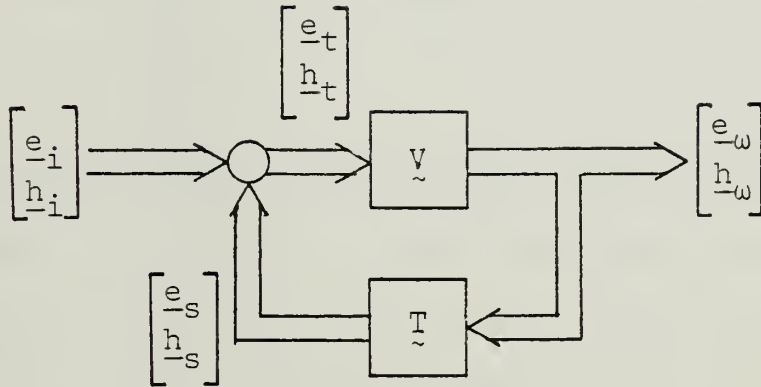


Figure 1. Field Feedback

What remains, then, is to construct the matrices \tilde{Y} and \tilde{T} to fit the problem at hand. It should be pointed out that the magnetic field alone is involved in the wire-scatterer problem as developed here. So $[e_x | h_x]^T$ is replaced by h_x . The field translation matrices \tilde{Y} and \tilde{T} , though developed in exactly the same way, will be considerably simplified as compared to the general scatterer case.

B. THE WIRE SCATTERING PROBLEM

Given a perfectly conducting thin wire in free space, and a plane wave of known amplitude incident from a known direction, it is required to find the current induced on the wire and the

field scattered by the wire at any point in space. Finding the induced current is equivalent to finding the field on the wire surface, since $\vec{J} = \hat{n} \times \vec{H}$, where \hat{n} is the unit vector normal to the surface. Normalized coordinates will be used throughout the problem, and are given by

$$(R, Z, \phi) = (K_0 r, K_0 z, \phi).$$

The coordinates (r, Z, ϕ) are standard circular cylindrical coordinates, and $K_0 = 2\pi/\lambda_0$ is the free space wavenumber of the time-harmonic field. The situation is depicted in Figure 2. Use of these normalized coordinates will allow the formation of a compact and useful form of the CAP equations.

The wire radius is a , given in terms of λ_0 , the free space wavelength. Then the normalized radius is $R_a = 2\pi a/\lambda_0$. The wire length is L , also given in wavelengths. So $Z_L = 2\pi L/\lambda_0$. The incidence angle of the plane wave is α , measured as shown in Figure 2. Since perfect conductivity is assumed, fields and currents will exist only on the surface of the wire. And since a very thin wire will be assumed, where $a \ll \lambda_0/10$, the current at the wire ends may be set to zero.

The problem will not be solved in terms of the usual electric and magnetic fields, \vec{E} and \vec{H} , or the scalar potential, V . Instead, use will be made of the magnetic vector potential, \vec{A} . The current and scattered fields will be presented and calculated in terms of the CAP formulation discussed below.

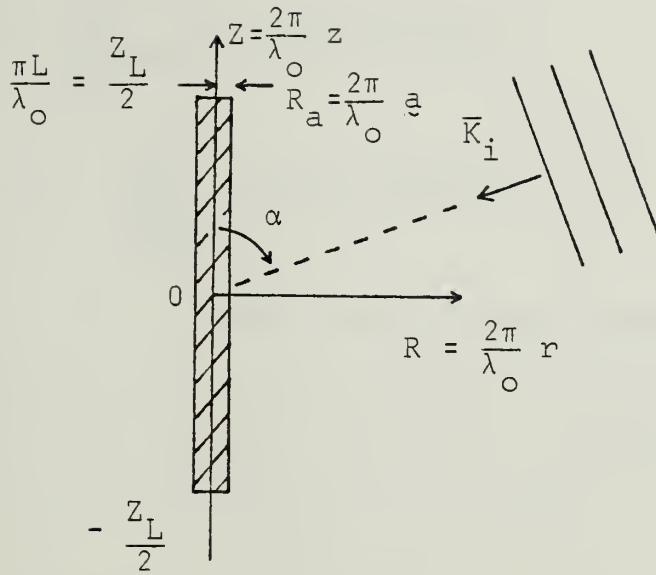


Figure 2. Normalized Coordinates

C. COUPLED AZIMUTHAL POTENTIALS

The CAP formulation [3] has been developed to handle previously intractable time-harmonic field problems involving continuously and discretely inhomogeneous bodies of revolution. With this limitation of axial symmetry, all electromagnetic field components can be expanded via exponential Fourier series in the ϕ coordinate. The model fields can then be represented by two coupled azimuthal potentials. These potentials satisfy a system of coupled partial differential equations, as well as a variational criterion, which will be developed here.

Using the normalized coordinates in Figure 2, the total fields are decomposed into azimuthal modes:

$$\bar{E}(R, Z, \phi) = \sum_{m=-\infty}^{\infty} \bar{e}_m(R, Z) \exp(jm\phi) \quad (5a)$$

$$\eta_0 \bar{H}(R, Z, \phi) = \sum_{m=-\infty}^{\infty} \bar{h}_m(R, Z) \exp(jm\phi) \quad (5b)$$

where $\eta_0 = 120\pi$. By substitution of these expansions into Maxwell's equations, it can be shown that all modal field components can be generated from two coupled azimuthal potentials $\psi_1(R, Z, m)$ and $\psi_2(R, Z, m)$, using

$$\hat{\phi} \times \bar{e}_m = jf_m(m\hat{\phi} \times \nabla \psi_1 - R\mu_r \nabla \psi_2) \quad (6a)$$

$$\hat{\phi} \cdot \bar{e}_m = \psi_1/R \quad (6b)$$

$$\hat{\phi} \times \bar{h}_m = jf_m(m\hat{\phi} \times \nabla \psi_2 + R\epsilon_r \nabla \psi_1) \quad (6c)$$

$$\hat{\phi} \cdot \bar{h}_m = \psi_2/R \quad (6d)$$

where $\hat{\phi}$ is the unit azimuthal vector, ∇ is the two dimensional gradient operator, and

$$f_m[R, Z] = [\mu_r(R, Z)\epsilon_r(R, Z)R^2 - m^2]^{-1} \quad (7)$$

The Euler-Lagrange variational technique will be discussed more fully in the exposition of the finite element method below. It is sufficient to note here that this technique finds the solution of the system partial differential

equations as the stationary point of a functional of the potentials and their first derivatives. This stationary point is defined as the point (ψ_{10}, ψ_{20}) at which the variation of F , δF , vanishes for perturbations $(\delta\psi_1, \delta\psi_2)$ about that point.

The functional F is a surface integral of the Lagrangian L , where

$$L = f_m [\nabla\psi_1 \cdot (R\epsilon_r \nabla\psi_1 + m\hat{\phi} \times \nabla\psi_2) + \nabla\psi_2 \cdot (R\mu_r \nabla\psi_2 - m\hat{\phi} \times \nabla\psi_1)] - (\epsilon_r \psi_1^2 + \mu_r \psi_2^2)/R \quad (3)$$

The functional F is integrated over the constant azimuth planar meridian cross section Ω of the volume in which the solution is of interest.

It is convenient at this point to change variables, and introduce a simplifying assumption. From (6b) and (6d) we have $e_{\phi m}(R, Z) = \psi_1/R$ and $h_{\phi m}(R, Z) = \psi_2/R$. So finding only the azimuthal components of the modal fields, $e_{\phi m}$ and $h_{\phi m}$, will yield a complete solution through (6a) and (6c). Now, since a thin wire is assumed, the phase variation of the incident field from side to side on the wire may be neglected. Then the induced current will be a function of Z alone; $\vec{J} = J_Z \hat{Z}$. Therefore the scattered fields will be azimuthally invariant, so that $\vec{E}(R, Z, \phi) = \vec{e}_0(R, Z)$ and $\eta_0 \vec{H}(R, Z, \phi) = \vec{h}_0(R, Z)$. Furthermore, since $J_Z = \hat{n} \times \vec{H} = H_\phi$ and since

$$\vec{E} = \frac{1}{j\omega\epsilon} \nabla \times \vec{H} = \frac{1}{j\omega\epsilon} \left[-\hat{R} \frac{\partial H_{\phi}}{\partial Z} + \hat{Z} \frac{1}{R} \frac{\partial}{\partial R} (R H_{\phi}) \right],$$

it follows that $e_{\phi 0} = 0$, and $\bar{h}_0 = h_{\phi 0}$. The number of modes has now been reduced to one, the $h_{\phi 0}$ mode.

Observe that (6a) and (6c) no longer involve coupled potentials. This allows the Lagrangian to be decoupled, and it may now be written

$$L = f_0 \{ \nabla(Rh_{\phi 0}) \cdot [R_{\mu r} \nabla(Rh_{\phi 0})] \} - \mu_r R h_{\phi 0}^2. \quad (9)$$

So the functional is

$$F = \int_{\Omega} L(R, Z, h_{\phi 0}, \nabla h_{\phi 0}) dR dZ \quad (10)$$

It remains to find $h_{\phi 0}(R, Z)$ to make F stationary in Ω for given Dirichlet boundary conditions. This will be done by use of the finite element method.

III. COMPUTATIONAL PROCEDURES

The constructions of the \tilde{V} and \tilde{T} matrices have little in common other than the coordinate system. The finite element method is used to generate \tilde{V} . \tilde{T} is derived from the magnetic vector potential in this perfect conductor case, while if a dielectric body were used, both electric and magnetic vector potentials would be required to construct \tilde{T} . The use of numerical methods obviously implies that the current and fields will be found only at discrete points. As discussed in Section II.C., only points in a constant azimuth meridian plane need be considered. The region between the wire surface and the boundary at which the fields are to be calculated is divided into triangular elements. These are areas of integration in the finite element method. The divisions and the nodal numbering scheme are shown in Figure 3. There are a total of N_W points along the wire, and N_B points along the boundary.

A. FINITE ELEMENT METHOD

This method is one whereby the region of interest is divided into a number of overlapping subregions of a specified shape. Then the problem solution function θ is approximated by defining the solution as a linear combination of the products of unknown coefficients with "basis" functions defined over

over each of the overlapping subregions. These basis functions are usually sectionally linear, and, in very simple terms, are used to "fill in" the approximation between points. A weighted residual approximation of the solution θ , commonly known as the Ritz method, can then be made by the application of the discretized Euler-Lagrange variational procedure, subject to the appropriate boundary conditions. The rigorous development of each of these parts of the finite element method is not necessary here, but the background required for a basic understanding of the method will be given below.

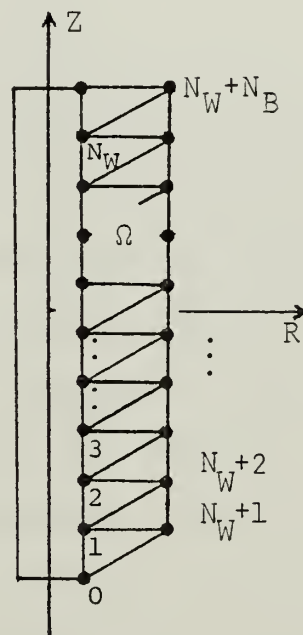


Figure 3. Solution Points

1. Basis Function Expansions

In order to solve a problem numerically, some method of approximating the solution using a finite number of unknowns must be found. Also, the method's convenience must be balanced against the desired accuracy. A general term for such an approximation is a "basis function expansion" of a function θ [2]. The type of expansion used in the finite element method for a one-dimensional problem is given by

$$\theta_N(X) = \sum_{i=1}^N \theta_i u_i(X) \quad (11)$$

where θ_N is the discrete version of θ , the θ_i are the values of $\theta(X)$ at the discrete points X_i , and the $U_i(X)$ are the basis functions at the points X_i . Linear basis functions are usually employed in FEM calculations, though quadratic or higher-order polynomial functions could be used to obtain greater accuracy. Linear basis functions for a one-dimensional problem are shown in Figure 4. Note that the node spacing is irregular. This allows tailoring of the expansion to better approximate the solution, and, in two or higher dimensional cases, may be necessary because of the shape of the solution region. If neither of these are necessary, regular node spacing can be used with some advantage to reduce complexity. The basis functions u_i are seen

to have unit value at their respective nodes x_i , and are zero for $x_{i-1} > x > x_{i+1}$, $1 \leq i \leq N$.

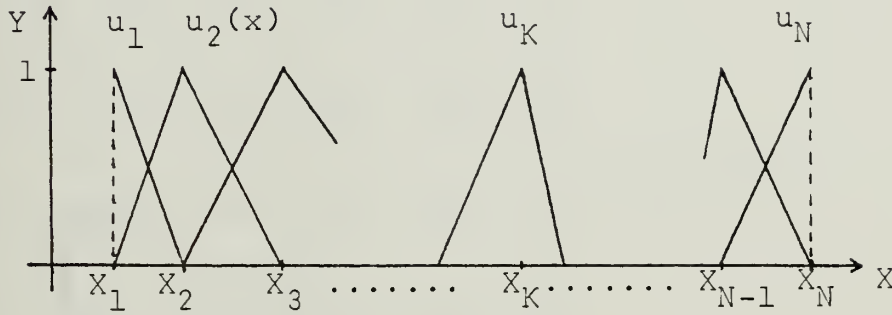


Figure 4. Linear Basis Functions

A two-dimensional linear basis function often used is the "pyramid" function; its two-dimensional projection is shown in Figure 5. A rectangular region Ω in the x - y plane has been discretized by division into the triangular elements shown. The boundary $\partial\Omega_{3,2}$ in Ω of the function $u_{3,2}(x,y)$ has been outlined to make the shape clear.

The function has a value of one at the center node, and is zero along and outside the periphery. Its equation can be written

$$u_{3,2}(x,y) = u_{3,2}^j(x,y), \quad j = a, f \quad (12)$$

where the component functions are planar segments of the form

$$u_{3,2}^j = \alpha x + \beta y + \gamma \quad (13)$$

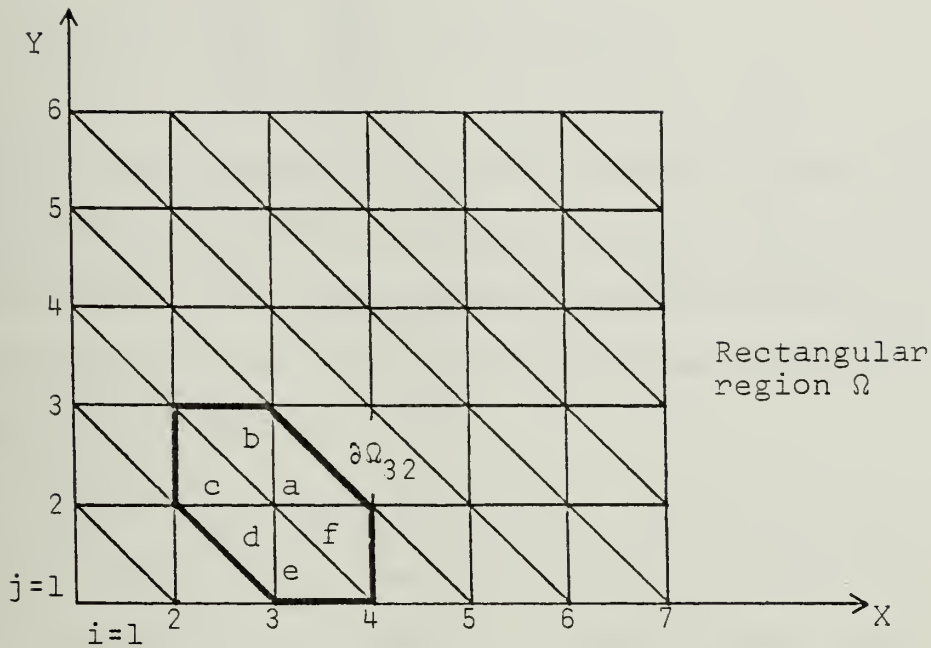


Figure 5. Two-Dimensional Finite Element Mesh

Then α, β, γ must be functions of (x, y) so that $u_{32}^j(x_3, y_2) = 1$, $u_{32}^j(x_i, y_j) = 0$, $i \neq 3$, $j \neq 2$, for integer (i, j) .

As in the one-dimensional case, the basis functions overlap; that is, a function is centered around each node in the region or on the boundary. Of course, on the boundary of Ω at least half of the function is "lost" outside Ω . The overall appearance of the basis function array in three dimensions might be imagined as a crystalline surface of multifaceted peaks centered over the nodes, with raised valleys running between. If a function $\theta(x, y)$ were defined over Ω ,

its expansion could be written

$$\theta_N(x,y) = \sum_{i=j}^7 \sum_{j=1}^6 \theta_{ij} u_{ij}(x,y) \quad (14)$$

If the exact values of θ_{ij} were known, θ_N would be a multifaceted approximation to $\theta_{(x,y)}$, equal only at the nodes x_{ij} . Then, within the limitations of machine accuracy and computing time, the greater the node density the better the approximation θ_N will be.

The wire scattering problem expands the field, $h_{\phi 0}$, by use of these pyramid basis functions. Referring to Figure 3, it is seen that the region Ω covered by the triangular elements will not contain any complete pyramids, but this is not really necessary. It will prove convenient to use a sequential node coordinate system rather than the (i,j) Cartesian description of (12). Let n be the node coordinate, where $1 \leq n \leq N$, $N = N_W + N_B$. Then the approximating expansion $h_{\phi N}$ of $h_{\phi 0}$ can be written

$$h_{\phi N}(R,Z) = \sum_{n=1}^N h_n u_n(R,Z) \quad (15)$$

Note that the top and bottom wire nodes are not represented. This is because of the assumption that $h_{\phi 0} = 0$ at these points.

Two field vectors can now be defined. The nodal wire-surface field is

$$\underline{h}_w = \underline{h}_n, \quad n = 1, N_W \quad (16)$$

The nodal boundary field is

$$\underline{h}_B = \underline{h}_n, \quad n = H_w + 1, N \quad (17)$$

These vectors contain the approximate values of h_{ϕ_0} at the nodes of the triangular mesh.

2. Euler-Lagrange Variational Technique

Consider the differential equation $A\theta=f$, which together with certain boundary conditions, describes some physical problem in a region Ω . The complex scalar wave (Helmholtz) equation, $A = [\nabla^2 + k^2]\theta=0$ is an example. The differential equation is related to the functional $F(\theta)$, where

$$F(\theta) = \int_{\Omega} L(\theta, D_x \theta, D_y \theta, x, y) d\Omega \quad (18)$$

This relationship is a fundamental result of the calculus of variations, and simply stated, is the fact that the functional $F(\theta)$ is stationary at the "point" θ_0 which also satisfies the differential equation. That is, if the particular function θ_0 can be found which causes the derivative (or first variation) of $F(\theta)$ to vanish, then $F(\theta)$ is said to be stationary, and θ_0 is said to be the stationary point of $F(\theta)$; θ_0 is then the solution of the equation $A\theta=f$ [5].

Observe that the vanishing of $dF/d\theta$ implies that a minimum, maximum, or saddle point of F occurs $\theta=\theta_0$. In many physical problems F is associated with the potential energy of systems and thus finding θ_0 is sometimes termed the

"minimization" of F . The problem now presents a choice of computational methods. The differential equation might be approximated by a discrete system, say finite differences, or the variational integral, F , can be "minimized" over a finite number of trial functions, as is done by the finite element method.

It is necessary in this procedure to find the Lagrangian L for use in $F(\theta)$ [4]. This L must be such that its insertion in the Euler-Lagrange equation produces the differential equation that is to be solved. As an example, the Euler-Lagrange equation for the two independent variable case is given by

$$\frac{\partial L}{\partial \theta} - \frac{\partial}{\partial X} \left[\frac{\partial L}{\partial D_x \theta} \right] - \frac{\partial}{\partial Y} \left[\frac{\partial L}{\partial D_y \theta} \right] = 0 \quad (19)$$

There is no definite way to discover L for any given problem, but it usually yields to informed guessing.

The problem's boundary conditions present no unmanageable difficulties in this formulation. If θ is specified on the boundary (Dirichlet boundary conditions) nothing else need be done. If θ is unspecified on the boundard, the stationary solution will automatically fulfill the Neumann boundary condition, $\frac{d\theta}{dn} = 0$, also known as the natural boundary condition. Boundary conditions of a more complicated type will require the functional F to be modified, but this procedure will not

be necessary here. It can be easily shown by using the field generating equations in [6], that the natural boundary condition here results in a zero tangential electric field on the wire surface.

3. Application to the Thin-Wire Problem

As discussed in Section II, the driving force in the scattering problem is the incident plane wave. Then, the boundary conditions to be applied are the natural condition along the wire, for nodes $n=1, N_w$, and a Dirichlet condition along the outer boundary of Ω ; $h_{\phi O} = h_t$ (total field). The Dirichlet condition $h_{\phi O} = 0$ has also been imposed on the top and bottom wire nodes. These correspond to boundary conditions along the top and bottom node rows of a larger mesh, as in Figure 5.

The minimization of F for the wire scattering problem is carried out as follows. F is discretized by substituting $h_{\phi N}$ for $h_{\phi O}$, which yields the approximate functional

$$F(h_{\phi N}) = \int_{\Omega} [f_o \{ \nabla(Rh_{\phi N}) \cdot R\mu_r \nabla(Rh_{\phi N}) \} - R\mu_r h_{\phi N}^2] dRdZ \quad (20)$$

The exact functional $F(h_{\phi O})$ is made stationary about the solution $h_{\phi O}$ by differentiating F with respect to $h_{\phi O}$. This makes F stationary about every point on $h_{\phi O}$. Since the approximate solution is to be found only at a finite number (N_w) of points, the functional needs to be made stationary only at those points. This is done by a simultaneous solution of the N_w stationary condition equations

$$0 = \frac{dF}{dh_i} (h_{\phi N}) = 2 \int_{\Omega} \left[\frac{1}{R} \nabla R \frac{dh_{\phi N}}{dh_i} \cdot \nabla R h_{\phi N} - R \frac{dh_{\phi N}}{dh_i} h_{\phi N} \right] dR dZ, \quad i = N_w \quad (21)$$

where h_i is the unknown value of $h_{\phi N}$ at the node $n=i$, and $u_r=1$. Writing $h_{\phi N}$ explicitly,

$$\int_{\Omega} \left[\frac{1}{R} \nabla R u_i \cdot \nabla R \sum_{n=1}^N h_n u_n - R u_i \sum_{n=1}^N h_n u_n \right] dR dZ = 0, \quad i=1, N_w \quad (22)$$

or, since $\sum_{n=1}^N h_n$ is a linear operator with no coordinate dependence,

$$\sum_{n=1}^N h_n \int_{\Omega} \left[\frac{1}{R} \nabla R u_i \cdot \nabla R u_n - R u_i u_n \right] dR dZ = 0, \quad i=1, N_w \quad (23)$$

Boundary conditions at the top and bottom wire nodes are already included in these equations. Application of the total field boundary condition is accomplished by observing that the h_n , $n=N_w+1, N$ are known, where, using (15), $\underline{h}_B = \underline{h}_t$. So by splitting the sum the useful minimization equations for $F(h_{\phi N})$ are found to be

$$\sum_{n=1}^{N_w} C_{in} h_n + \sum_{n=N_w+1}^N C_{in} h_n = 0, \quad i=1, N_w \quad (24a)$$

where

$$C_{in} = \int_{\Omega} \left[\frac{1}{R} \nabla R u_i \cdot \nabla R u_n - R u_i u_n \right] dR dZ \quad (24b)$$

The matrix equation to be used for computation can be formed directly from (24). First, recall that the basis functions u_n are zero on and outside of the boundary $\partial\Omega_n$. This means that the product of non-overlapping basis functions is zero. For example, in Figure 3, $u_3 \cdot u_1 = 0$. Thus

$$u_i u_n = 0 \quad , \quad |n-i| \geq 2 \quad (25a)$$

and

$$\nabla R u_i \cdot \nabla R u_n = 0 \quad , \quad |n-i| \geq 2 \quad (25b)$$

This behavior is very useful in that it produces banded coefficient matrices. Special techniques can be used to invert large banded matrices very quickly. Writing out a few equations should make the matrix construction clear.

$$\begin{aligned} i=1: & \quad C_{11}h_1 + C_{12}h_2 + C_{1N_w+1}h_{N_w+1} + C_{1N_w+2}h_{N_w+2} = 0 \\ i=2: & \quad C_{21}h_1 + C_{22}h_2 + C_{23}h_3 + C_{2N_w+2}h_{N_w+2} + C_{2N_w+3}h_{N_w+3} = 0 \\ i=3: & \quad C_{32}h_2 + C_{33}h_3 + C_{34}h_4 + C_{3N_w+3}h_{N_w+3} + C_{3N_w+4}h_{N_w+4} = 0 \end{aligned} \quad (26)$$

The system equation can therefore be written

$$\underline{\underline{A}}\underline{\underline{h}}_w = -\underline{\underline{B}}\underline{\underline{h}}_B \quad (27)$$

where the $N_w \times N_w$ coefficient matrix $\underline{\underline{A}}$ contains the basis function integrals for $i=1, N_w, n=1, N_w$ and the $N_w \times N_w + 1$ matrix $\underline{\underline{B}}$ contains the integrals for $i=1, N_w, n=N_w+1, N$. Both $\underline{\underline{A}}$ and $\underline{\underline{B}}$ are diagonal and have the forms

$$\underline{\underline{A}}: \begin{bmatrix} X & X & & & \\ X & X & X & & 0 \\ & X & X & X & \\ & & & \ddots & \\ 0 & & & X & X & X \\ & & & & X & X \end{bmatrix} \quad \underline{\underline{B}}: \begin{bmatrix} X & X & & & \\ & X & X & & 0 \\ & & X & X & \\ & & & \ddots & \\ 0 & & & X & X \\ & & & & X & X \end{bmatrix}$$

The wire field $\underline{\underline{h}}_w$ due to the boundary field $\underline{\underline{h}}_B$ is now known, since

$$\underline{\underline{h}}_w = -\underline{\underline{A}}^{-1}\underline{\underline{B}}\underline{\underline{h}}_B = \underline{\underline{V}}\underline{\underline{h}}_t \quad (28)$$

Equation (28) is the forward path in the system of Figure 1. The actual calculation of the A_{in} , B_{in} will be discussed in Section III.C.

B. SCATTERED FIELD INTEGRAL

1. Vector Potential Formulation

The development of the feedback path is less complicated than the forward path construction given in III.A. The

thin-wire approximation is applied to the familiar classical vector potential \bar{A} , and a matrix equation formulation built on a one-dimensional basis function expansion. The result will be an approximation giving the near field produced by a wire-surface field or current.

From the inhomogeneous Helmholtz equation

$$\nabla^2 \bar{A} + k^2 \bar{A} = -\bar{J} \quad (29)$$

it is seen, since $\bar{J} = J_z \hat{Z}$ by assumption, that $\bar{A} = A_z \hat{Z}$. Then it follows from the vector potential defining equation

$$\bar{H} = \nabla \times \bar{A} \quad (30)$$

that

$$H_\phi = -\frac{\partial}{\partial R} A_z(R, Z) \quad (31)$$

The azimuthal invariance of \bar{H} has been made explicit in (31).

A commonly used expression for \bar{A} [1] is given as an integration of a weighted point-source Green's function $G(\bar{r}', \bar{r})$ over the current source where

$$G(\bar{r}', \bar{r}) = \frac{1}{4\pi} \frac{e^{-jk_0 |\bar{r} - \bar{r}'|}}{|\bar{r} - \bar{r}'|} \quad (32)$$

Then

$$\bar{A}(\bar{r}) = \int_{V'} \bar{J}(\bar{r}') G(\bar{r}', \bar{r}) dV' \quad (33)$$

This general situation is shown in Figure 6.

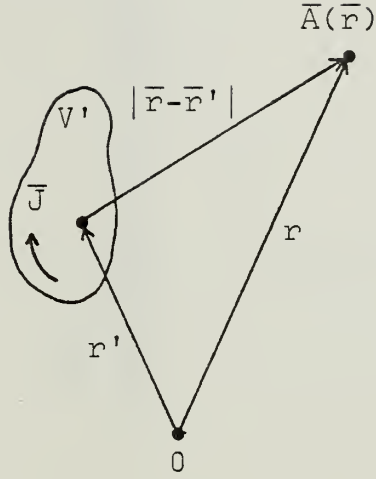


Figure 6

2. Scattered Field Matrix Equation

The formulation is easily applied to the thin-wire case. Recalling that $h_{\phi 0} = \eta_0 H_\phi$, and assuming that the current J_Z lies along the Z axis, \bar{A} , for the thin wire, is

$$\eta_0 A_Z(R, Z) = \int_S \int h_\phi(Z') \frac{e^{-j|D|}}{4\pi|D|} R_a d\phi dZ' \quad (34)$$

where, $|D| = \sqrt{R^2 + (Z - Z')^2}$, as seen in Figure 7, and the integration is over S , the wire surface. Now, putting (34) in (31) yields

$$h_{\phi 0}(R, Z) = \frac{R_a R}{2} \int_{-1/2}^{1/2} \int_{Z_L}^{Z_L} h_{\phi 0}(Z') \left[\frac{j}{|D|^2} + \frac{1}{|D|^3} \right] e^{-j|D|} dZ' \quad (35)$$

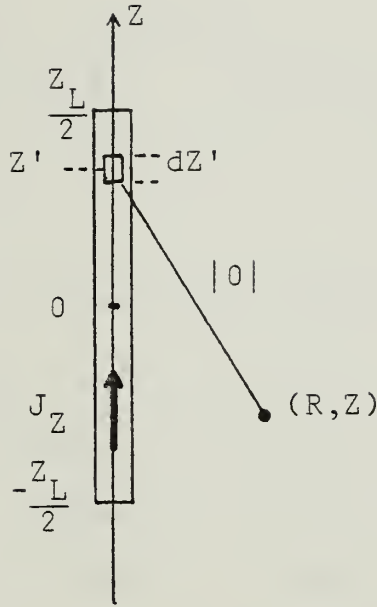


Figure 7

This $h_{\phi_0}(R, Z)$ is approximately the scattered field, $h_s(R, Z)$, radiated by the wire carrying an induced current J_Z . This wire current, in the form of $h_{\phi_0}(Z')$, must be approximated by a basis function expansion so that $h_s(R, Z)$ can be computed. Since $h_{\phi_0}(Z')$ is a function of Z only, the one-dimensional linear basis functions shown in Figure 4 may be used. Then, for the same N_w nodes along the wire, as in Section III.A.,

$$h_{\phi_0}(Z') = \sum_{n=1}^{N_w} h_n u_n(Z') \quad (36)$$

Notice that (36) defines the same nodal surface-field vector as (16). Substitution of (36) into (35) produces

$$h_s(R, Z) = \frac{R_a R}{2} \sum_{n=1}^{N_w} h_n \int_{Z'_{n-1}}^{Z'_{n+1}} u_n(Z') \left[\frac{j}{|D|^2} + \frac{1}{|D|^3} \right] e^{-j|D|} dZ' \quad (37)$$

The limits of integration reduce from $\pm Z_{L/2}$ to Z'_{n-1} , Z'_{n+1} because the basis function $u_n(Z')$ is zero for $Z'_{n-1} > Z' > Z_{n+1}$. Equation (37) can be used to construct the \tilde{T} matrix by noting that (37) gives the scattered field at one point (R, Z) . Then, by choosing a number of points in some region, a discrete field approximation can be constructed. The points chosen will be, unsurprisingly, just those N_B points along the finite element mesh border. So the matrix equation is

$$\underline{h}_s = \tilde{T} \underline{h}_w \quad (38a)$$

where

$$T_{bn} = \frac{R_a R}{2} \int_{Z'_{n-1}}^{Z'_{n+1}} u_n(Z') \left[\frac{j}{|D|^2} + \frac{1}{|D|^3} \right] e^{-j|D|} dZ' \quad (38b)$$

is the coefficient of the n -th value of the wire field, and $T_{bn} h_n$ is one term of the b -th value of the scattered field.

Finally, since $\underline{h}_t = \underline{h}_s + \underline{h}_{inc}$, an expression for the total field in terms of the incident and wire fields is

$$\underline{h}_t = \underline{h}_{inc} + \tilde{T} \underline{h}_w \quad (39)$$

The scattered field \underline{h}_s found in (38) is a near field expression. It is valid at any distance from the wire, but this behavior does not extend to the entire problem. If \underline{h}_s were to be found at some large distance from the wire, simply extending the radial width of Ω would not suffice. This is because FEM calculation accuracy degrades as the distance from the wire to the boundary, B_L , increases. The magnitudes of the electrostatic and induction fields decrease rapidly as R increases, so the point is quickly reached where they become effectively zero as far as computer calculations are concerned. The resulting incorrect total field values are a part of the FEM R -related inaccuracies. The greater part of the FEM error is found in the basis function expansion of \underline{h}_ϕ . The planar-section basis functions used are unable to accurately model the near field over a large radial distance, where "large", in this case, may be 1/100 of the wavelength.

To solve the far-field problem, the near-field solution must first be obtained for the wire field \underline{h}_w . Then (38) may be used to find \underline{h}_s along any boundary. For typical far-field problems, assumptions may be made to reduce the integral's complexity. Let β be the angle of the far-field point, measured from the Z axis at the origin. Then $R = k_o r \sin\beta$, where r is the spherical radius of the point. The far-field assumption is

$$|D| = k_o r - Z' \cos\beta \quad (\text{in phase term of (38b)}) \quad (40a)$$

$$|D| = k_o r \quad (\text{in denominators}) \quad (40b)$$

So the radiation field along a spherical arc of radius r is given by (38), where T_{bn} is

$$T_{bn} = j \frac{a \sin \beta}{2r} e^{-jk_o r} \int_{Z'_{n-1}}^{Z'_{n+1}} u_n(Z') e^{jZ' \cos \beta} dZ' \quad (41)$$

C. PROBLEM IMPLEMENTATION

Combining equations (27) and (39) gives

$$\underline{h}_w = -(\underline{A} + \underline{B}\underline{T})^{-1} \underline{B} \underline{h}_{inc} \quad (42)$$

This is, of course, the same equation as is represented in Figure 1, where $\underline{V} = -\underline{A}^{-1}\underline{B}$. The system "transfer matrix" is defined by

$$\underline{h}_w = (\underline{I} - \underline{V} \cdot \underline{T})^{-1} \cdot \underline{V} \cdot \underline{h}_{inc} \quad (43a)$$

Simple matrix algebra leads to a simplification of this result

$$\underline{h}_w = -(\underline{A} + \underline{B} \cdot \underline{T})^{-1} \cdot \underline{B} \cdot \underline{h}_{inc} \quad (43b)$$

Multiplying this equation by $(\underline{A} + \underline{B}\underline{T})$ yields (42), so the system equation as derived does behave as a feedback system.

The only variable remaining to be identified is \underline{h}_{inc} , the incident field vector. The incident plane wave \underline{h}_{inc} can be

expressed in the normalized cylindrical coordinate system as

$$h_{\phi}(R,Z) = je^{-jZ\cos\alpha} J_0'(R\sin\alpha) \quad (44)$$

where J_0' is the derivative of the zeroth-order Bessel function. Since R will be kept small, as discussed in Section III.B., (44) may be simplified by replacing $J_0'(R\sin\alpha)$ with the first few terms of its series expansion

$$J_0'(R\sin\alpha) \doteq -\left(\frac{R\sin\alpha}{2}\right) + \left(\frac{R\sin\alpha}{16}\right)^3 - \left(\frac{R\sin\alpha}{384}\right)^5 \quad (45)$$

Then h_{inc} may be calculated at the boundary nodes by use of (44) and (45).

Now that expressions for all of the quantities in (42) have been found, the computer program can be devised to carry out the calculations. The use of an existing routine, CSMINV, for the inversion of $(\tilde{A} + \tilde{B}\tilde{T})$ reduces the number of major computations to two: equation (24b) for the \tilde{A} and \tilde{B} elements, and equation (38b) for the scattered field coefficients T_{bn} .

The integration of (34b) becomes algebraically messy, but is otherwise straightforward. Because of the basis function's behavior, the integration area is reduced from Ω to $\partial\Omega$, the region of non-zero overlap of u_i and u_n . This integration over $\partial\Omega$ may then be written as a sum of integrations over the triangular elements comprising $\partial\Omega$, since u_n is piecewise planar in the elements. Also, note that C_{in} is independent of Z in

the sense that the integration for any pair (i,n) of nodes, will be the same if that pair is translated along the wire. This means that one wire node may be selected, and the integrals concerning that node and its immediate neighbors will be the only ones required to construct \tilde{A} and \tilde{B} . For example, select $i=2$. Then C_{21} , C_{22} , C_{2N_w+2} and C_{2N_w+3} are the only integrals that need to be calculated. (Node three is not being neglected. Equation (24b) shows that $C_{23} = C_{32}$, but this is just C_{21} moved up one element. So $C_{23}=C_{21}$.)

In this simple narrow mesh case, the integration of (24b) is required over at most three elements (C_{22}), and the size and shape of all elements is the same. For many problems this will not be the case. For large meshes, and especially for skewed elements, it becomes very convenient computationally to change from a global to a local node system. Instead of moving from node to node, calculating all the coefficients about each node one at a time, an algorithm is devised to move from element to element, finding the integrals involving the three corner nodes over each element. This procedure effects a considerable simplification in the "bookkeeping" necessary to keep track of the nodal indices and coordinates.

The local node system employed here is shown in Figure 8. The integrals of the combinations of local nodes (k,l) are found over a upper and lower element. Then the integrals can be placed in their proper global positions. As an example,

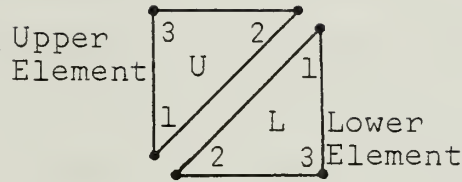


Figure 8. Local Node Indices

consider the upper element with global nodes $(2, 3, N_w + 3)$. The integrations of (24b) over U are found for local node pairs $(1,1), (1,2), (1,3), (3,1), (3,2)$, and $(3,3)$. Then the local node pair $(1,1)$ integral, $f(1,1)$ is put in \tilde{A} as one part in three of C_{22} , $f(1,2)$ is one part in two of C_{2N_w+3} in \tilde{B} , and $f(1,3) = C_{23}$ in \tilde{A} . Also, $f(3,1) = C_{32}$, $f(3,2)$ is part of C_{3N_w+3} , and $f(3,3)$ is part of C_{33} . The remaining three local node integrals over U are not needed in this case, but would be used in larger meshes.

For the thin mesh used here, the local node procedure improves only slightly the algorithm efficiency as compared to a global node procedure. The principle reason for its use was that an existing and successful subroutine was available to do local node integrations. This routine is named VARELA in the program. It requires only the local node ordering scheme and the coordinate (R, Z) of each local node to produce

a three by three matrix containing the integrations. As discussed above, the wire-scattering problem needs only two calls to VARELA to obtain the necessary values. The subroutine ABLOAD then fills \tilde{A} and \tilde{B} with these integrals.

The calculation of the coefficients T_{bm} is done by the familiar Gaussian quadrature method, using eight unequally spaced points. The interval of integration in (38b) is split into two segments, as in Figure 9. Then a change of variable is affected so that the limits of integration in each sub-interval are $X=+1$ to -1 . The Gaussian procedure then gives

$$\int_{-1}^{+1} f(x)dx \approx \sum_{i=1}^n w_i [f(x_i) + f(-x_i)] \quad (46)$$

where the values $\pm x_i$ and the weight factors w_i are tabulated in several references such as [6]. The code used to implement these integrations is contained in subroutine GFINT.

Equation (42) is coded in two subroutines, CFORM and ZCURRE. Routine CFORM produces the matrix product $(\tilde{A} + \tilde{B}\tilde{T})^{-1}\tilde{B} = \tilde{C}$, while ZCURRE calculates the incident field vector \tilde{h}_{inc} according to (44) and (45), then finds the wire field vector $\tilde{h}_w = \tilde{C} \tilde{h}_{inc}$.

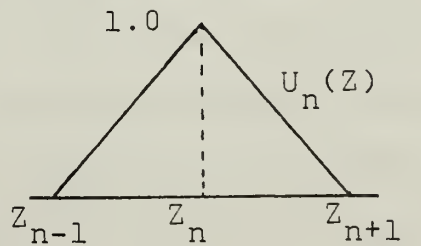


Figure 9

IV. RESULTS AND ANALYSIS

In many other time-harmonic field problems, FEM calculations yield good results with perhaps 20 to 30 nodes per wavelength. With higher node densities, say 50-75 perwavelength, the solution breaks down due to roundoff error in the computations. As will be shown, this does not appear to be the case with the field feedback formulation. Nodal densities as high as 100 per wavelength have been used without difficulty. Indeed, these high densities are required in order to achieve good convergence of the formulation. As yet, no satisfactory answer for this behavior has been found.

The only other parameter available to affect the convergence of the solution is B_L , the wire-to-boundary distance. As mentioned in section III.B.2., this parameter can be expected to be critical in achieving a good field approximation. Computed results show this to be true.

A great deal of effort was expended in looking for errors in the formulation before the solution behavior with respect to B_L and N_W was fully appreciated. It is still possible, no matter how unlikely, that some error still exists. If an error is present in the formulation, or code, it's effect is quite peculiar. By comparison with other FEM problems, the possible error causes two to three times the "normal" node

density to be needed, but otherwise seems to have no effect. That is, the results are satisfactory in all respects save node density required for convergence.

The primary comparison case chosen was a one-half wavelength wire with a radius of $1/50$ wavelength. This case was a compromise forced by excessive required computing for longer wires and questionable integral equation comparison results with shorter wires. These other cases were looked at, and some example results are included here. Their investigation, however, has not been exhaustively completed due to lack of time.

A. INTEGRAL EQUATION COMPARISON

The basis used for judging the convergence of the FFM computation was a standard and successful type of integral equation formulation, Hallen's equation for scattering by a thin conductive cylinder. This method assumes a \hat{z} directed current density, and finds this wire current by a simultaneous solution of two expressions for the vector potential, \bar{A} . One equation is just equation (33). The second is a different form of equation (20)

$$\nabla^2 \bar{A} + k^2 \bar{A} = j\omega\epsilon \bar{E}^S(\bar{r}) \quad (47)$$

where $\bar{E}^S(\bar{r})$ is the scattered electric field. Simple manipulations yield the integral equation for $I(z')$, [7]

$$\int_0^L I(Z') G(Z, Z') dZ' - j \int_0^Z I(Z') \frac{Z(Z')}{Z_0} \sin k(Z-Z') dZ' + C \sin kZ + D \cos kZ = U(Z) \quad (48)$$

where A is an impedance per unit length, C and D are constants of integration, and U contains the incident field. Equation (48) is coded in subroutine INTEQ.

Results for the $1/2 \times 1/50$ wavelength case are shown on pages A-1 through A-38 of Appendix A. F^3 calculations are shown as a solid line, while integral equation computations are displayed as the "X" curve. The parameters of each case are given below the graph. The magnitude plots are scaled in milliamperes along x , and wavelengths along y . The wire is to be seen lying along the y axis, and is conveniently demarcated by the zero end values of the integral equation curve. The current phase plots have the same y axis units, and are scaled in degrees along x .

Graphs A-1 through A-24 show F^3 convergence with an increasing number of nodes. Values of N_w are 20, 40, 70 and 100, with three plane wave incidence angles (ALPHA) used in each case. In these plots, the plane wave is incident from the upper right for ALPHA=30 and 60 degrees. ALPHA=90° is broadside incidence. Convergence of the current magnitude

is plainly seen at all incidence angles. For $\alpha=90^\circ$, the error is 15.5% at the wire center for $N_w=20$, but only 2.5% for $N_w=70$. Similarly, the phase error decreases from 18° to 1° . Comparing the $N_w=70$ and $N_w=100$ cases, it is seen that the extra nodes make very little difference in the quality of the solution. Convergence has been essentially accomplished at $N_w=70$, and the additional memory and computing time for $N_w=100$ are not really necessary. The convergence is less satisfying for incidence angles other than 90° . At $\text{ALPHA}=30^\circ$, for example, the magnitude is not skewed quite enough, while the phase error increases toward the wire bottom. This situation does not improve as N_w increases.

Graphs A-25 through A-38 show FFM convergence as a function of B_L . All F^3 calculations are made with $N_w=28$. The behavior shown in these plots is characteristic of all cases of wire length and radius. For B_L much too large, the magnitude is too low and the phase is off by as much as 90° . As B_L decreases, the magnitude rises, overshoots, and then settles back towards the correct, convergent value. The phase moves smoothly down to the correct value. Notice that the F^3 curves are nearly identical for $\text{DR}=\text{DZ}/32$ and $\text{DR}=\text{DZ}/64$. This implies that convergence has been reached by the time DR has decreased to $\text{DZ}/32$, or $B_L=.0005\lambda_0$. For this case the convergence point of B_L is actually about $B_L=.001\lambda_0$, as shown in A-1 through A-25. Results for several other cases of wire length and radius are shown in Appendix B. The one and two wavelength wire

calculations show that more nodes are required, assuming that $B_L = .001\lambda_0$ is still adequate since A_L has not changed. If 70 nodes are required for a good answer at $Z_L = \lambda_0/2$, then for two wavelengths as many as 300 nodes might be necessary. Similarly, well over 100 nodes could be needed for the one wavelength wire. The one wavelength case indicates that this is probably true. The F^3 solution for $N_w = 100$ is perceptibly better than the $N_w = 70$ solution, especially for off-axis incidence angles.

Appendix C contains graphs for two different cases: $A_L = 1/100\lambda_0$ while $Z_L = \lambda_0/2$ or $Z_L = \lambda_0/4$. Graphs C-1 through C-4 again show convergence value is no longer $B_L = .001\lambda_0$, but is smaller than $B_L = .0005\lambda_0$.

Plots C-7 through C-10 show the quarter-wavelength wire case. It appears from the FFM curves that convergence has been almost reached for $N_w = 40$. This calls into question the accuracy of the integral equation solution. This possible inaccuracy should not be too surprising, however, since the wire is relatively thick for it's length, and the integral equation does much better for very thin wires.

An "error isolation" check was made on the F^3 system by testing the feedback path. A fictitious sinusoidal wire current was generated and its radiated field calculated via $\underline{h}_s = \underline{T} \underline{h}_w$. This field was compared to that given in reference [8]. The comparison is shown in plots C-11 and C-12. The two field calculations are equal, to the fourth significant digit. This indicates that the feedback path formulation and program coding is correct.

B. ERROR ANALYSIS

Consideration of the near field behavior reveals the reason for the critical dependence of the solution on B_L . The magnetic field magnitude in the very near field is dominated by a $1/R^2$ term, as can be deduced from equation (37). This is depicted in Figure 10. Also shown are two dashed lines which are the linear basis function expansion of the field. It is clear from the figure that the approximation of the field deteriorates as A_L decreases, if B_L is held constant. Thus it is seen why $B_L = .001\lambda_0$ is adequate for $A_L = .02\lambda_0$ while $B_L = .0005\lambda_0$ to obtain the best convergence with $A_L = .01\lambda_0$. It is noted, however, that even at this best convergence value of B_L , the F^3 solution is not as close to the integral equation solution as in the $A_L = .02\lambda_0$, $B_L = .001\lambda_0$ case. This fact can also be explained by consideration of the basis function approximation's behavior. While decreasing B_L improves the field approximation very near the wire, the approximation becomes worse in the neighborhood of $R = B_L$.

It thus appears that there is a limit to the usefulness of this formulation of the F^3 solution to the wire-scattering problem. The primary difficulty lies in the inaccuracy of the linear basis function expansion used in the FEM calculation. A much better basis function may contain a term proportional to $1/R^2$. This would greatly reduce the sensitivity of the solution to B_L .

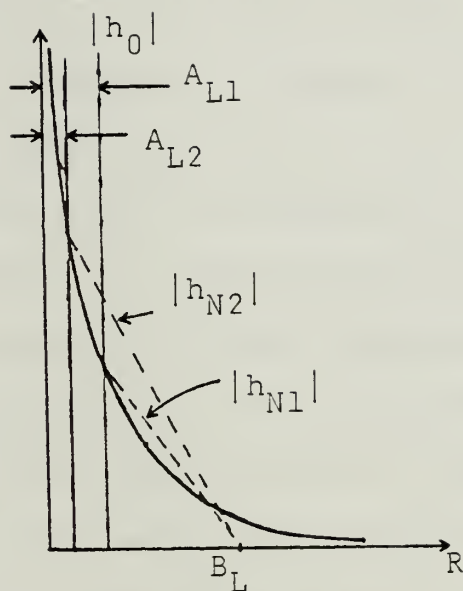


Figure 10

There is another source of error which is inherent in any sort of computer solution: roundoff. Simple calculations will be affected in the sixth or seventh significant digit by the use of single-precision arithmetic on the IBM-360. If only a few operations were required, this error could be ignored. But when solving large systems of equations many thousands of operations are required, and accuracy can be severely degraded.

A rough guide to the degree of trust to be placed in a solution can be had in the condition number of an inverted matrix. This number provides an upper bound on error propagation in a system due to the inaccuracy of finite-precision

arithmetic. For example, in the system $\underline{X} = \underline{\tilde{A}}^{-1}\underline{Y}$, a condition number of 1000 for $\underline{\tilde{A}}^{-1}$ would cause errors in the third significant digit of \underline{Y} to appear as errors in the third, second or even first significant digit of \underline{X} .

This condition number is a measure of the similarity of the system equations. In the wire-scatterer case, as the solution points are placed closer together, the field values at these nodes become more indistinguishable. Hence the equations relating the field values at neighboring nodes become more nearly the same. The system solution, then, becomes sensitive to errors in the less significant digits.

Condition numbers of system matrices for the cases discussed here range from about 250 to 1000. Cases with fewer nodes and larger values of B_L have lower condition numbers, while as N_w increases and/or B_L decreases, the condition number increases rapidly. This is another reason why a good solution is more difficult to achieve for very thin or long wires. The use of a basis function more suited to the field behavior would allow larger values of B_L to be employed. This would lower the system condition number significantly, and improve the solution's accuracy and trustworthiness. Other than this and keeping N_w as small as possible, there is nothing that can be done to avoid the problems reflected in the condition number.

Even if the errors mentioned above could be eliminated, the results of both the F^3 and integral equation calculations

would still not represent the fields with complete accuracy. The assumptions made in both formulations are not strictly true for any wire of finite thickness. Current flows on the surface of the wire, not in the center, as assumed in the vector potential formulation.

Field phase variation from side to side of the wire is not zero, so there is an azimuthal component of current as well as the \hat{z} -directed current assumed. And because this $\hat{\phi}$ -directed current exists, the current is not zero at the wire ends. But, since essentially the same types of approximations are made for both solution methods, it is not possible to ascertain, from the comparisons made here, the degree to which either solution represents the actual fields.

V. CONCLUSIONS

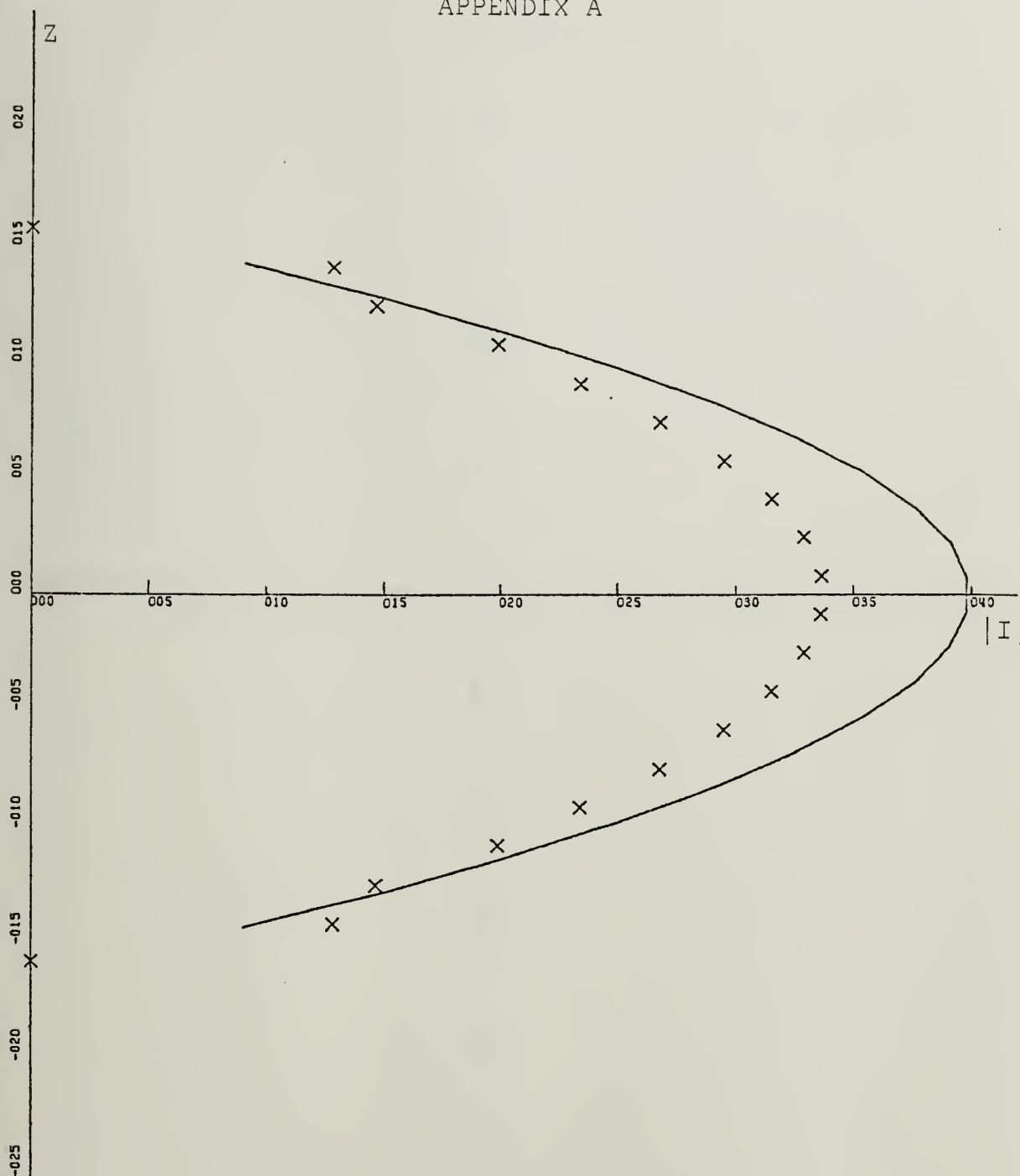
As a result of this investigation, the field-feedback formulation has been shown to be a sound technique for the computation of electromagnetic scattering problems. It has been demonstrated that F^3 calculations compare very favorably with results obtained by the conventional integral equation formulation. The success of this initial development is not unqualified, however. The two deficiencies previously discussed, basis function unsuitability and excessive number of required nodes, could present formidable difficulties in problems where a priori knowledge of field behavior is not available, or where bodies large compared to a wavelength are used.

The discrepancy between required and expected node density is particularly troublesome, as this fact is as yet unexplained. If high node densities are actually required by the method and are not just the result of some formulational error, then the attendant large matrices will limit the usefulness of F^3 computations because of the great amount of computer memory required.

In any case, the flexibility of the finite-element method when used in the coupled-azimuthal potential formulation should allow numerous heretofore difficult problems to be attacked. The ease with which mixed boundary conditions can

be met for complicated inhomogeneous scattering bodies, and the accuracy and simplicity of the vector potential formulation promise a wide applicability for the field feedback formulation.

APPENDIX A



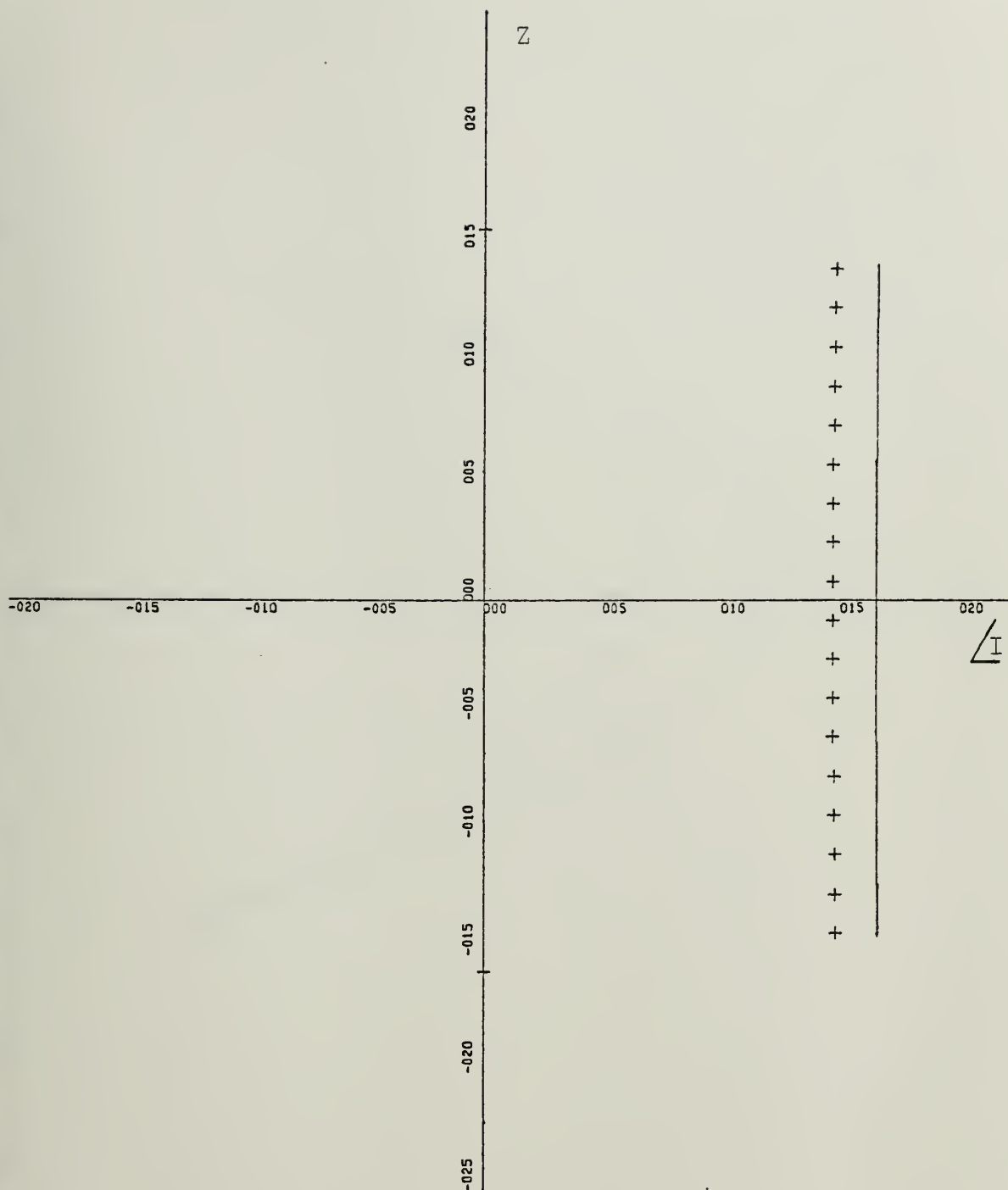
X-SCALE=5.00E-04 UNITS INCH.

Y-SCALE=5.00E-01 UNITS INCH.

CURRENT MAGNITUDE : FEM/T=SOLID : INT.EQ=X

ZL=.5:AL=0.02:BL=0.001:ALFA=90:NW=20

A-1



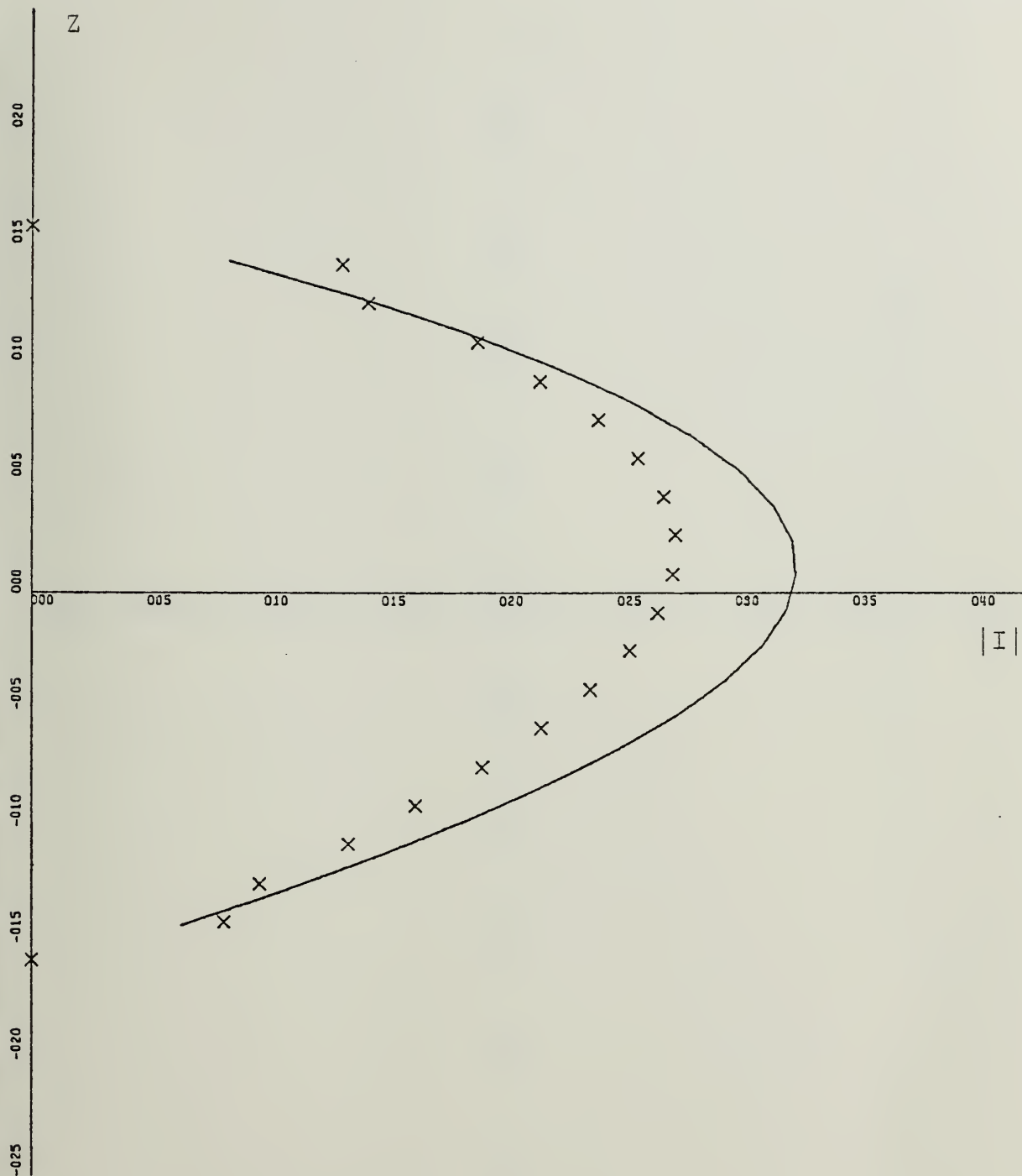
X-SCALE=5.00E+01 UNITS INCH.

Y-SCALE=5.00E-01 UNITS INCH.

CURRENT PHASE : FEM/T=SOLID : INT.EQ=PLUS

ZL=.5:AL=0.02:BL=0.001:ALFA=90:NW=20

A-2

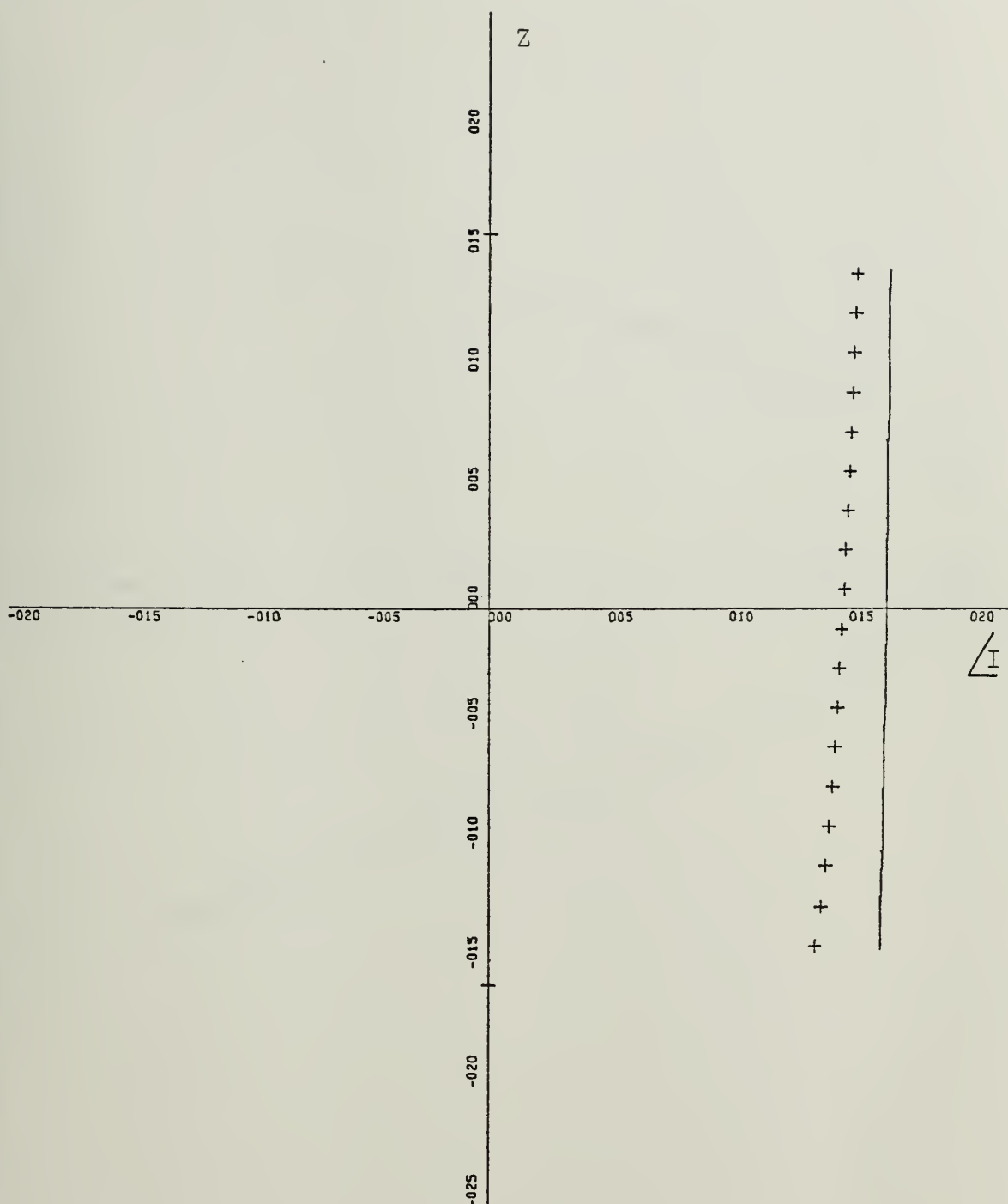


X-SCALE=5.00E-04 UNITS INCH.

Y-SCALE=5.00E-01 UNITS INCH.

CURRENT MAGNITUDE : FEM/T=SOLID : INT.EQ=X

ZL=.5:AL=0.02:BL=0.001:ALFA=60:NW=20



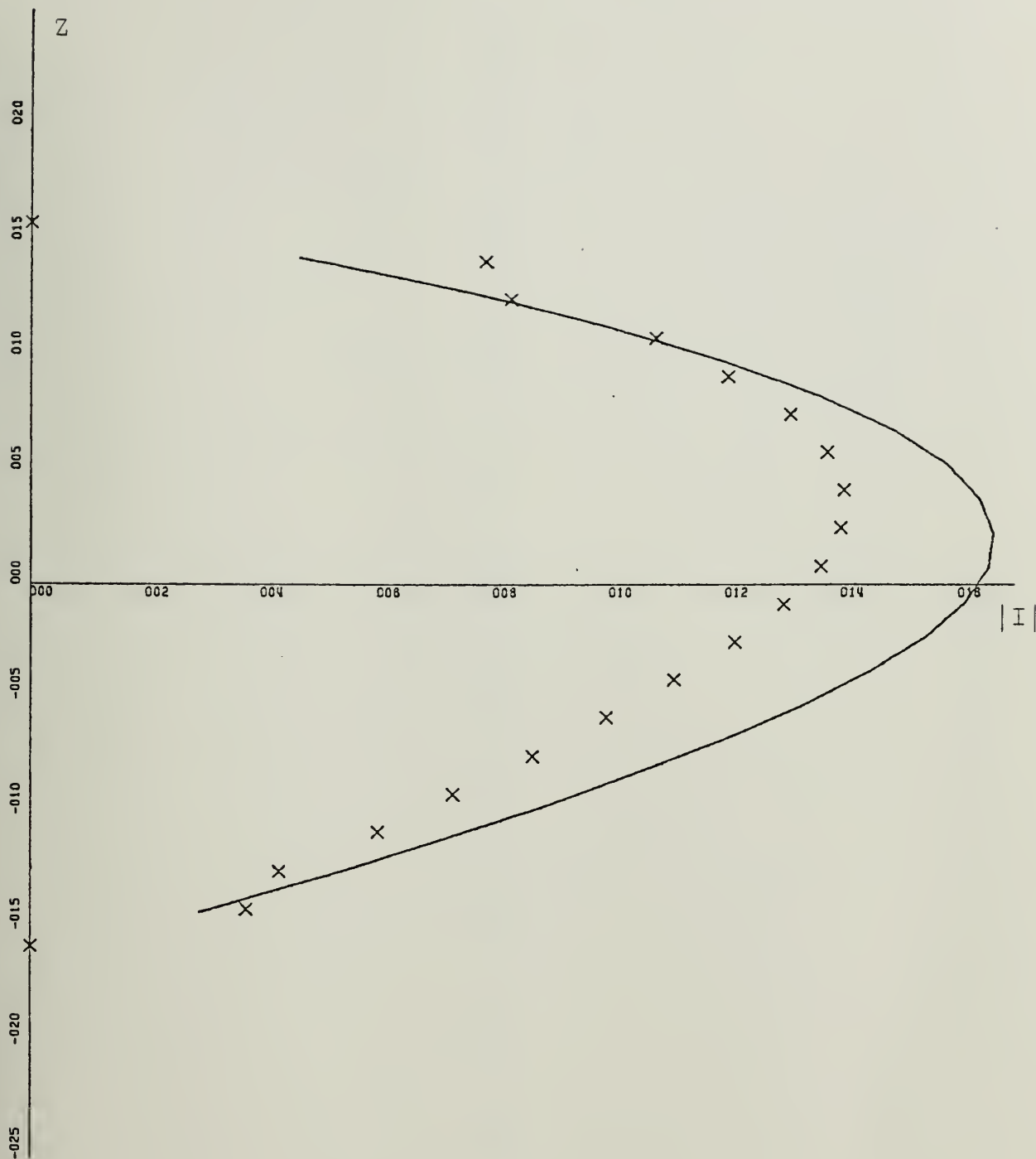
X-SCALE=5.00E+01 UNITS INCH.

Y-SCALE=5.00E-01 UNITS INCH.

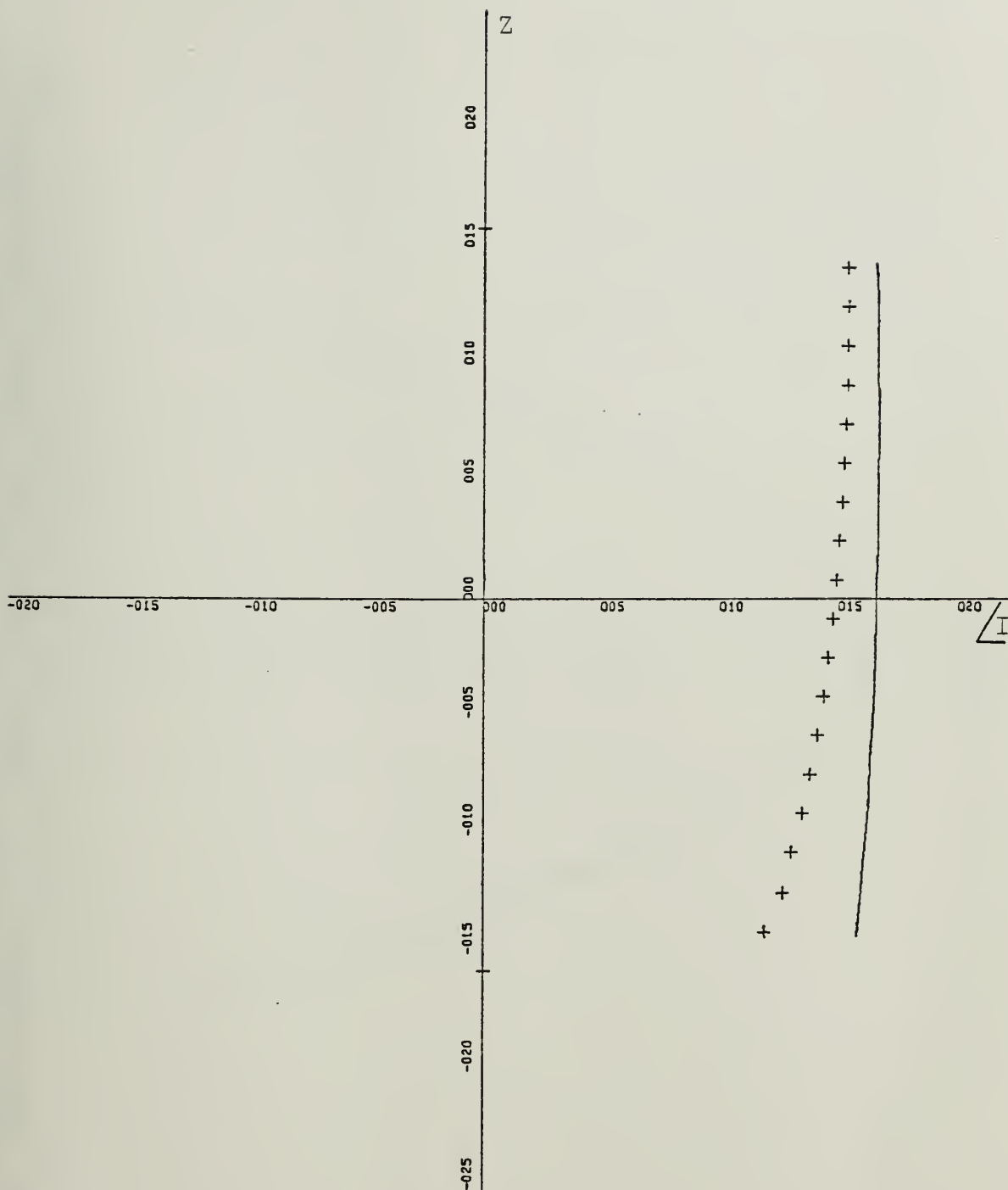
CURRENT PHASE : FEM/T=SOLID : INT.EQ=PLUS

ZL=.5:AL=0.02:BL=0.001:ALFA=60:NW=20

A-4



X-SCALE=2.00E-04 UNITS INCH.
 Y-SCALE=5.00E-01 UNITS INCH.
 CURRENT MAGNITUDE : FEM/T=SOLID : INT.EQ=X
 ZL=.5:AL=0.02:BL=0.001:ALFA=30:NW=20
 A-5



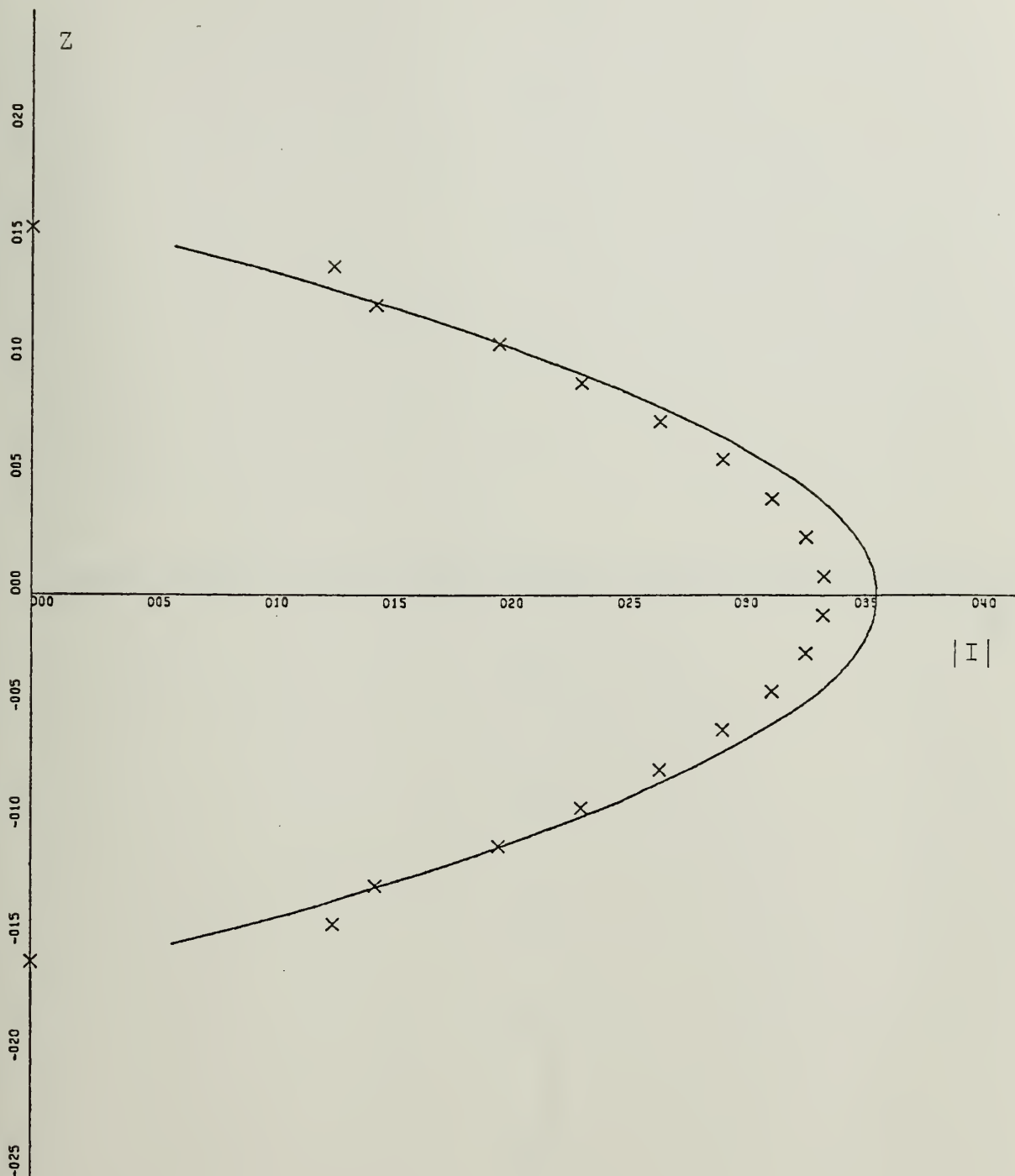
X-SCALE=5.00E+01 UNITS INCH.

Y-SCALE=5.00E-01 UNITS INCH.

CURRENT PHASE : FEM/T=SOLID : INT.EQ=PLUS

ZL=.5:AL=0.02:BL=0.001:ALFA=30:NW=20

A-6



X-SCALE=5.00E-04 UNITS INCH.

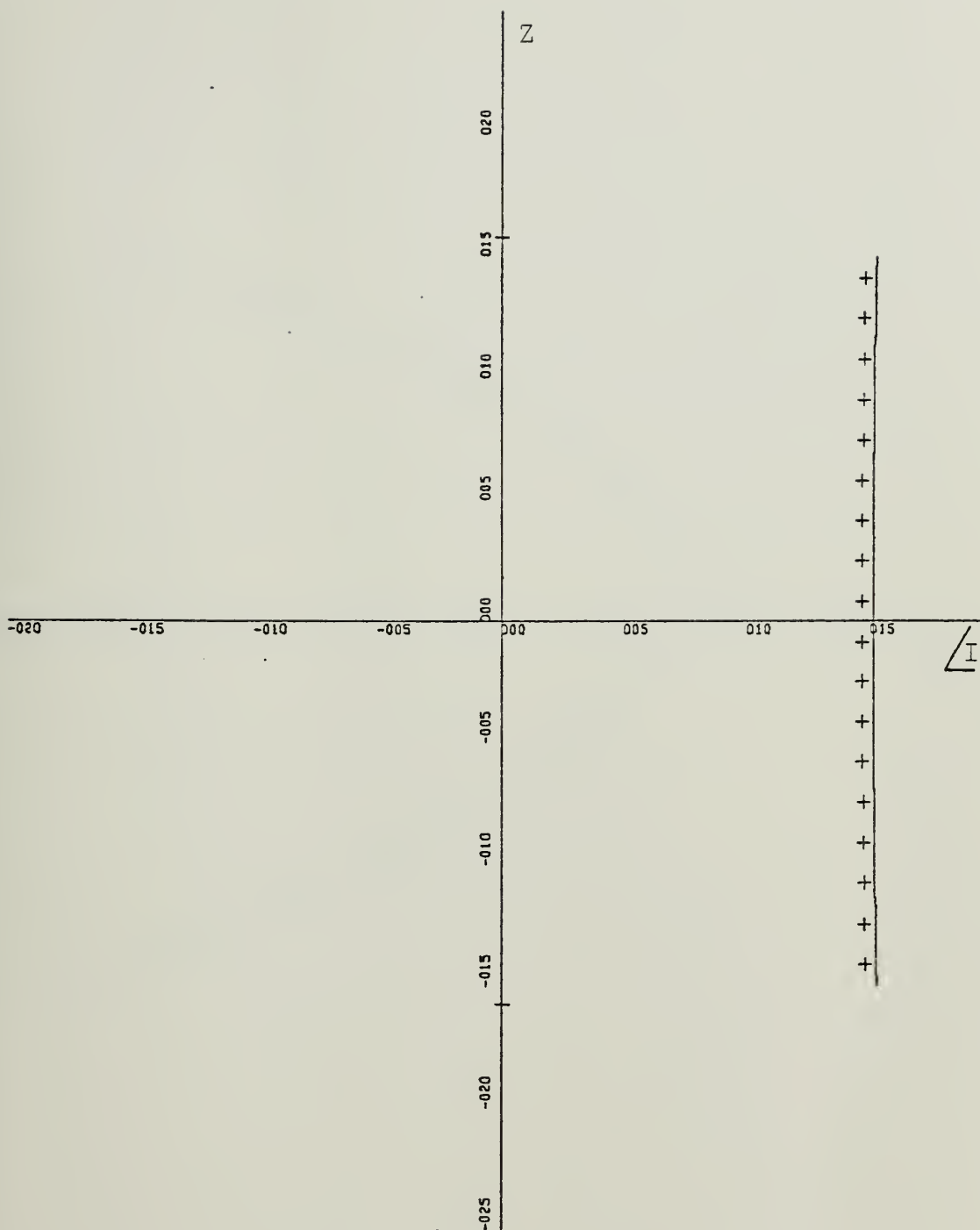
Y-SCALE=5.00E-01 UNITS INCH.

CURRENT MAGNITUDE : FEM/T=SOLID : INT.EQ=X

ZL=.5:AL=0.02:BL=0.001:ALFA=90:NW=40

A-7





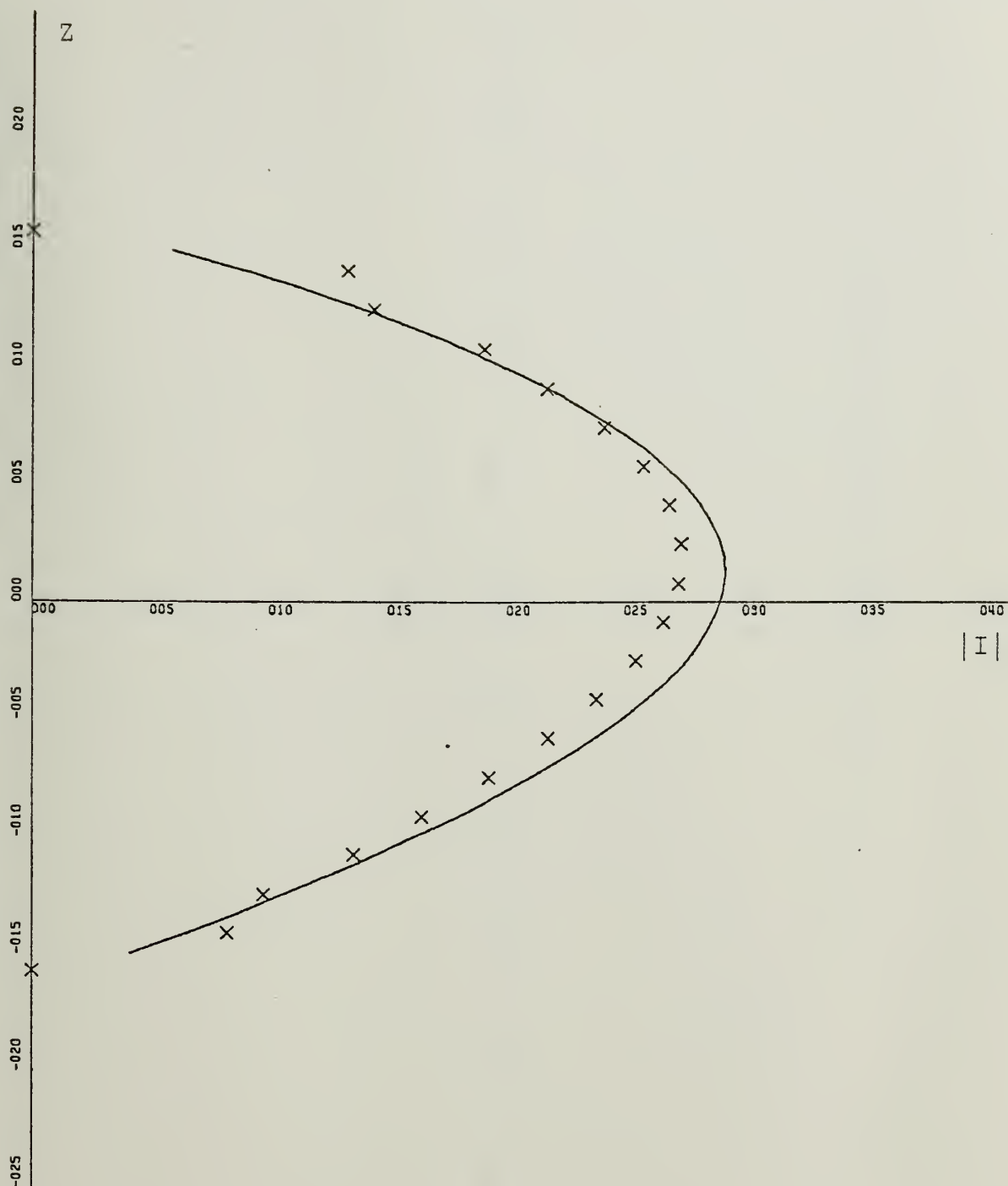
X-SCALE=5.00E+01 UNITS INCH.

Y-SCALE=5.00E-01 UNITS INCH.

CURRENT PHASE : FEM/T=SOLID : INT.EQ=PLUS

ZL=.5:AL=0.02:BL=0.001:ALFA=90:NW=40

A-8



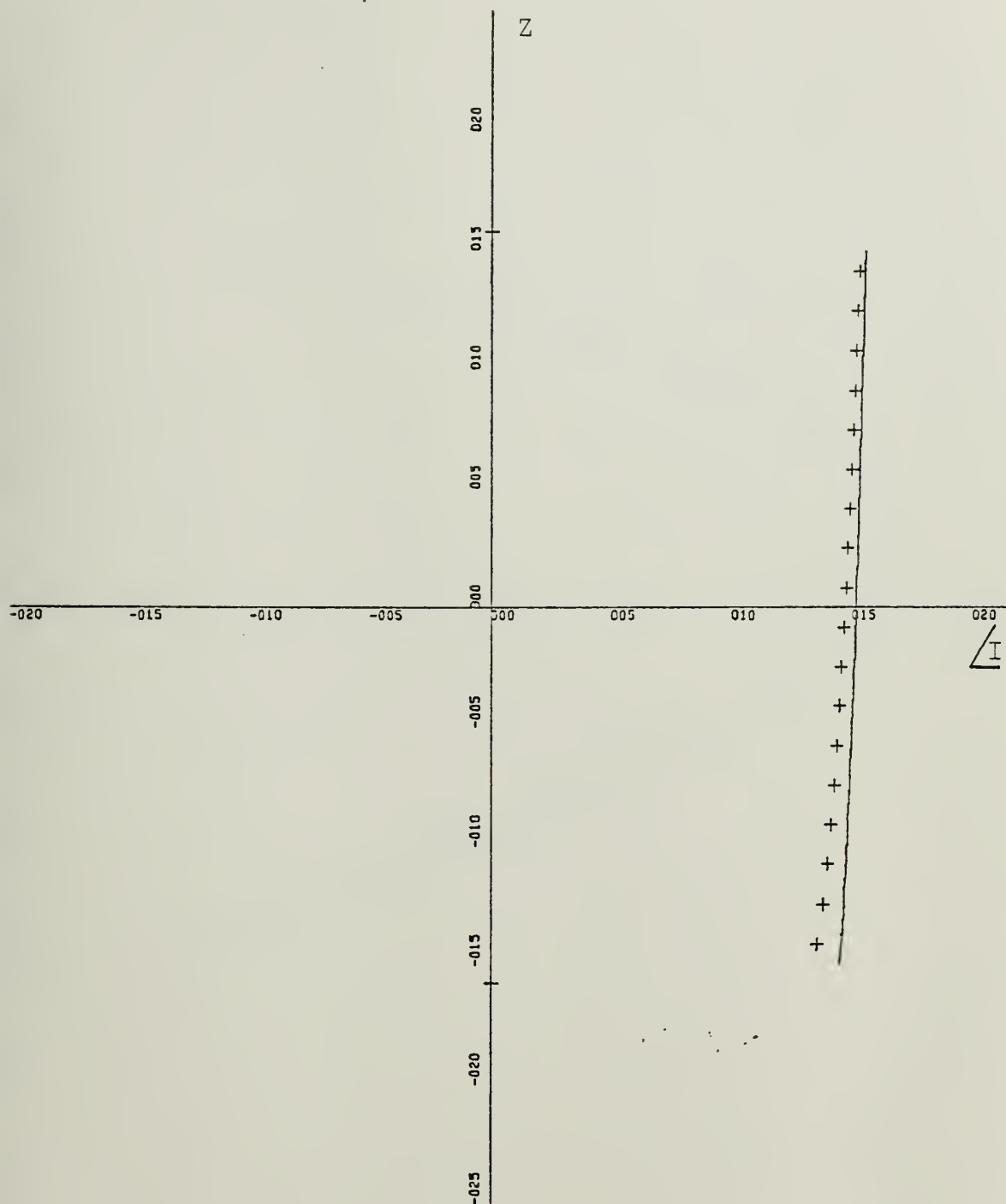
X-SCALE=5.00E-04 UNITS INCH.

Y-SCALE=5.00E-01 UNITS INCH.

CURRENT MAGNITUDE : FEM/T=SOLID : INT.EQ=X

ZL=.5:AL=0.02:BL=0.001:ALFA=60:NW=40

A-9



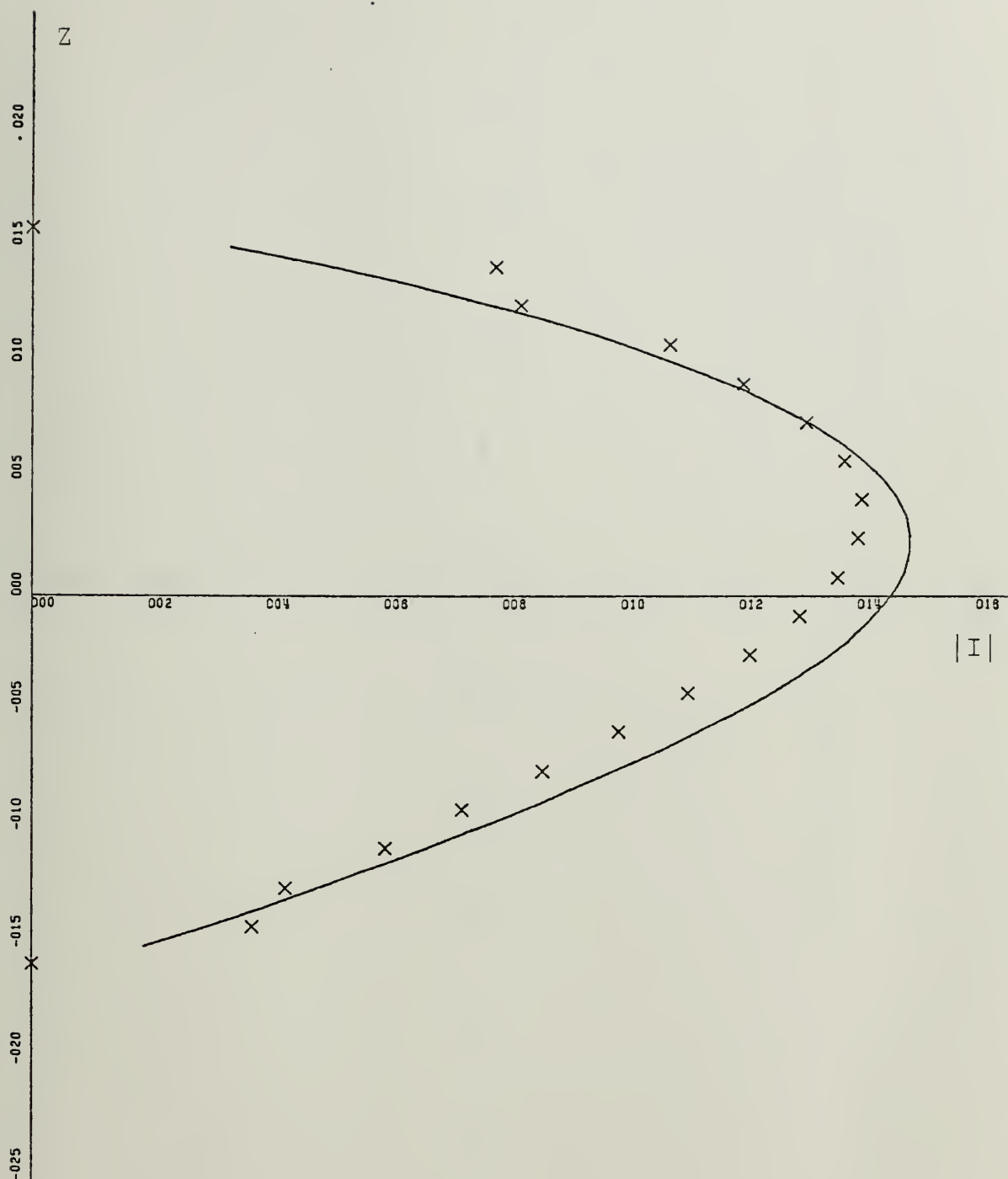
X-SCALE=5.00E+01 UNITS INCH.

Y-SCALE=5.00E-01 UNITS INCH.

CURRENT PHASE : FEM/T=SOLID : INT.EQ=PLUS

ZL=.5:AL=0.02:BL=0.001:ALFA=60:NW=40

A-10



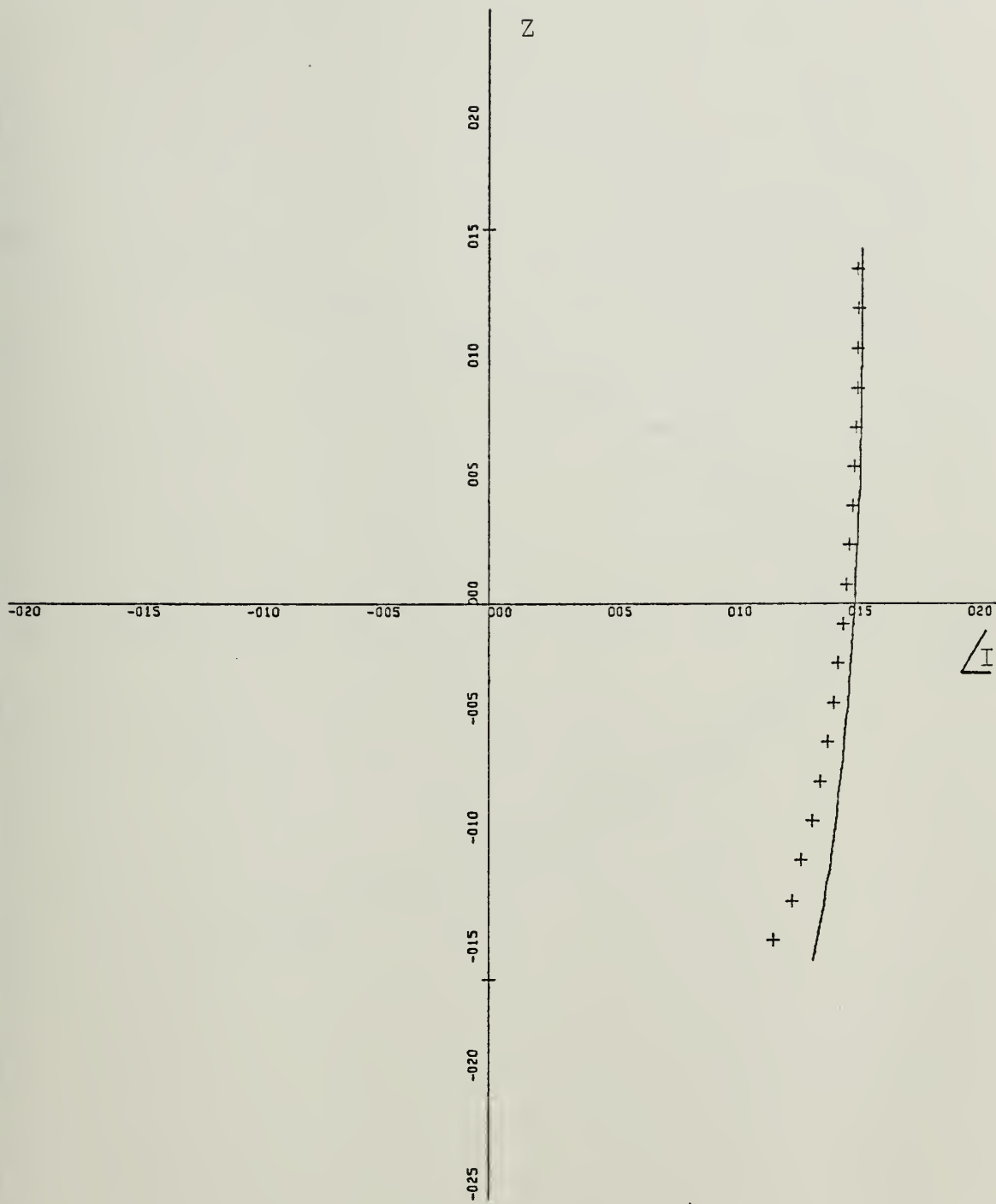
X-SCALE=2.00E-04 UNITS INCH.

Y-SCALE=5.00E-01 UNITS INCH.

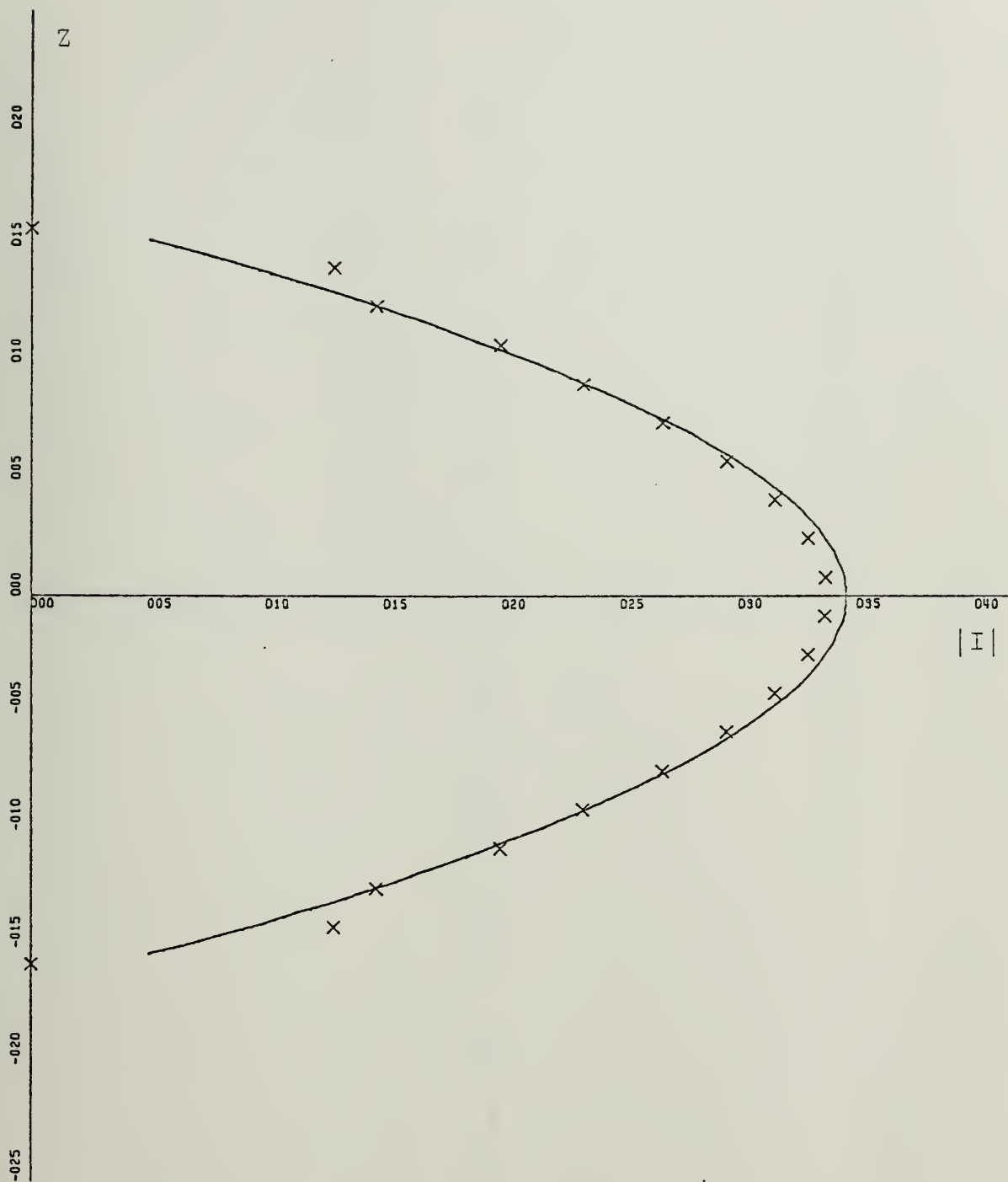
CURRENT MAGNITUDE : FEM/T=SOLID : INT.EQ=X

ZL=.5:AL=0.02:BL=0.001:ALFA=30:NW=40

A-11

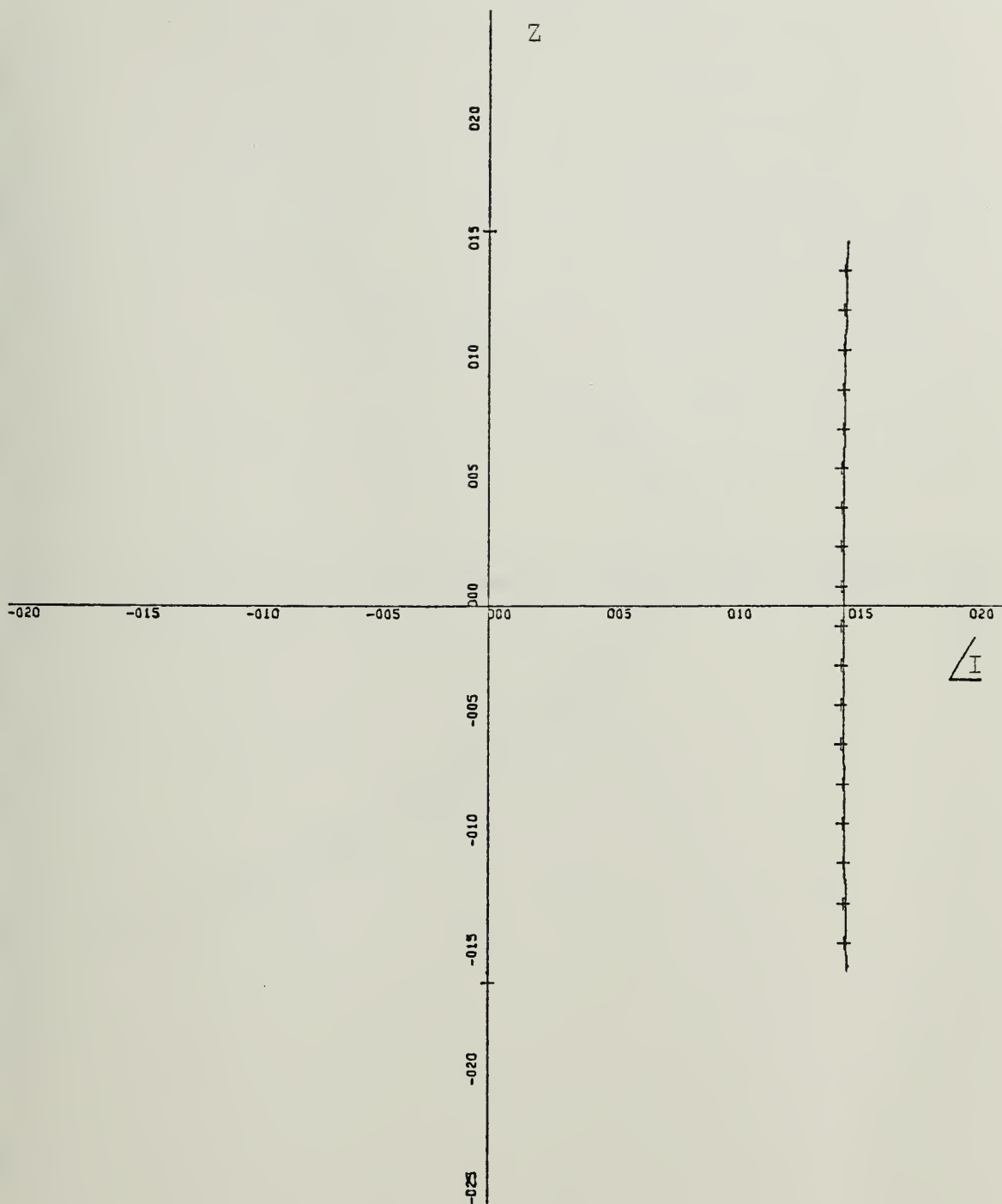


X-SCALE=5.00E+01 UNITS INCH.
 Y-SCALE=5.00E-01 UNITS INCH.
 CURRENT PHASE : FEM/T=SOLID : INT.EQ=PLUS
 ZL=.5:AL=0.02:BL=0.001:ALFA=30:NW=40
 A-12



X-SCALE=5.00E-04 UNITS INCH.
 Y-SCALE=5.00E-01 UNITS INCH.
 CURRENT MAGNITUDE : FEM/T=SOLID : INT.EQ=X
 ZL=.5:AL=0.02:BL=0.001:ALFA=90:NW=70

A-13



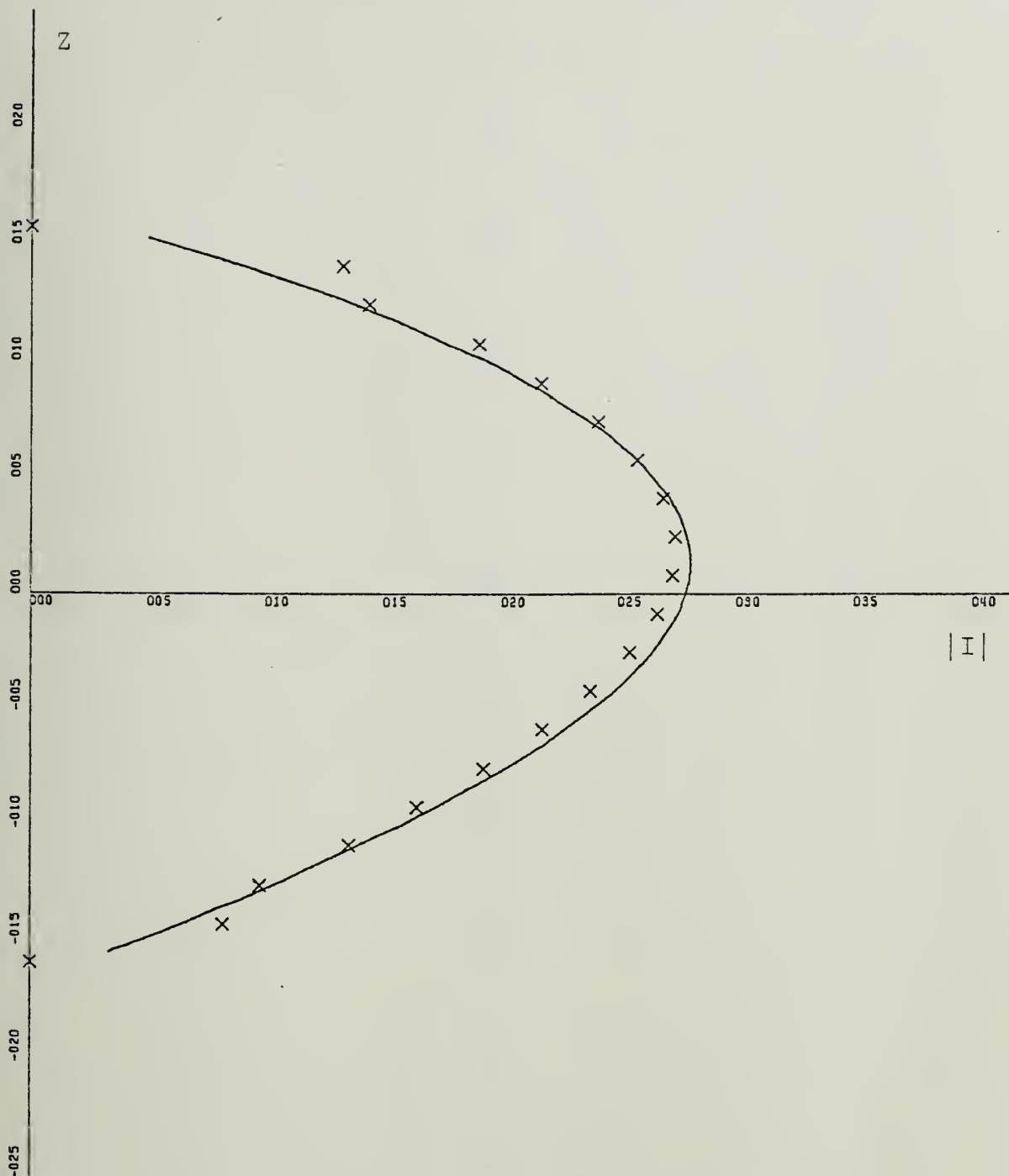
X-SCALE=5.00E+01 UNITS INCH.

Y-SCALE=5.00E-01 UNITS INCH.

CURRENT PHASE : FEM/T=SOLID ; INT.EQ=PLUS

ZL=.5:AL=0.02:BL=0.001:ALFA=90:NW=70

A-14



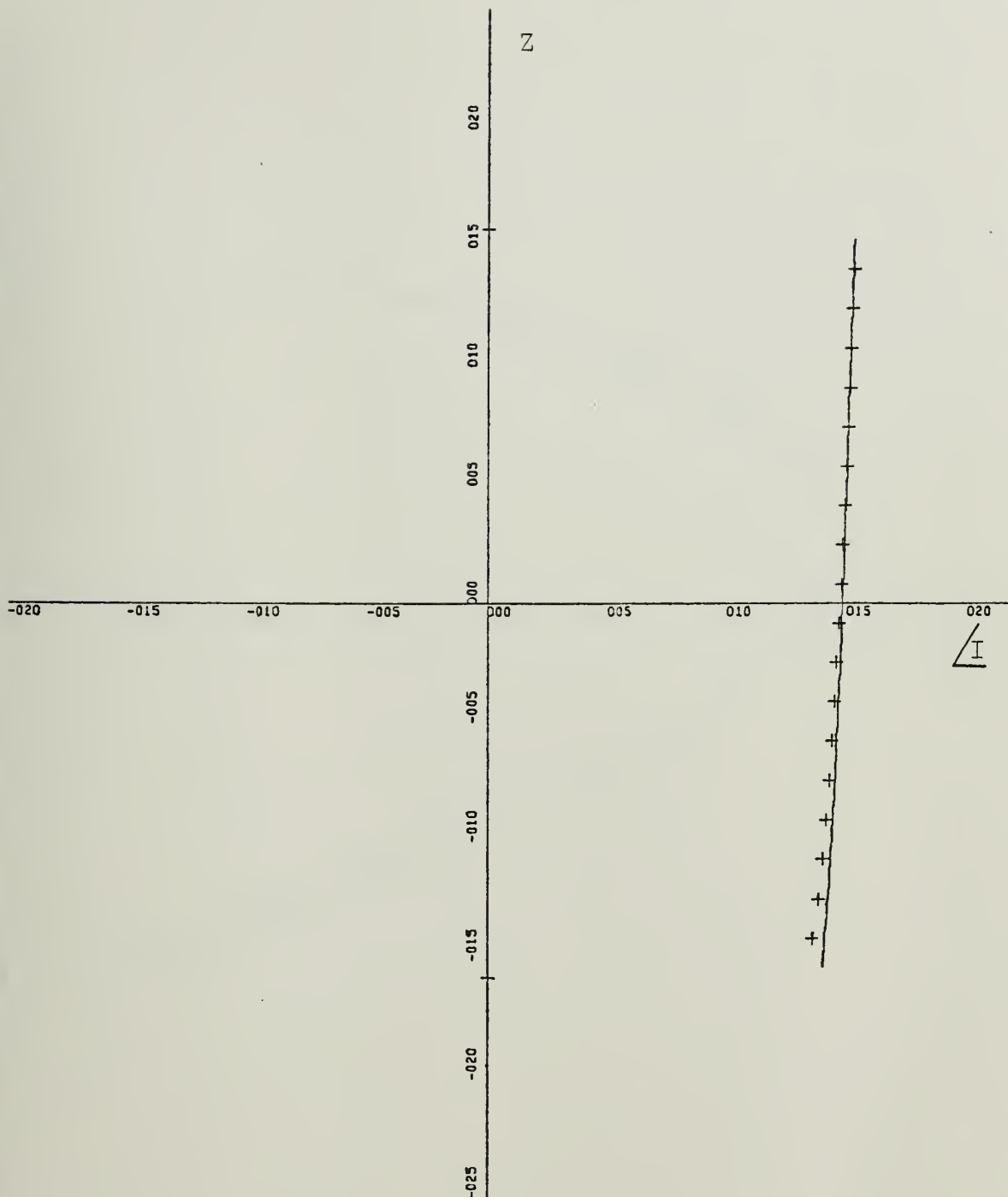
X-SCALE=5.00E-04 UNITS INCH.

Y-SCALE=5.00E-01 UNITS INCH.

CURRENT MAGNITUDE : FEM/T=SOLID : INT.EQ=X

ZL=.5:AL=0.02:BL=0.001:ALFA=60:NW=70

A-15



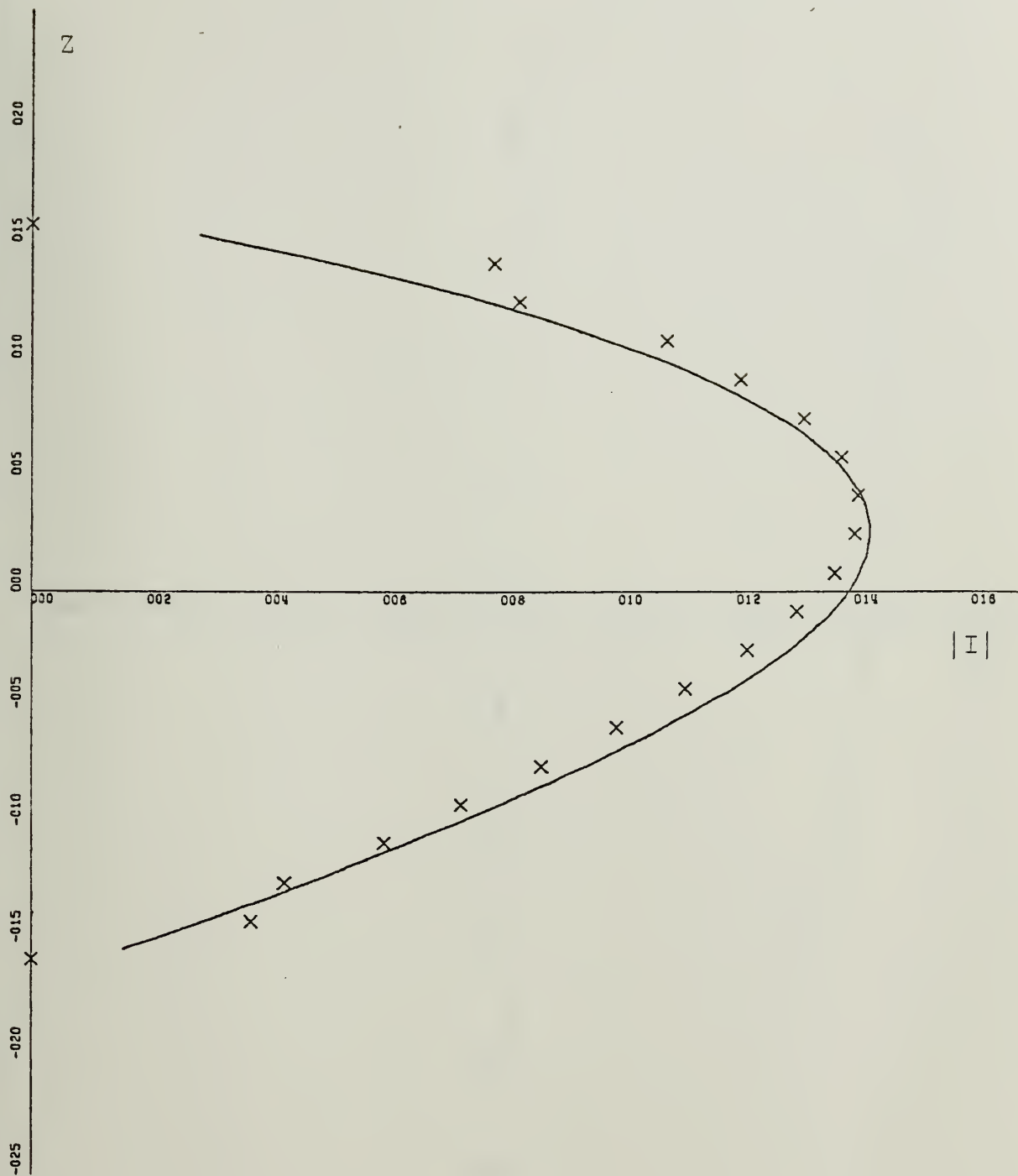
X-SCALE=5.00E+01 UNITS INCH.

Y-SCALE=5.00E-01 UNITS INCH.

CURRENT PHASE : FEM/T=SOLID : INT.EQ=PLUS

ZL=.5:AL=0.02:BL=0.001:ALFA=60:NW=70

A-16



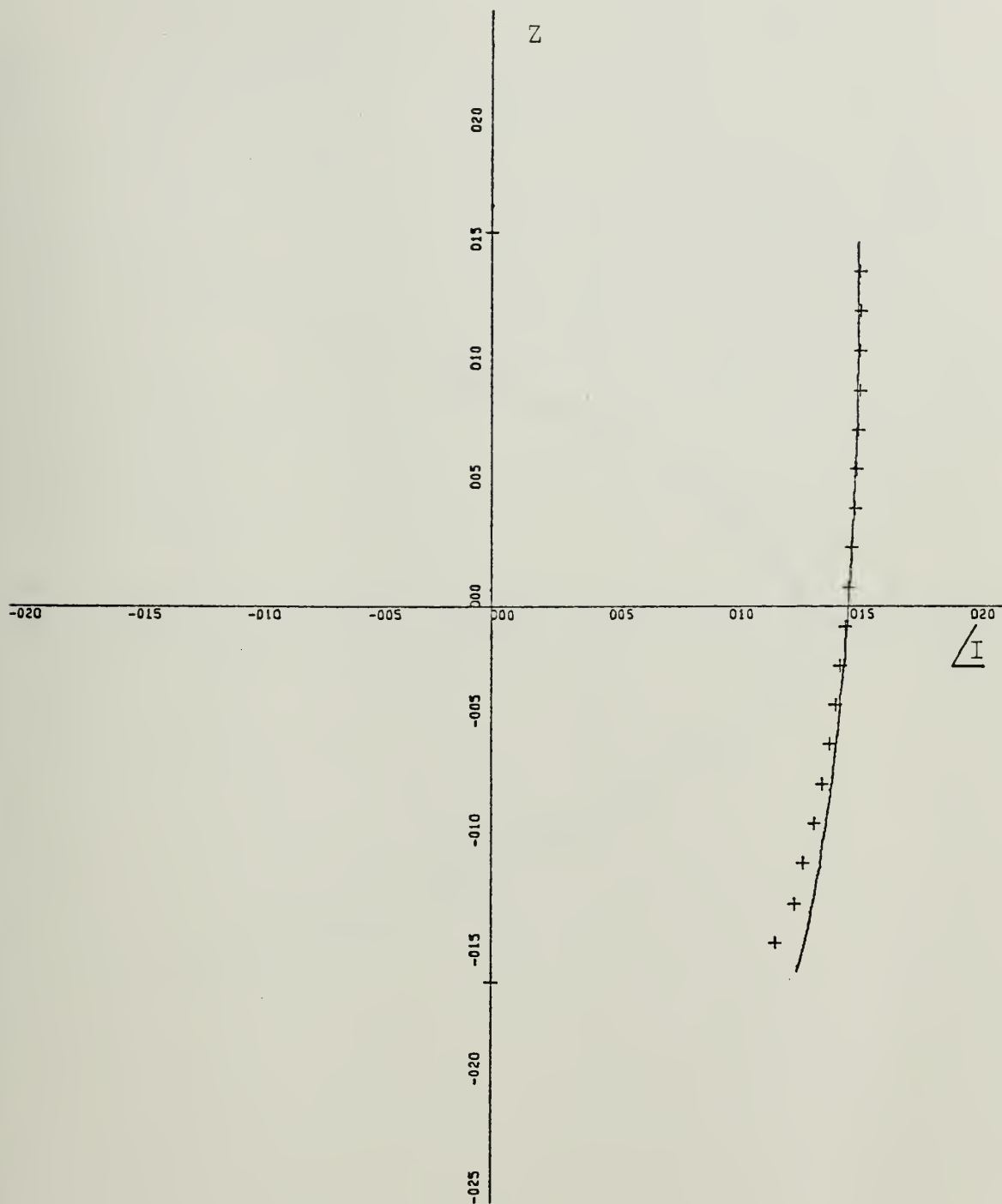
X-SCALE=2.00E-04 UNITS INCH.

Y-SCALE=5.00E-01 UNITS INCH.

CURRENT MAGNITUDE : FEM/T=SOLID : INT.EQ=X

ZL=.5:AL=0.02:BL=0.001:ALFA=30:NW=70

A-17



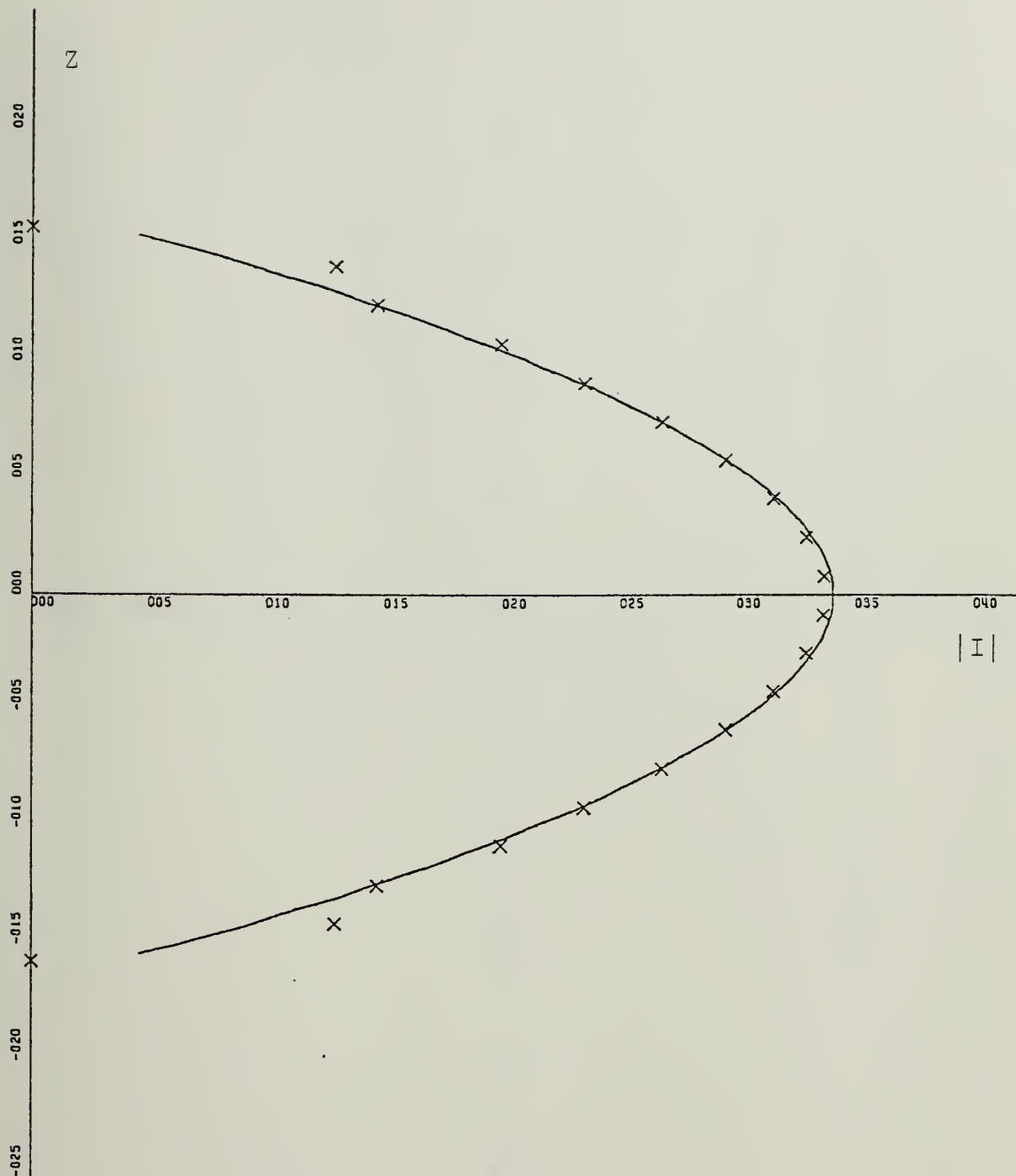
X-SCALE=5.00E+01 UNITS INCH.

Y-SCALE=5.00E-01 UNITS INCH.

CURRENT PHASE : FEM/T=SOLID : INT.EQ=PLUS

ZL=.5:AL=0.02:BL=0.001:ALFA=30:NW=70

A-18



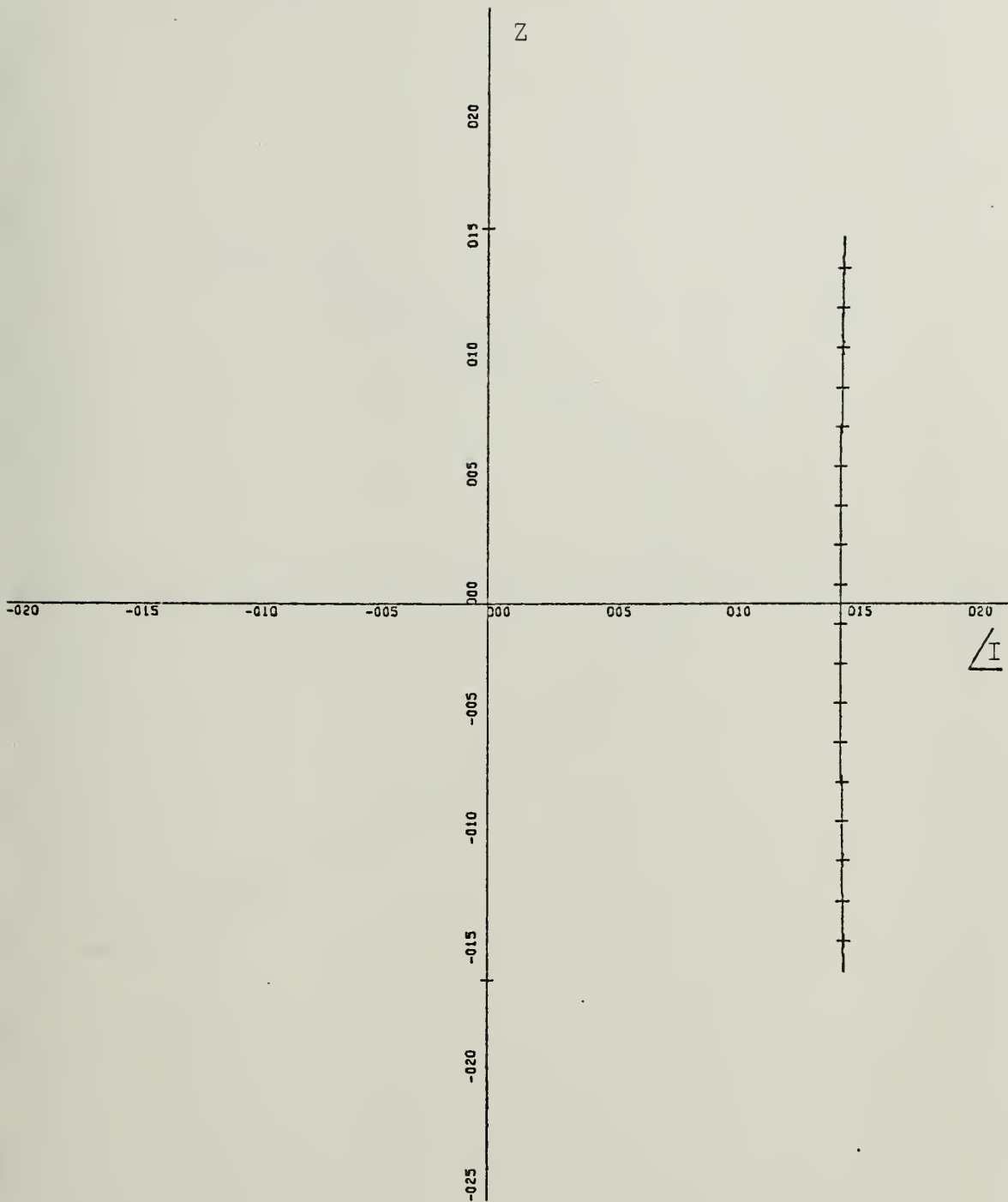
X-SCALE=5.00E-04 UNITS INCH.

Y-SCALE=5.00E-01 UNITS INCH.

CURRENT MAGNITUDE : FEM/T=SOLID : INT.EQ=X

ZL=0.5:AL=0.02:BL=0.001:ALFA=90:NW=100

A-19



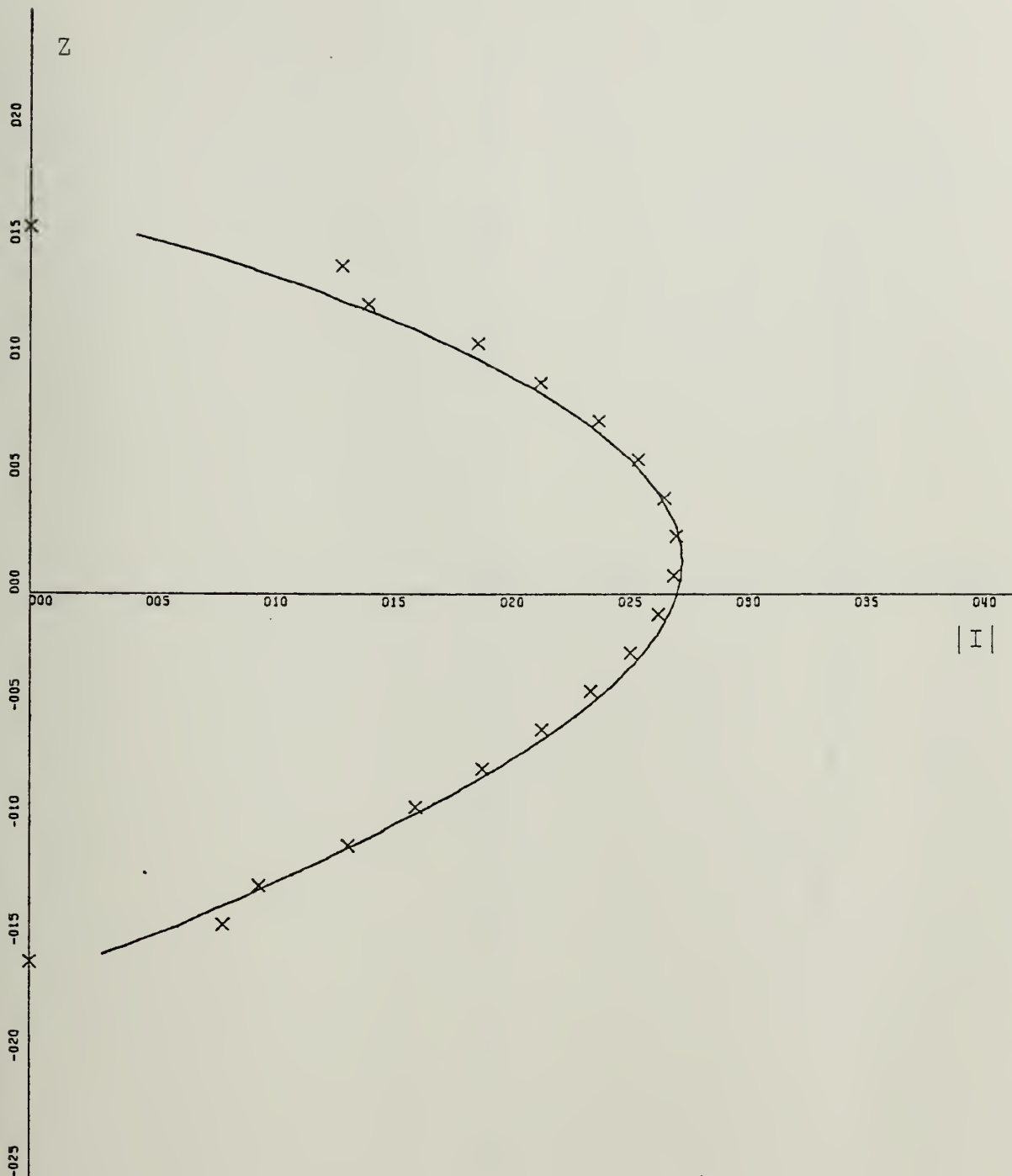
X-SCALE=5.00E+01 UNITS INCH.

Y-SCALE=5.00E-01 UNITS INCH.

CURRENT PHASE : FEM/T=SOLID : INT.EQ=PLUS

ZL=0.5:AL=0.02:BL=0.001:ALFA=90:NW=100

A-20



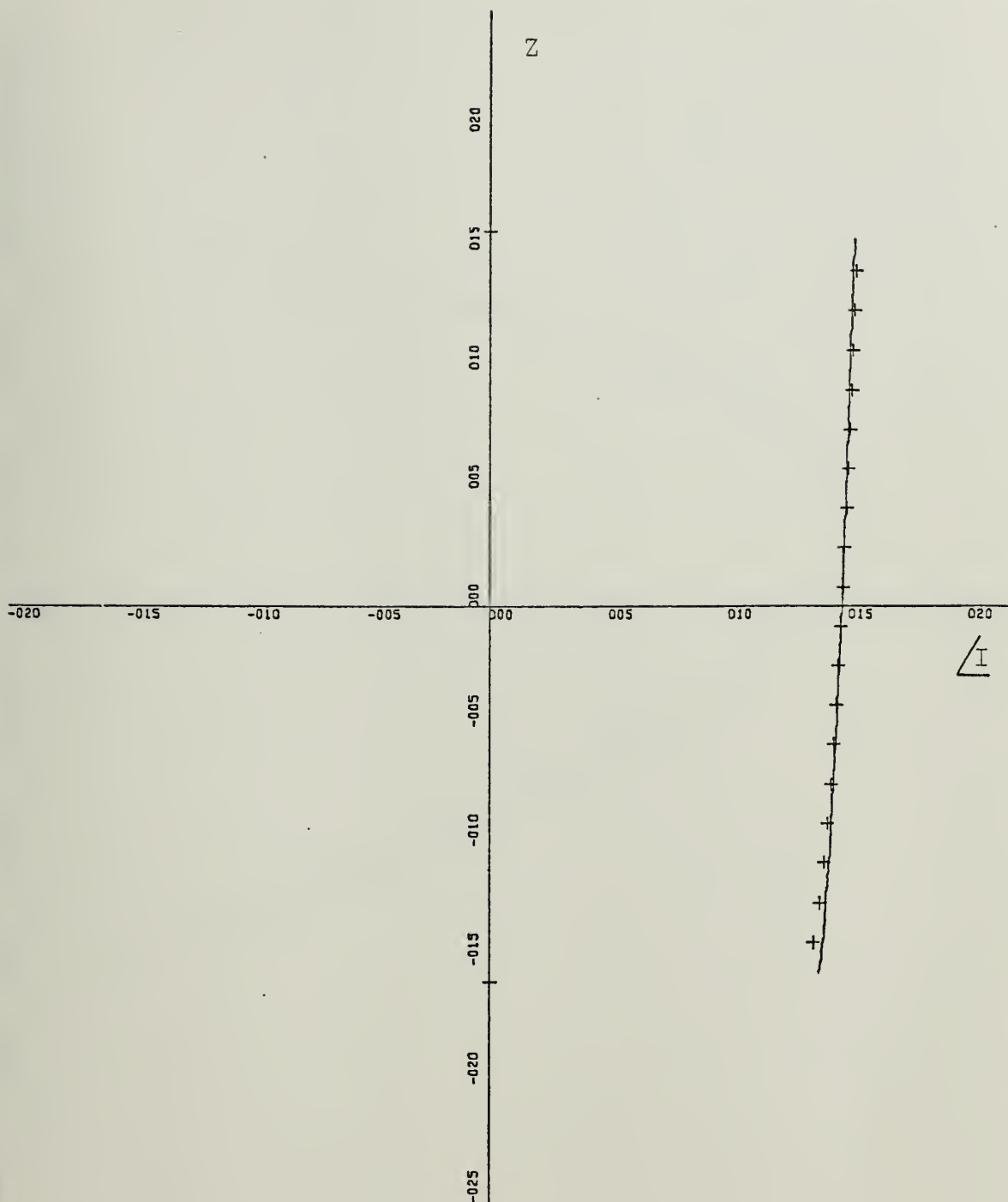
X-SCALE=5.00E-04 UNITS INCH.

Y-SCALE=5.00E-01 UNITS INCH.

CURRENT MAGNITUDE : FEM/T=SOLID : INT.EQ=X

ZL=0.5:AL=0.02:BL=0.001:ALFA=60:NW=100

A-21



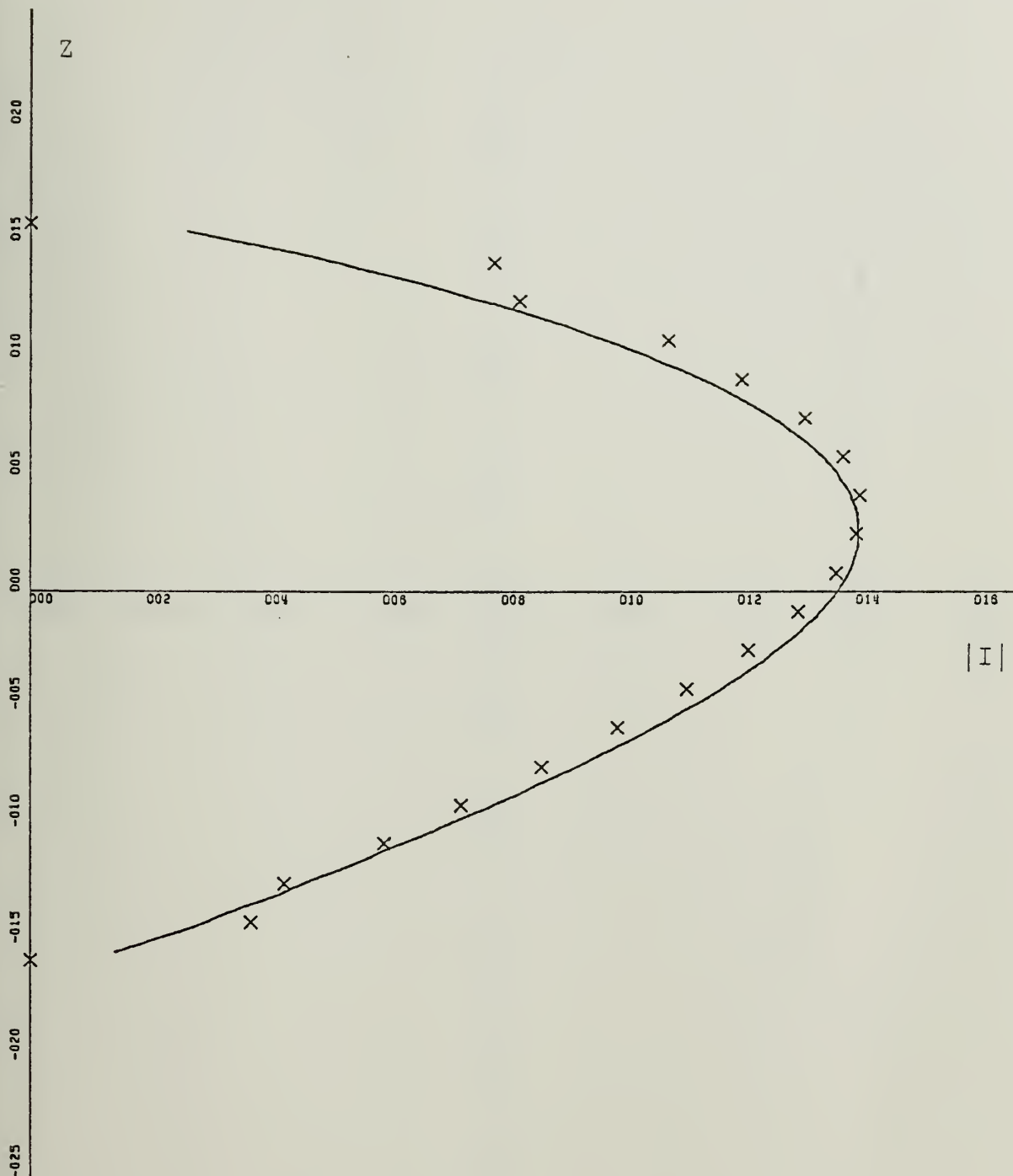
X-SCALE=5.00E+01 UNITS INCH.

Y-SCALE=5.00E-01 UNITS INCH.

CURRENT PHASE : FEM/T=SOLID : INT.EQ=PLUS

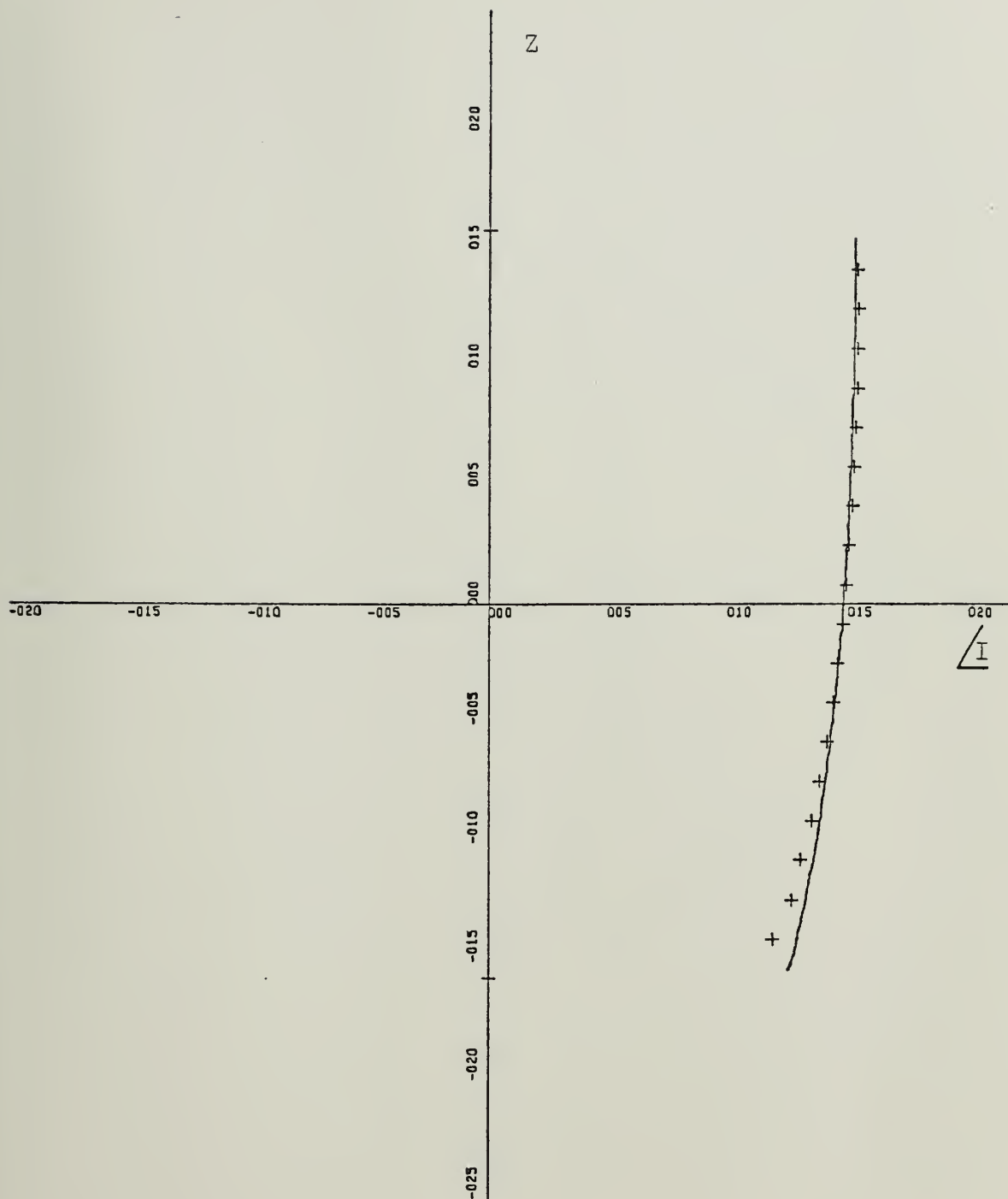
ZL=0.5:AL=0.02:BL=0.001:ALFA=60:NW=100

A-22



X-SCALE=2.00E-04 UNITS INCH.
 Y-SCALE=5.00E-01 UNITS INCH.
 CURRENT MAGNITUDE : FEM/T=SOLID : INT.EQ=X
 ZL=0.5:AL=0.02:BL=0.001:ALFA=30:NW=100

A-23



X-SCALE=5.00E+01 UNITS INCH.

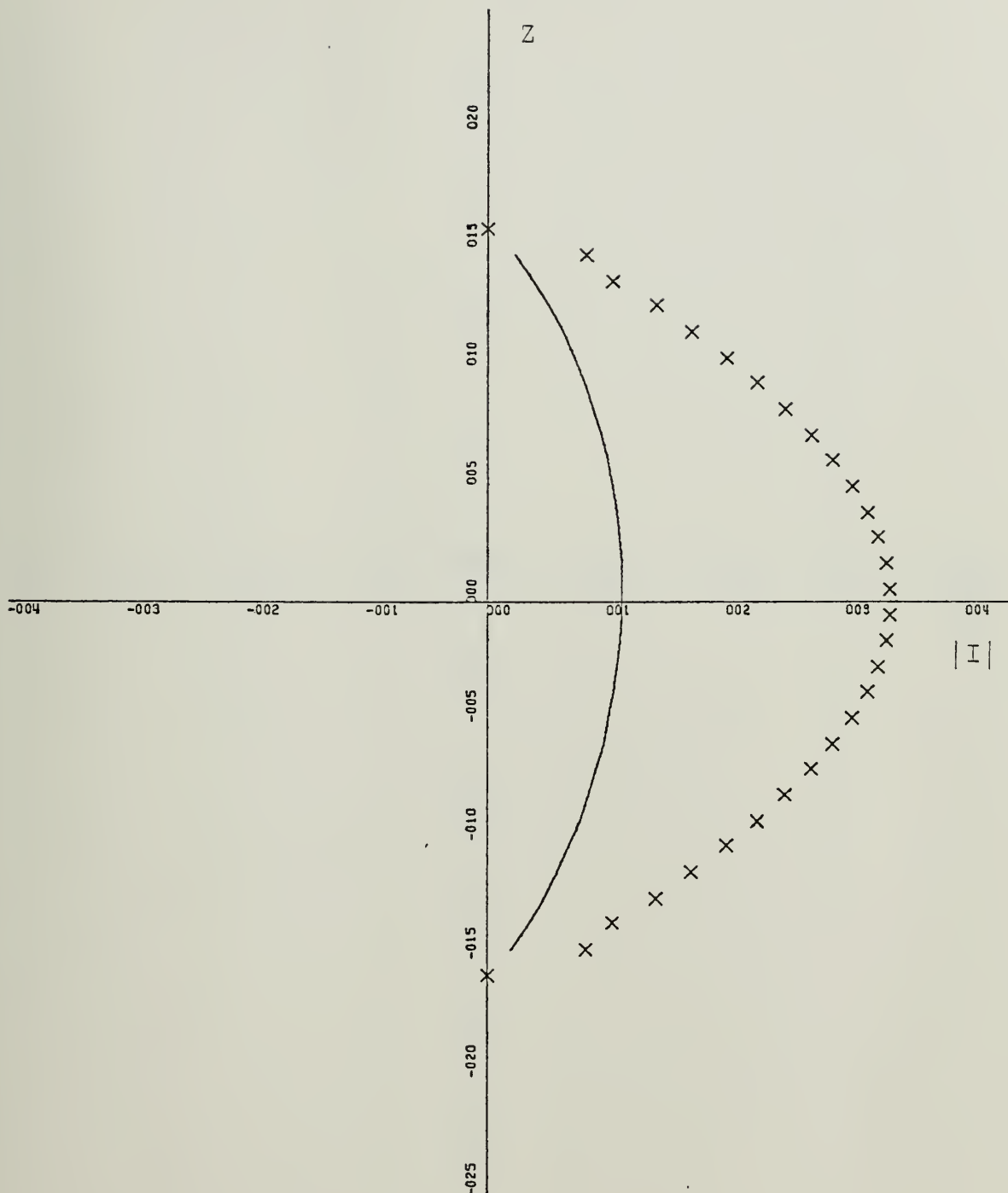
Y-SCALE=5.00E-01 UNITS INCH.

CURRENT PHASE : FEM/T=SOLID : INT.EQ=PLUS

ZL=0.5:AL=0.02:BL=0.001:ALFA=30:NW=100

A-24

72



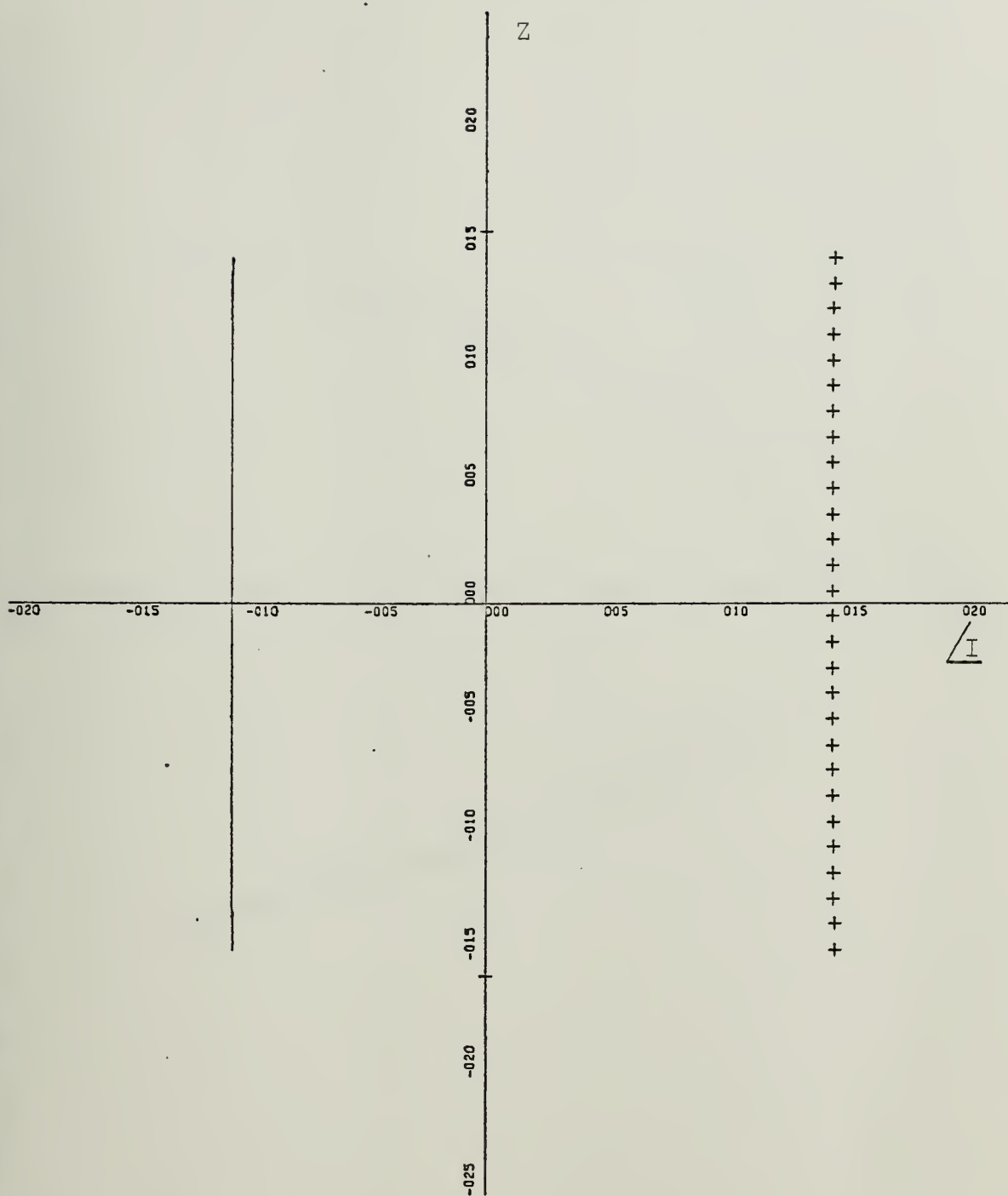
X-SCALE=1.00E-03 UNITS INCH.

Y-SCALE=5.00E-01 UNITS INCH.

CURRENT MAGNITUDE : FEM/T=SOLID : INT.EQ=X

ZL=.5 : AL=1/100 : DR=DZ/4 : ALFA=90

A-25



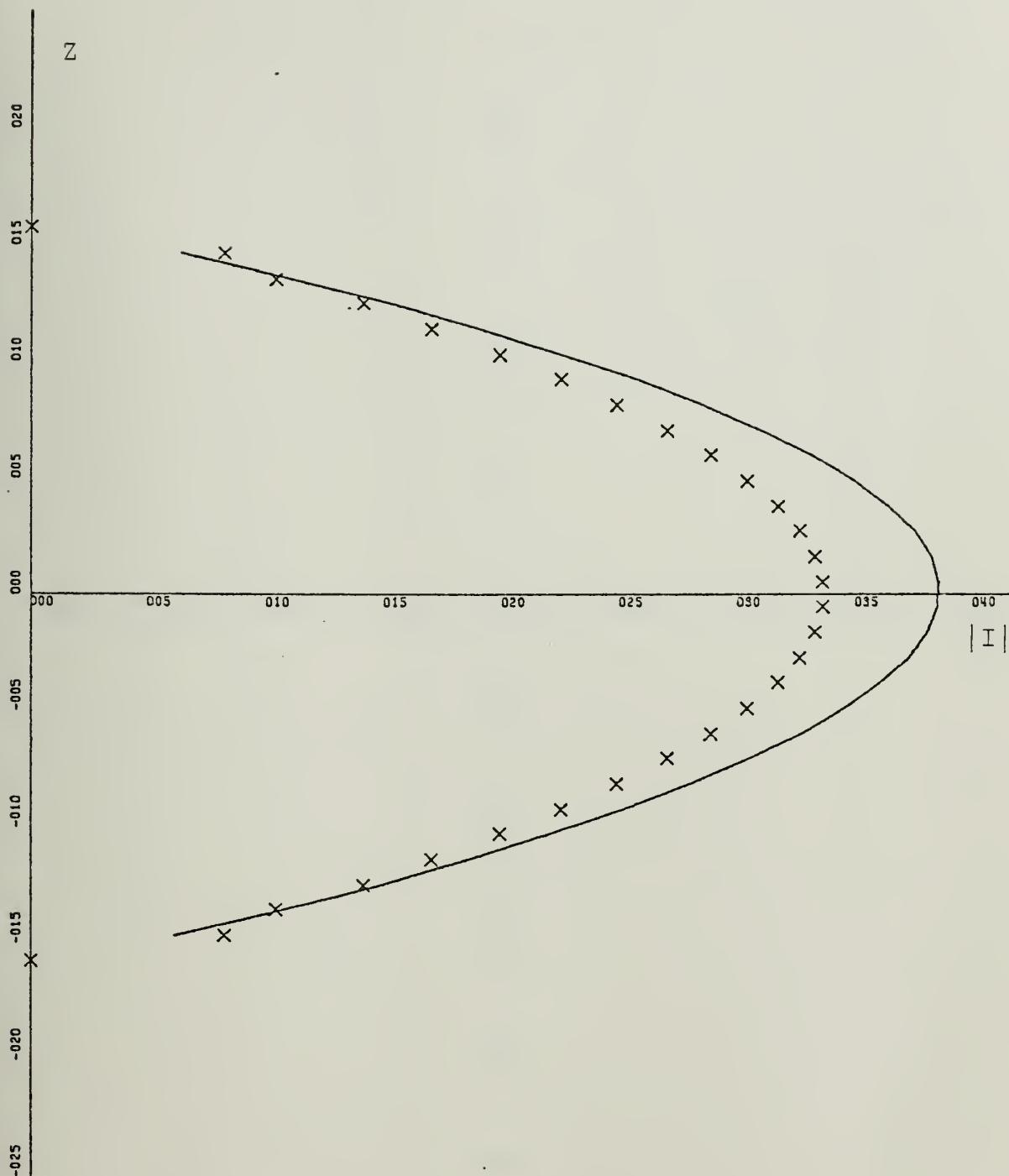
X-SCALE=5.00E+01 UNITS INCH.

Y-SCALE=5.00E-01 UNITS INCH.

CURRENT PHASE : FEM/T=SOLID : INT.EQ=PLUS

ZL=.5 : AL=1/100 : DR=DZ/4 : ALFA=90

A-26



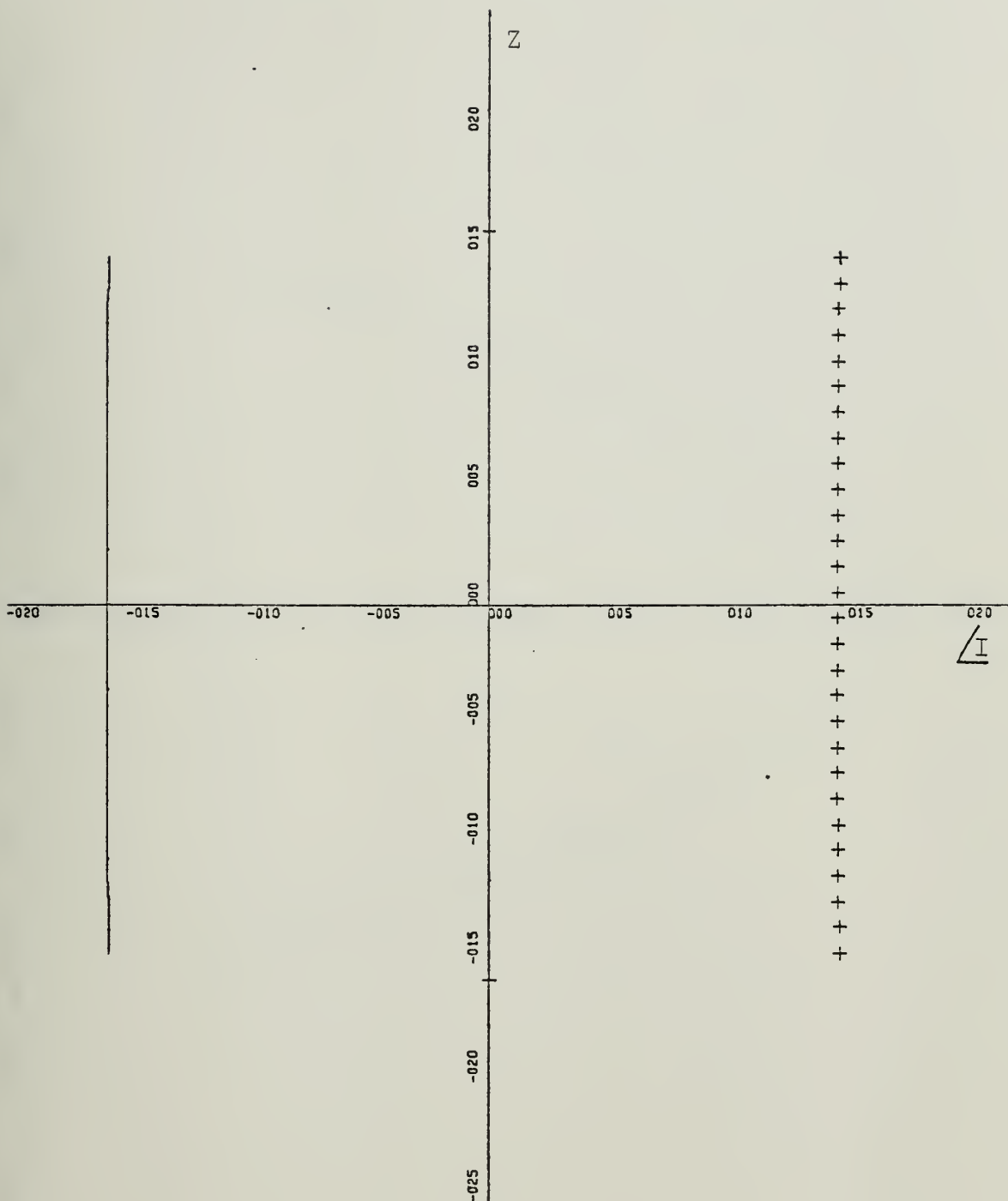
X-SCALE=5.00E-04 UNITS INCH.

Y-SCALE=5.00E-01 UNITS INCH.

CURRENT MAGNITUDE : FEM/T=SOLID : INT.EQ=X

ZL=.5 : AL=1/100 : DR=DZ/9.8 : ALFA=90

A-27



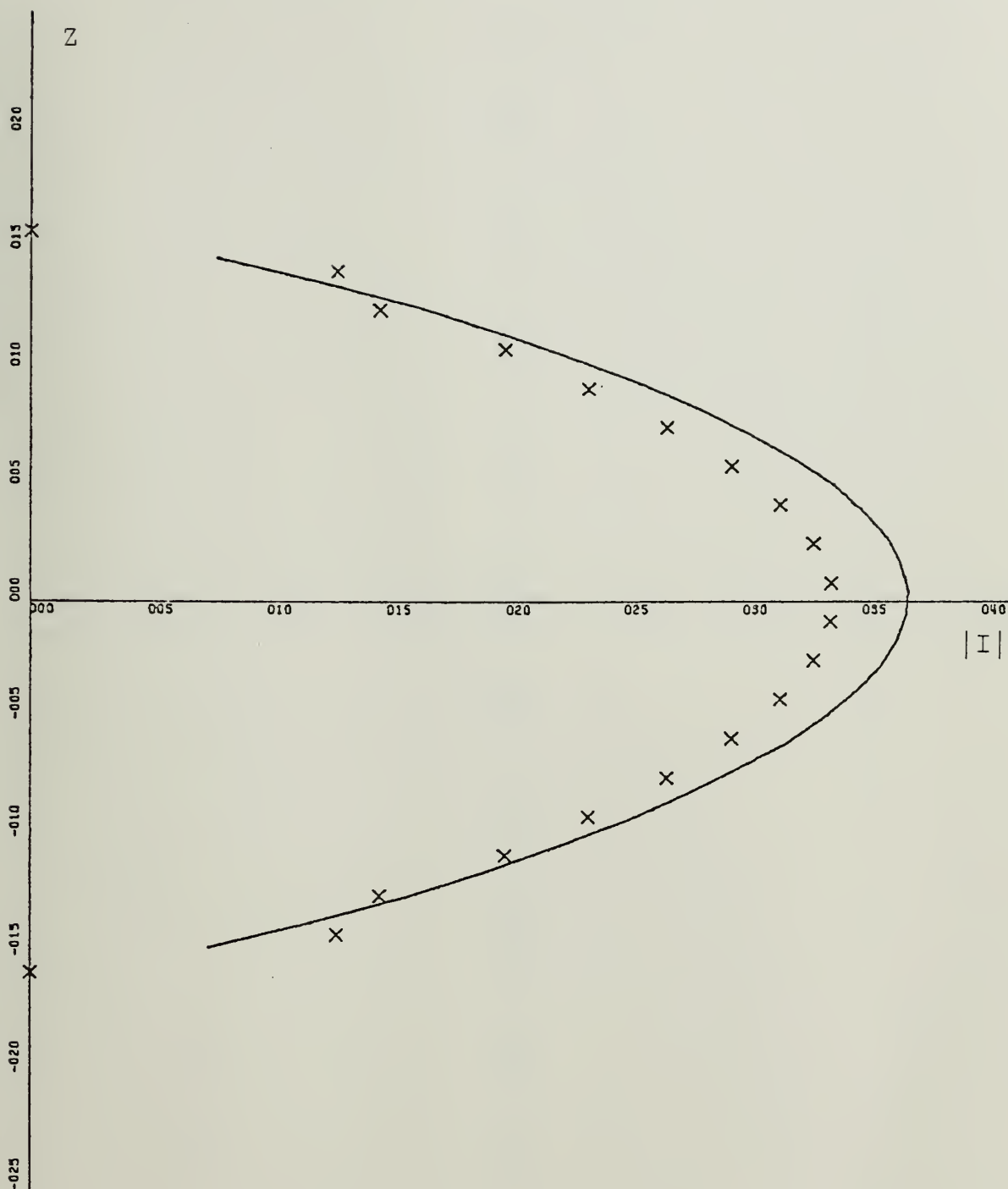
X-SCALE=5.00E+01 UNITS INCH.

Y-SCALE=5.00E-01 UNITS INCH.

CURRENT PHASE : FEM/T=SOLID : INT.EQ=PLUS

ZL=.5 : AL=1/100 : DR=DZ/9.8 : ALFA=90

A-28



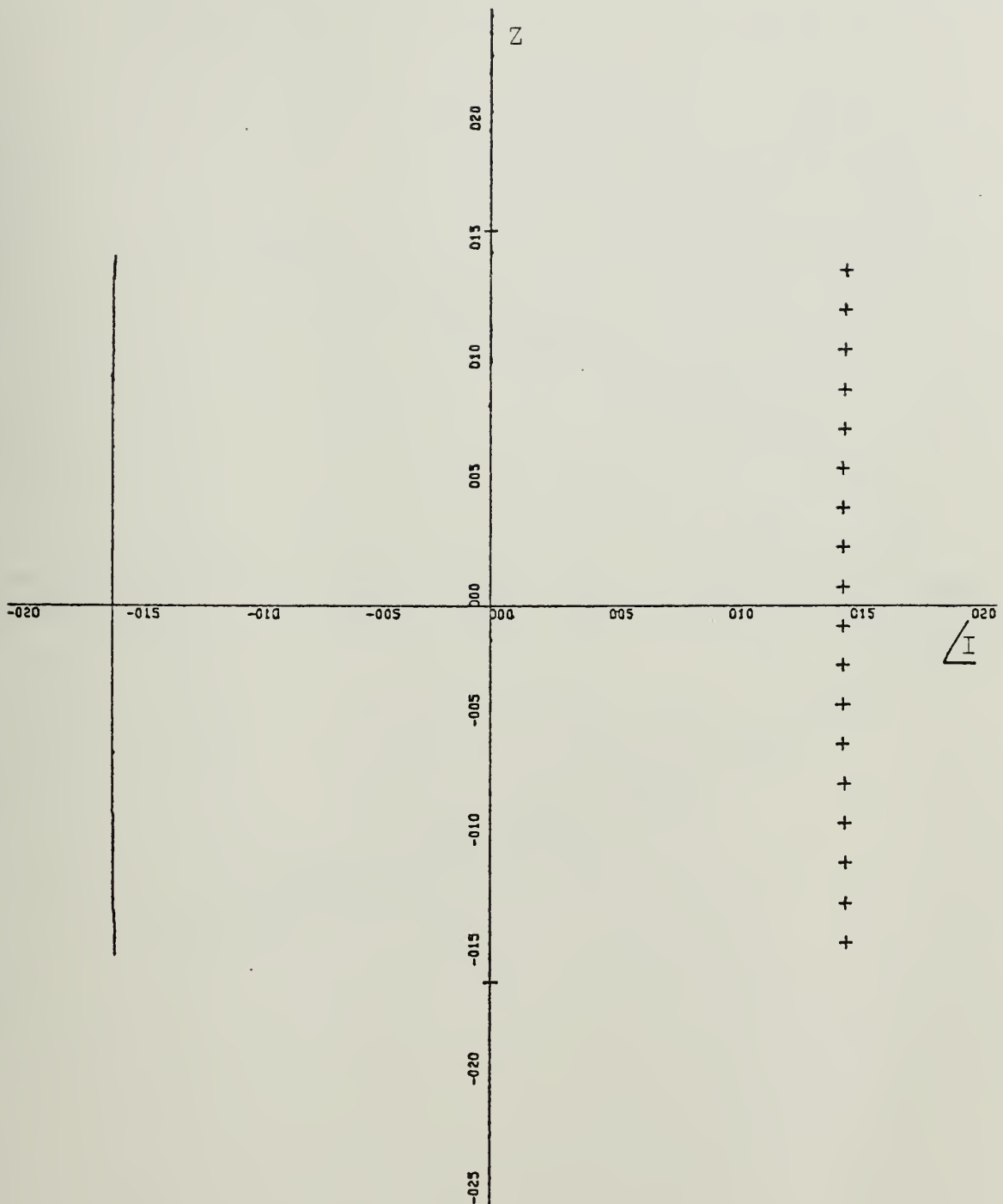
X-SCALE=5.00E-04 UNITS INCH.

Y-SCALE=5.00E-01 UNITS INCH.

CURRENT MAGNITUDE : FEM/T=SOLID : INT.EQ=X

ZL=.5 : AL=1/50 : DR=DZ/2 : ALFA=90

A-29



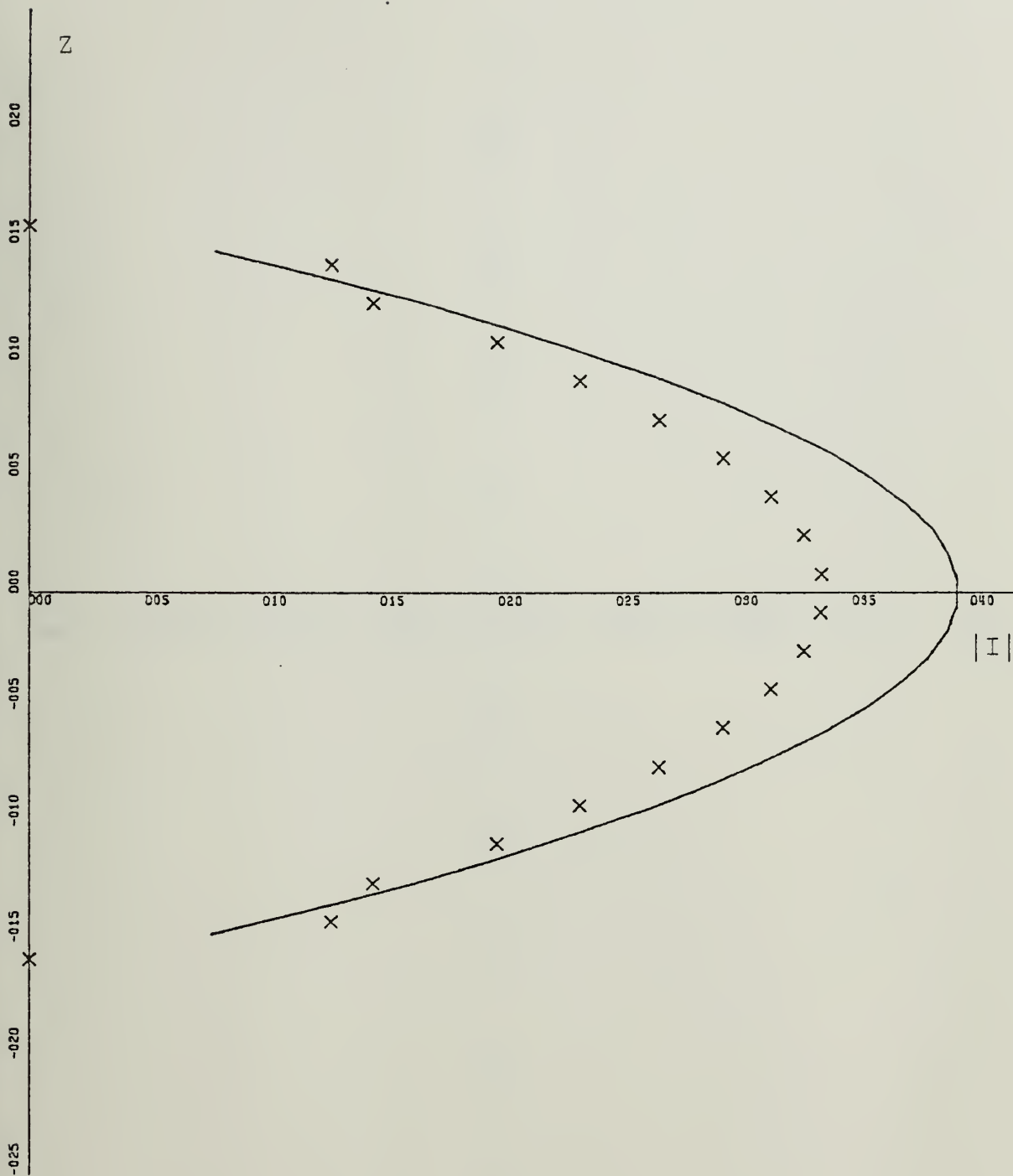
X-SCALE=5.00E+01 UNITS INCH.

Y-SCALE=5.00E-01 UNITS INCH.

CURRENT PHASE : FEM/T=SOLID : INT.EQ=PLUS

ZL=.5 : AL=1/50 : DR=DZ/2 : ALFA=90

A-30



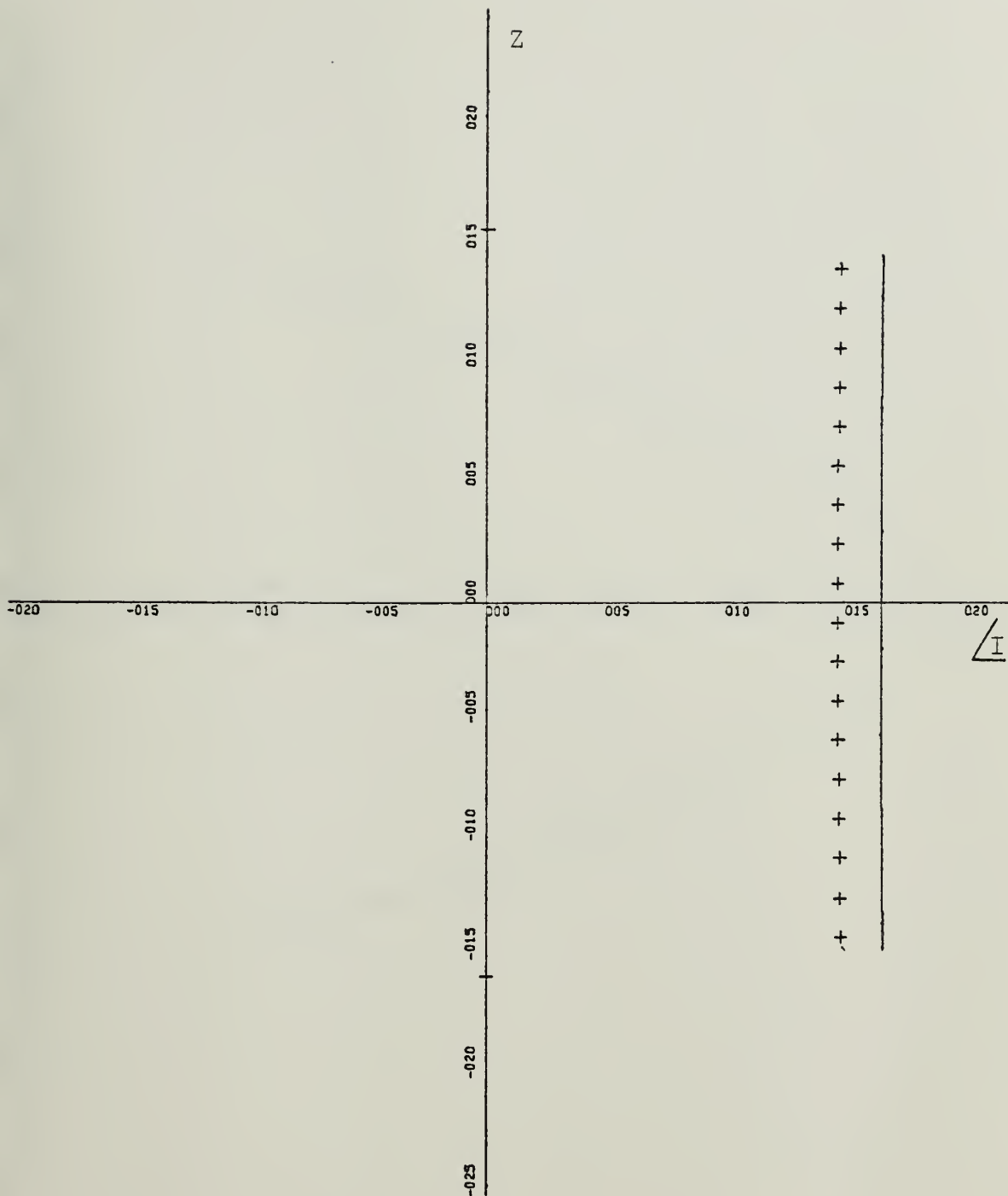
X-SCALE=5.00E-04 UNITS INCH.

Y-SCALE=5.00E-01 UNITS INCH.

CURRENT MAGNITUDE : FEM/T=SOLID : INT.EQ=X

ZL=.5 : AL=1/50 : DR=DZ/4 : ALFA=90

A-31



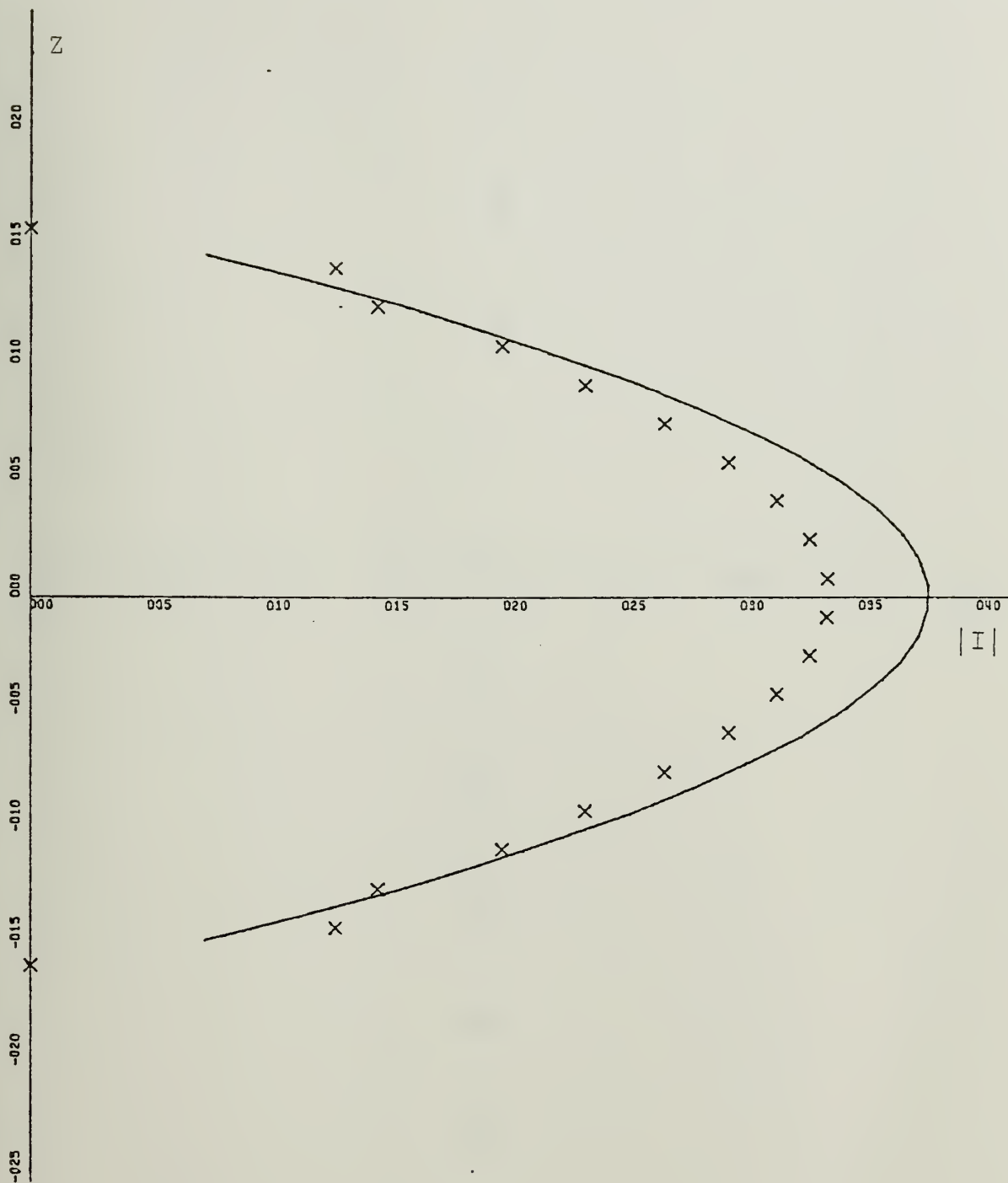
X-SCALE=5.00E+01 UNITS INCH.

Y-SCALE=5.00E-01 UNITS INCH.

CURRENT PHASE : FEM/T=SOLID : INT.EQ=PLUS

ZL=.5 : AL=1/50 : DR=DZ/4 : ALFA=90

A-32



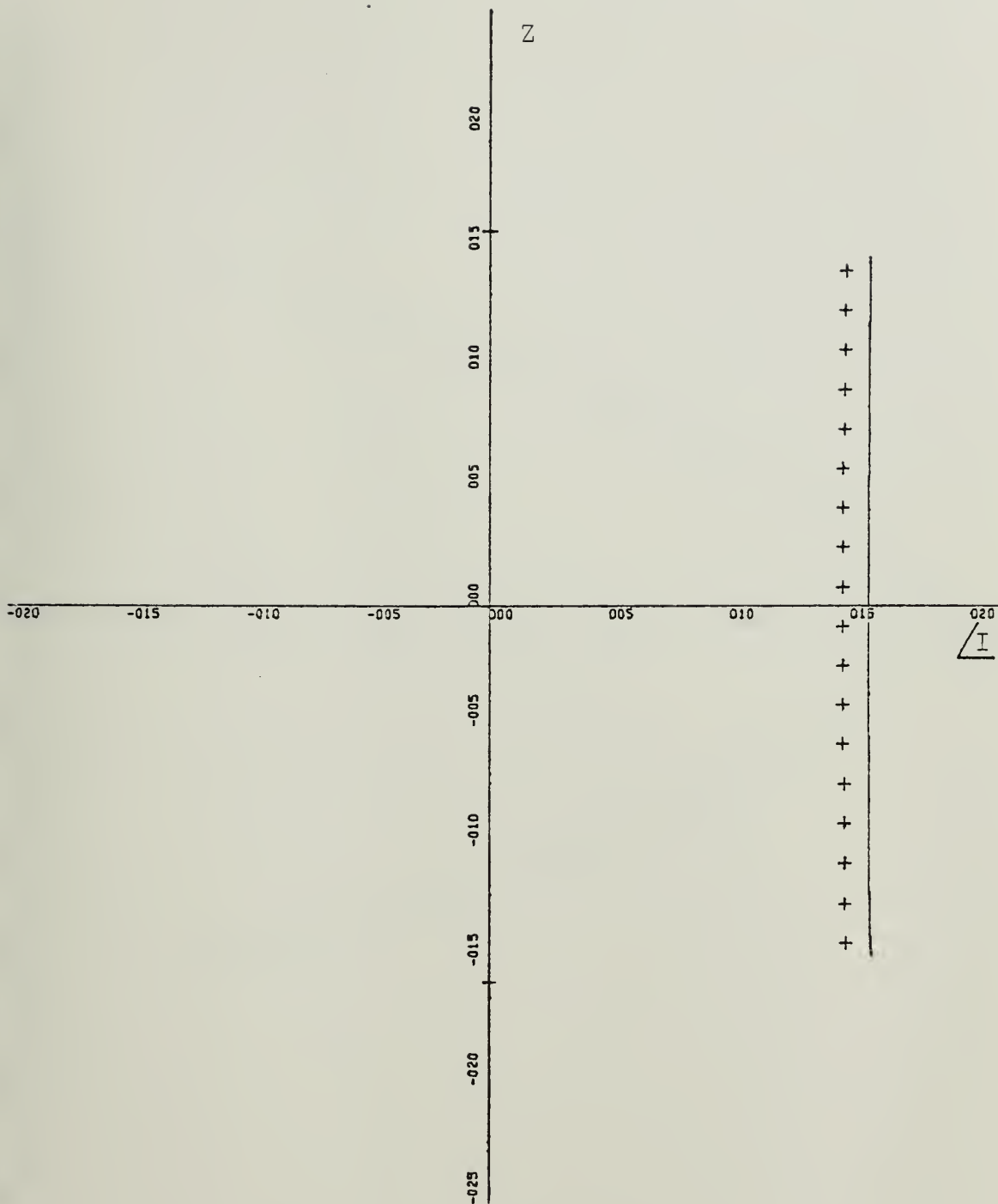
X-SCALE=5.00E-04 UNITS INCH.

Y-SCALE=5.00E-01 UNITS INCH.

CURRENT MAGNITUDE : FEM/T=SOLID : INT.EQ=X

ZL=.5 : AL=1/50 : DR=DZ/8 : ALFA=90

A-33



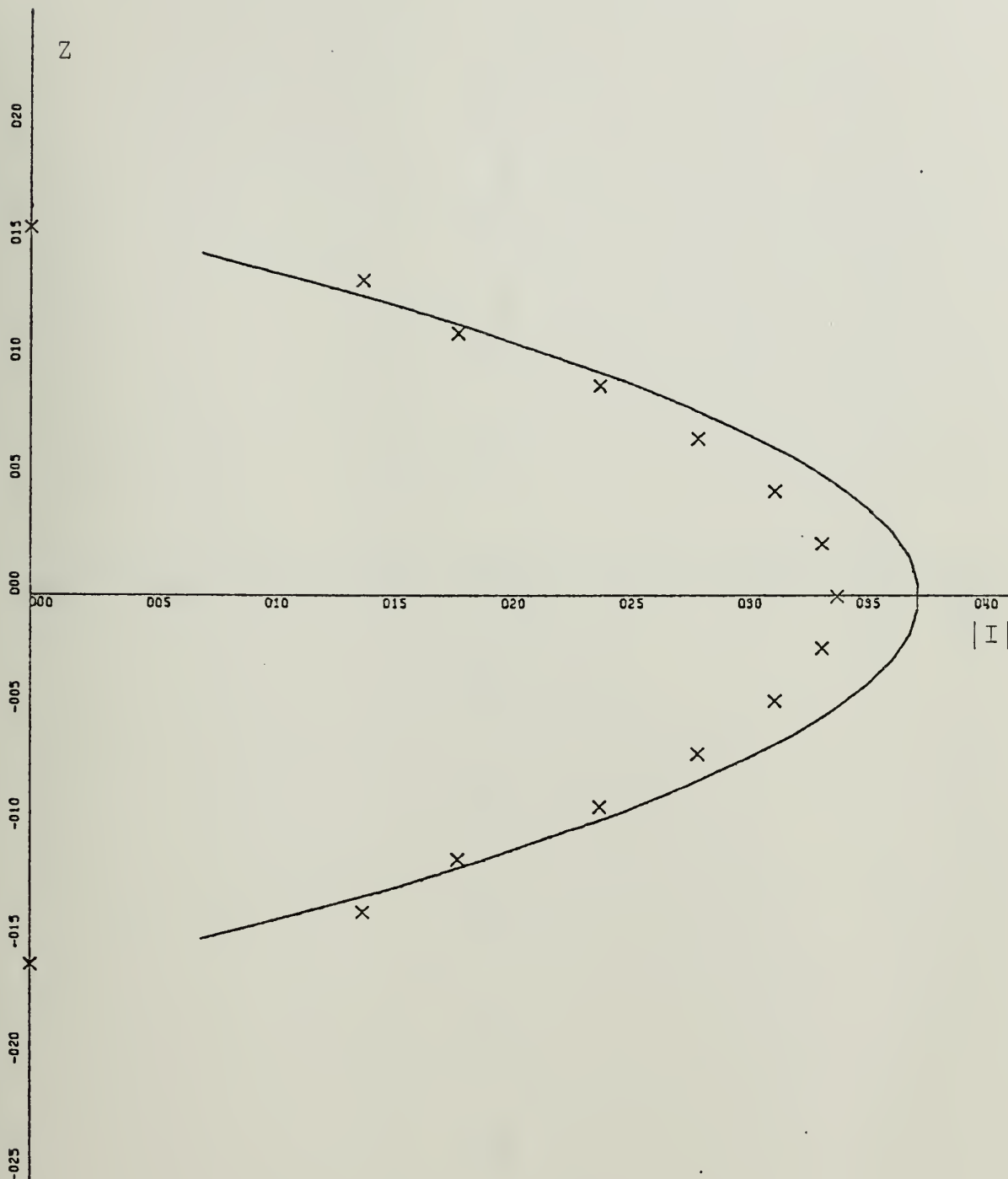
X-SCALE=5.00E+01 UNITS INCH.

Y-SCALE=5.00E-01 UNITS INCH.

CURRENT PHASE : FEM/T=SOLID : INT.EQ=PLUS

ZL=.5 : AL=1/50 : DR=DZ/8 : ALFA=90

A-34



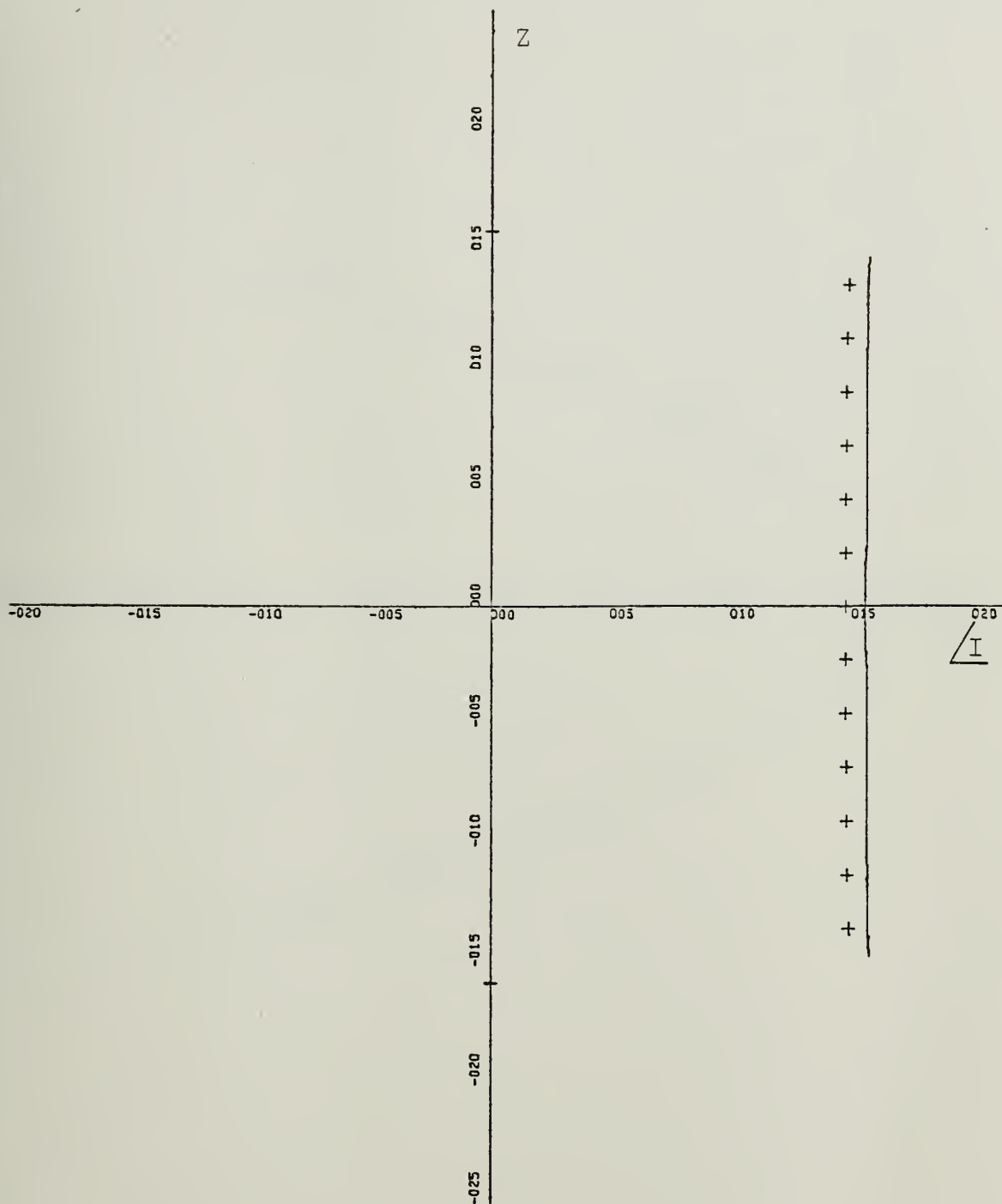
X-SCALE=5.00E-04 UNITS INCH.

Y-SCALE=5.00E-01 UNITS INCH.

CURRENT MAGNITUDE : FEM/T=SOLID : INT.EQ=X

ZL=.5 : AL=1/50 : DR=DZ/32 : ALFA=90

A-35



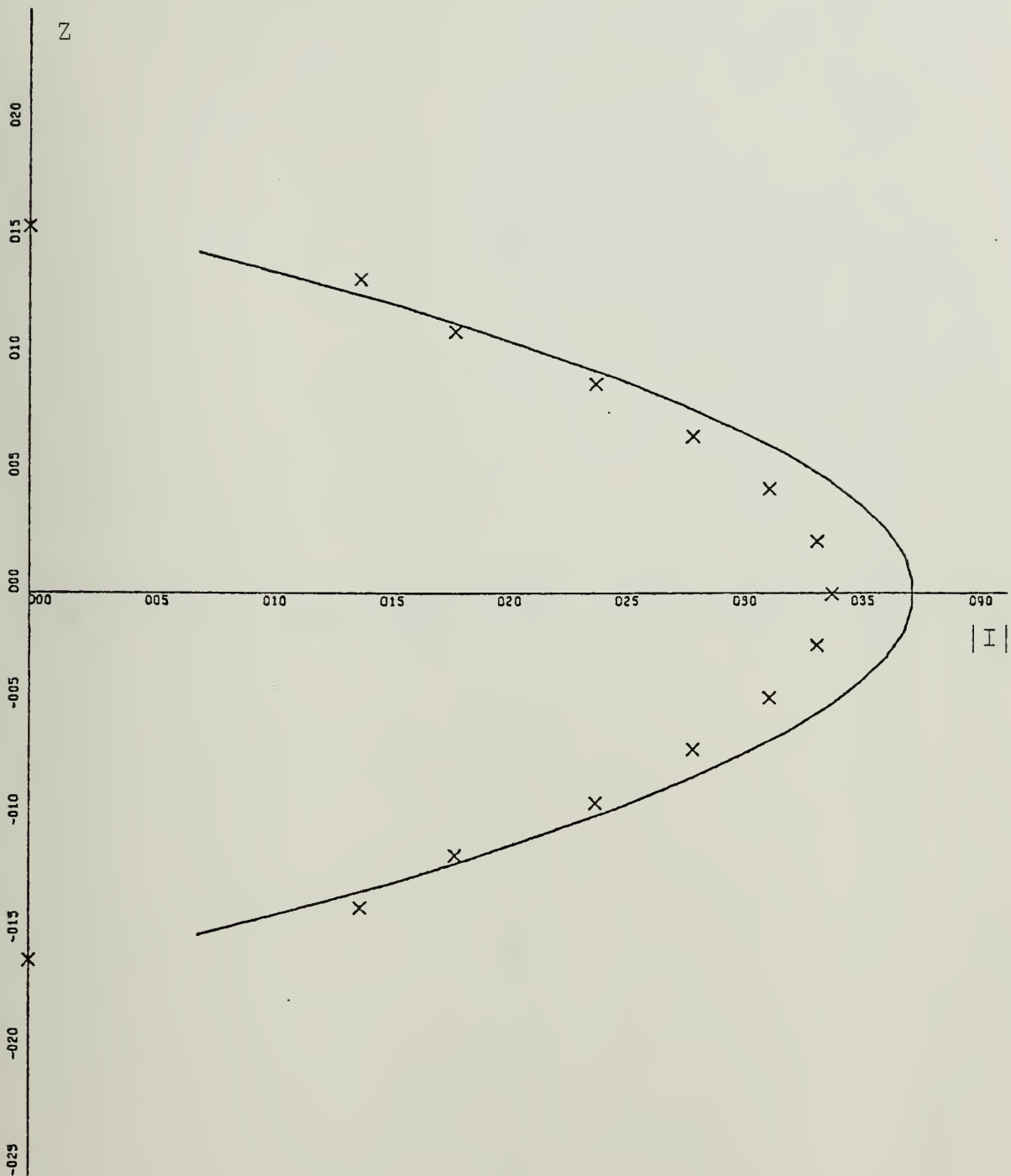
X-SCALE=5.00E+01 UNITS INCH.

Y-SCALE=5.00E-01 UNITS INCH.

CURRENT PHASE : FEM/T=SOLID : INT.EQ=PLUS

ZL=.5 : AL=1/50 : DR=DZ/32 : ALFA=90

A-36



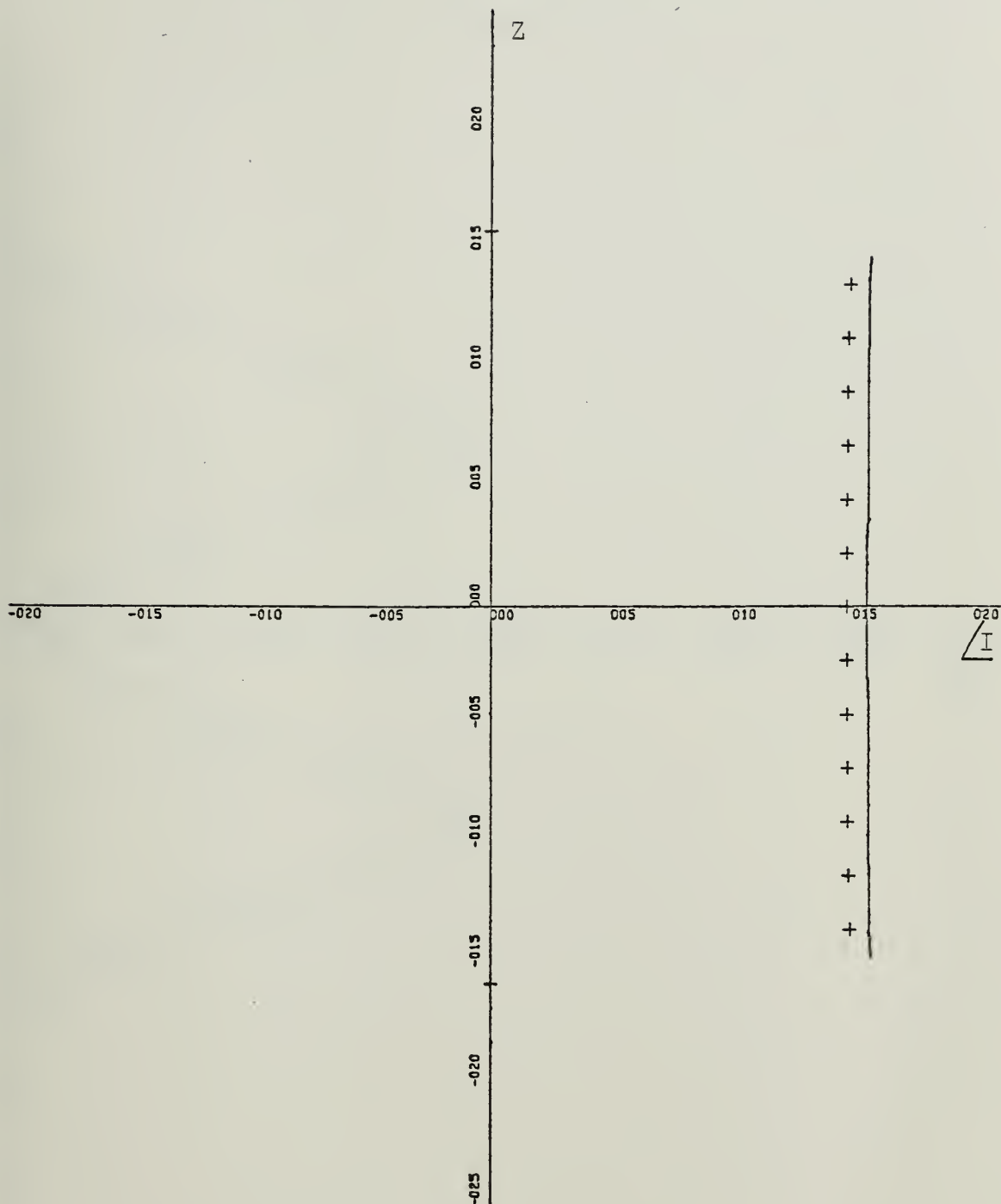
X-SCALE=5.00E-04 UNITS INCH.

Y-SCALE=5.00E-01 UNITS INCH.

CURRENT MAGNITUDE : FEM/T=SOLID : INT.EQ=X

ZL=.5 : AL=1/50 : DR=0Z/64 : ALFA=90

A-37



X-SCALE=5.00E+01 UNITS INCH.

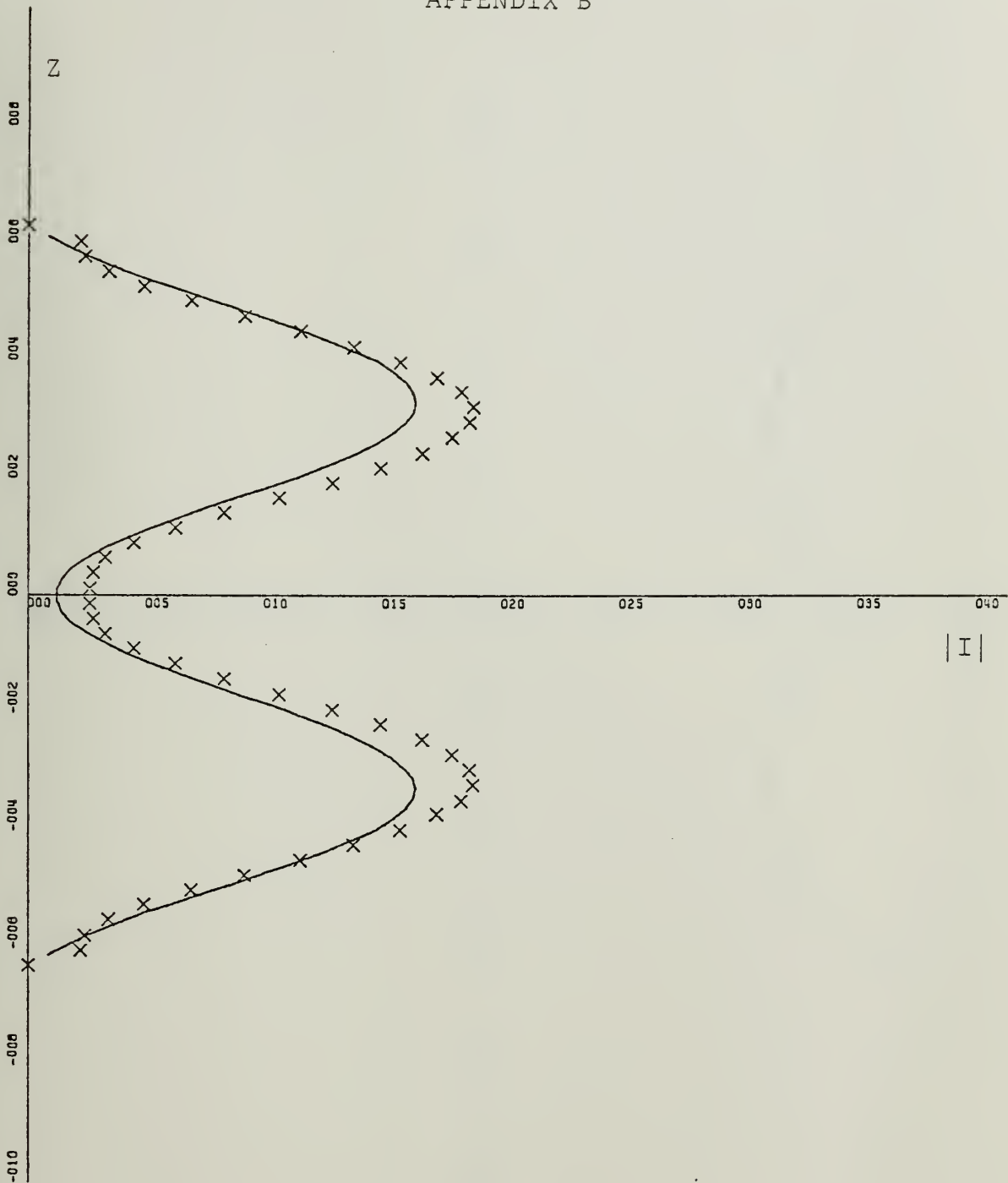
Y-SCALE=5.00E-01 UNITS INCH.

CURRENT PHASE : FEM/T=SOLID : INT.EQ=PLUS

ZL=.5 : AL=1/50 : DR=DZ/64 : ALFA=90

A-38

APPENDIX B

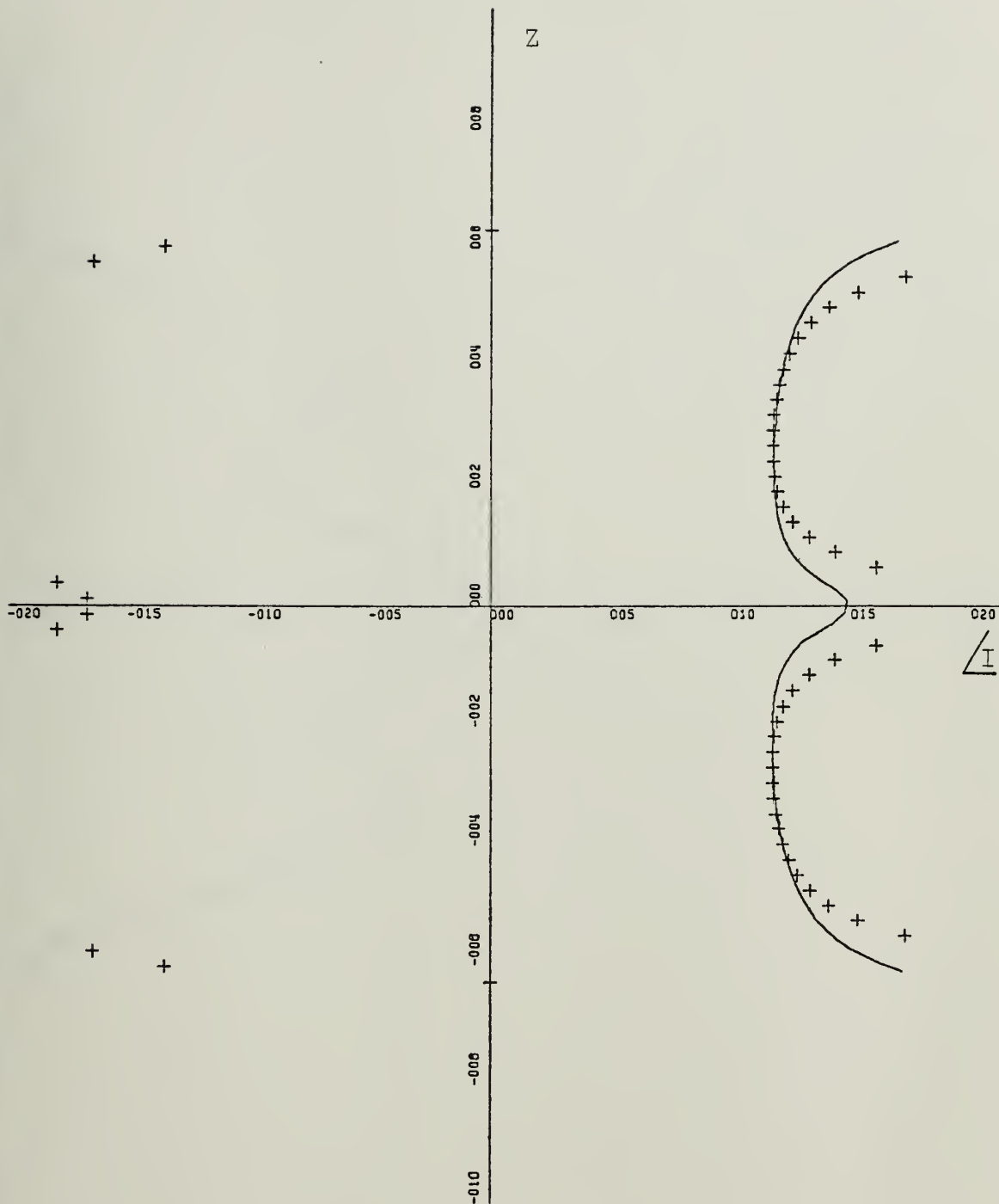


X-SCALE=5.00E-04 UNITS INCH.

Y-SCALE=2.00E+00 UNITS INCH.

CURRENT MAGNITUDE : FEM/T=SOLID : INT.EQ=X

ZL=2.0:AL=0.02:BL=0.001:ALFA=90:NW=70

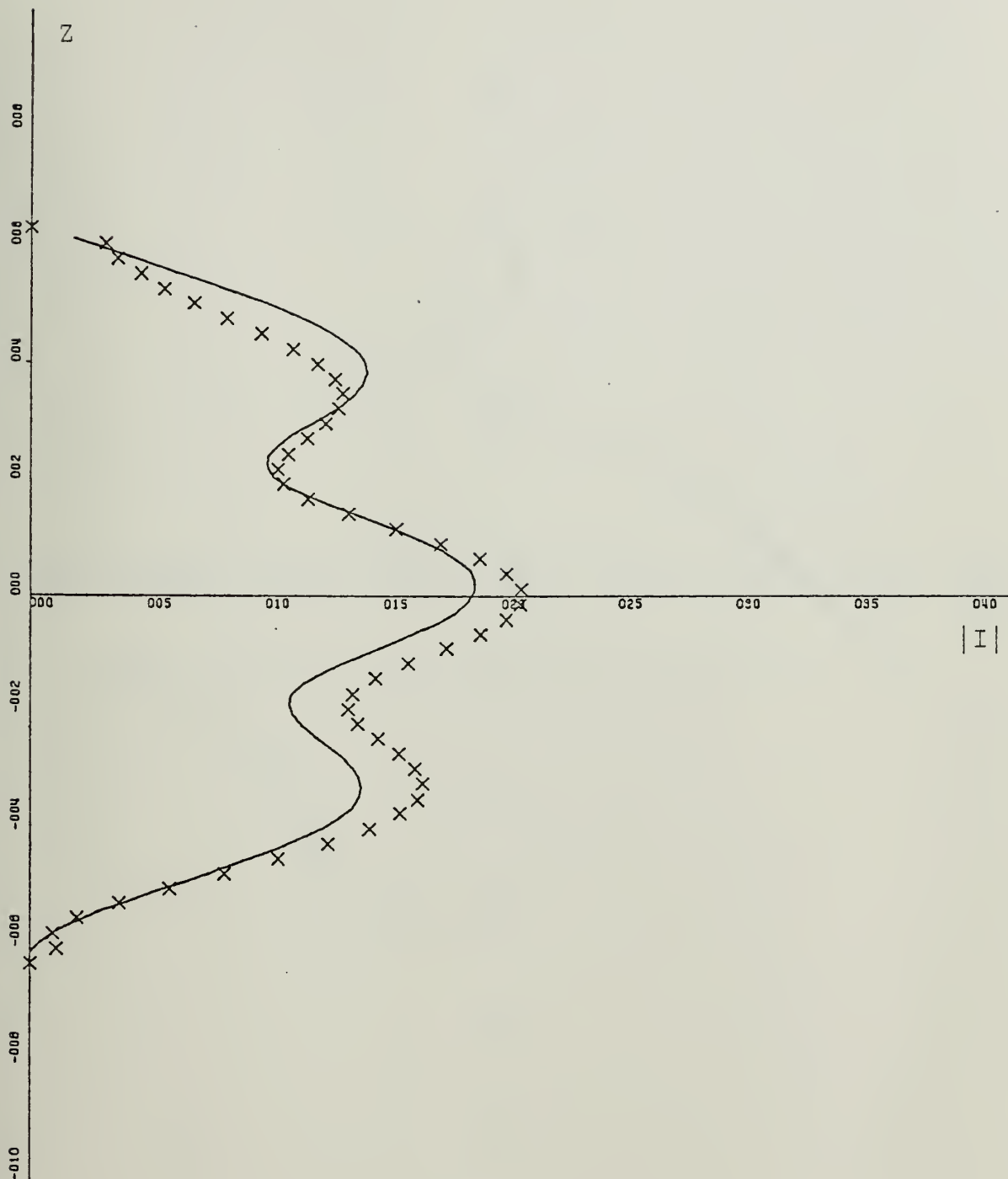


X-SCALE=5.00E+01 UNITS INCH.

Y-SCALE=2.00E+00 UNITS INCH.

CURRENT PHASE : FEM/T=SOLID : INT.EQ=PLUS

ZL=2.0:AL=0.02:BL=0.001:ALFA=90:NW=70

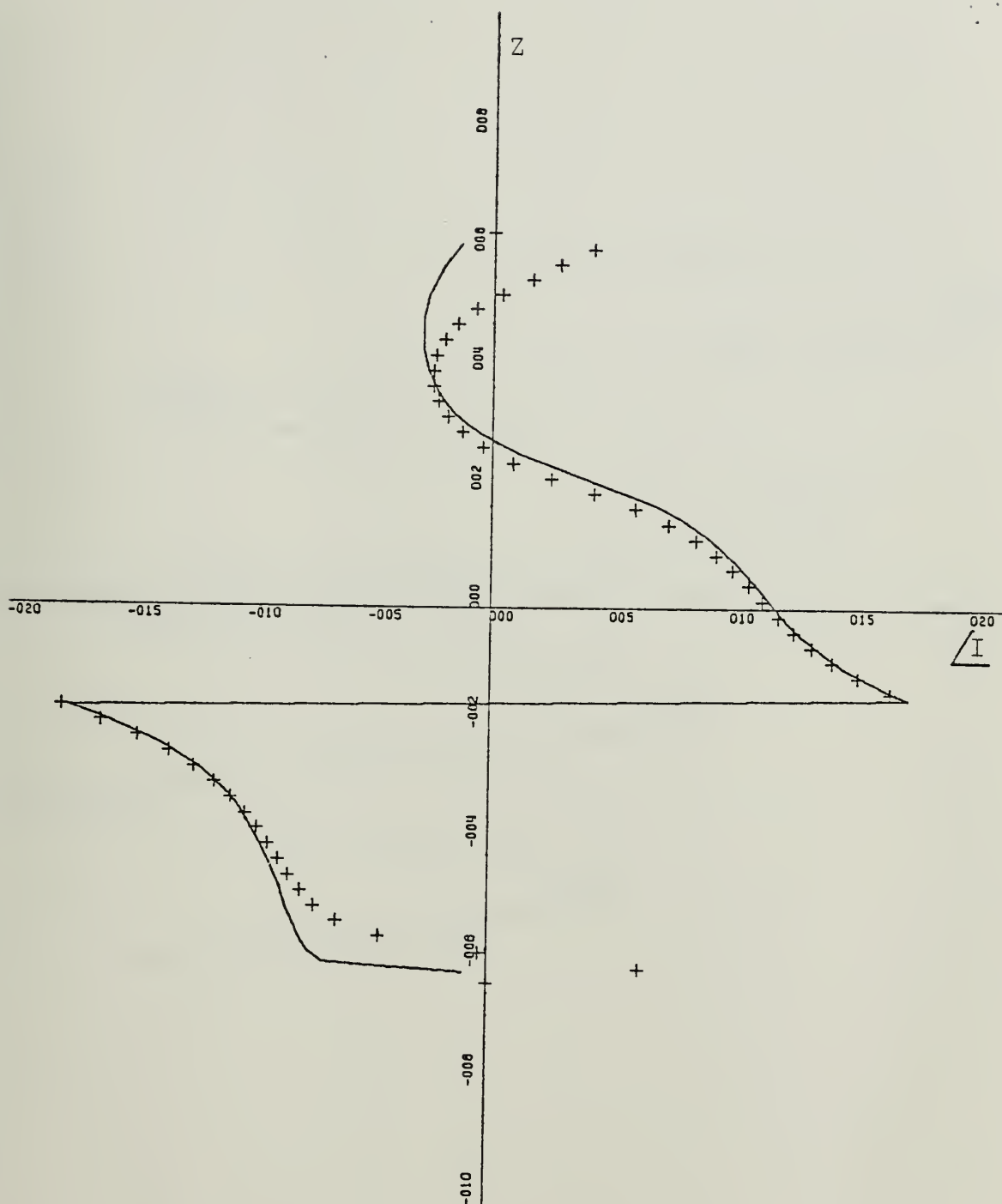


X-SCALE=5.00E-04 UNITS INCH.

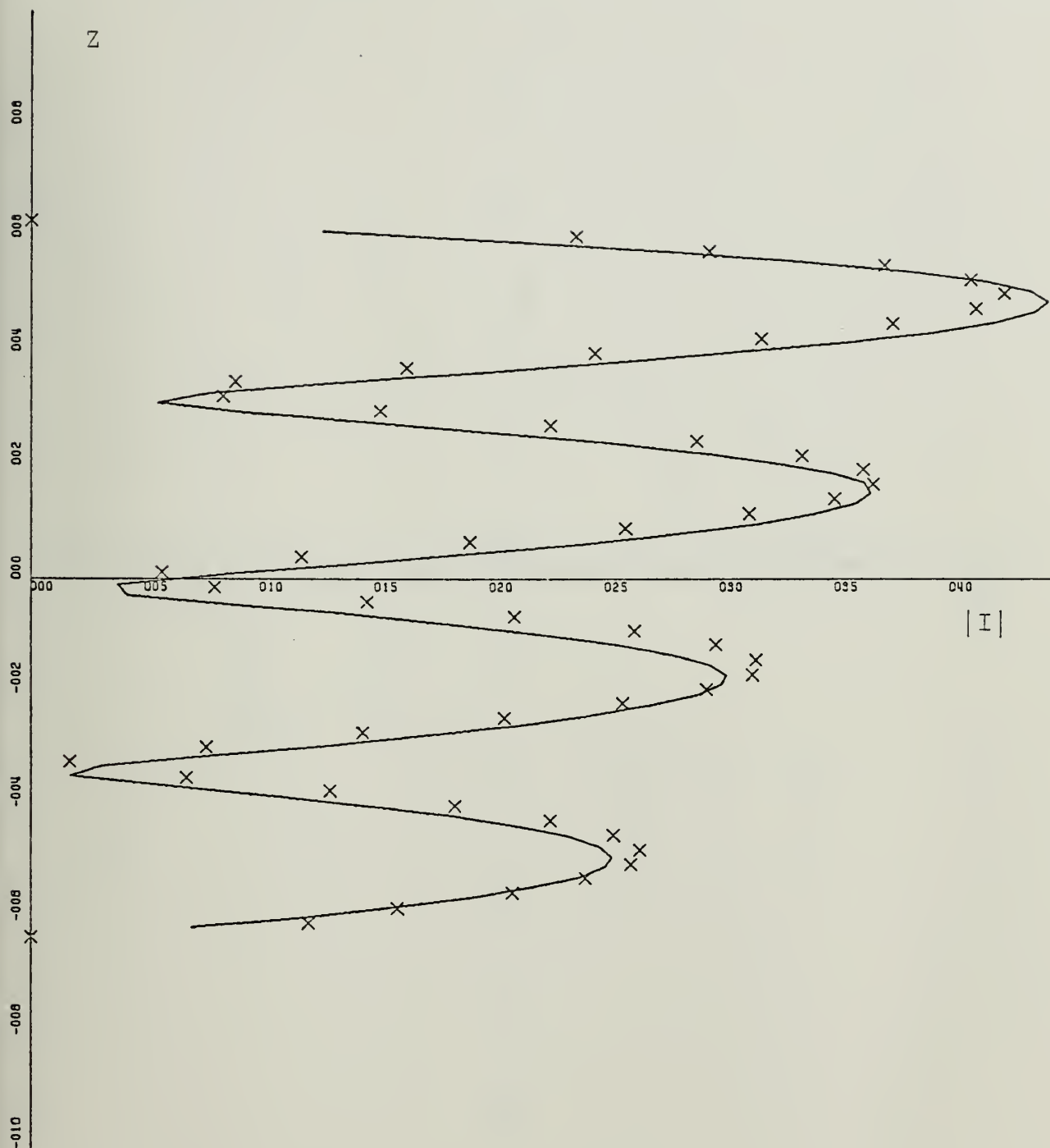
Y-SCALE=2.00E+00 UNITS INCH.

CURRENT MAGNITUDE : FEM/T=SOLID : INT.EQ=X

ZL=2.0:AL=0.02:BL=0.001:ALFA=60:NW=70



X-SCALE=5.00E+01 UNITS INCH.
Y-SCALE=2.00E+00 UNITS INCH.
CURRENT PHASE : FEM/T=SOLID : INT.EQ=PLUS
ZL=2.0:AL=0.02:BL=0.001:ALFA=60:NW=70

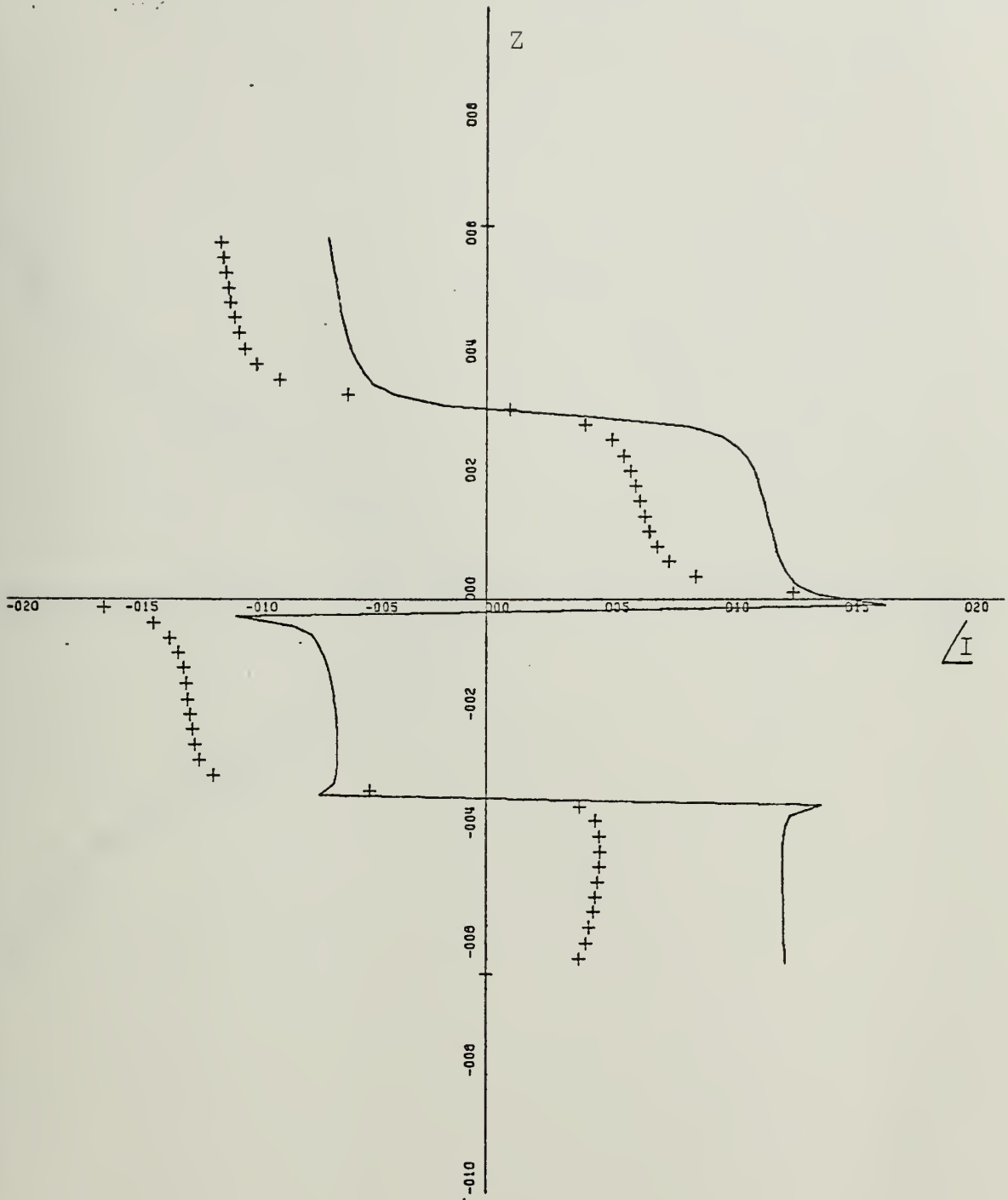


X-SCALE=5.00E-04 UNITS INCH.

Y-SCALE=2.00E+00 UNITS INCH.

CURRENT MAGNITUDE : FEM/T=SOLID : INT.EQ=X

ZL=2.0:AL=0.02:BL=0.001:ALFA=30:NW=70

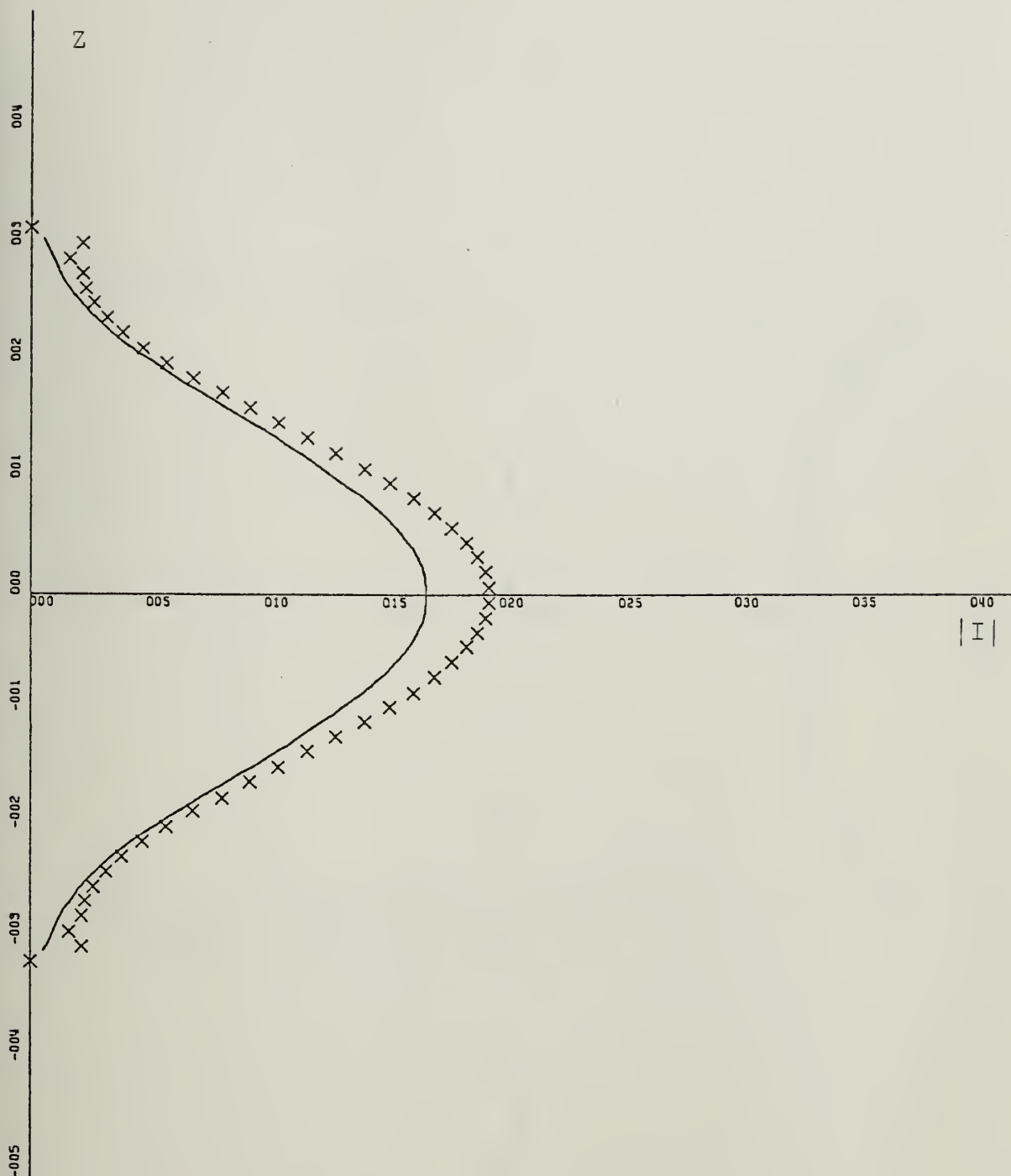


X-SCALE=5.00E+01 UNITS INCH.

Y-SCALE=2.00E+00 UNITS INCH.

CURRENT PHASE : FEM/T=SOLID : INT.EQ=PLUS

ZL=2.0:AL=0.02:BL=0.001:ALFA=30:NW=70

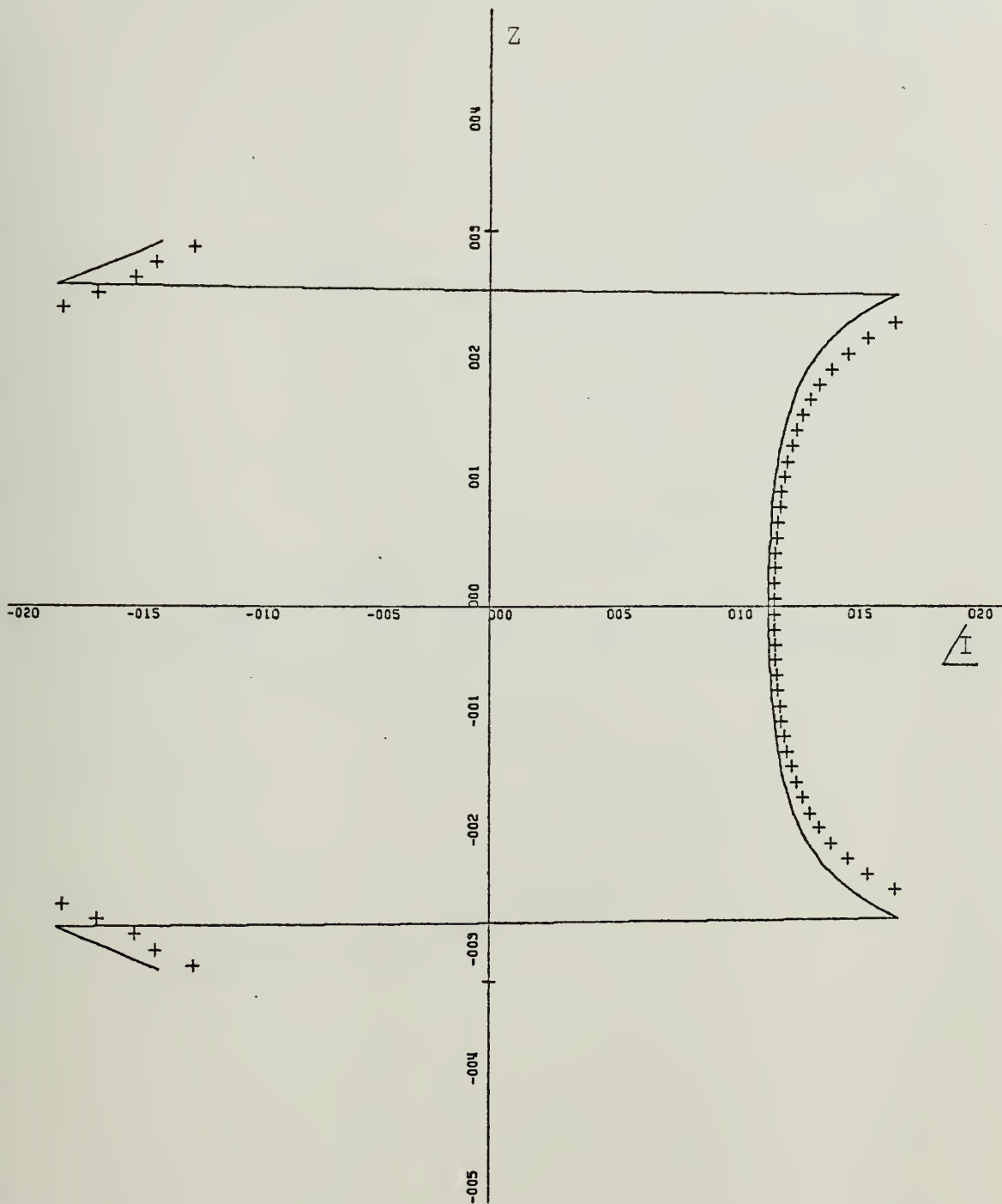


X-SCALE=5.00E-04 UNITS INCH.

Y-SCALE=1.00E+00 UNITS INCH.

CURRENT MAGNITUDE : FEM/T=SOLID : INT.EQ=X

ZL=1.0:AL=0.02:BL=0.001:ALFA=90:NW=70

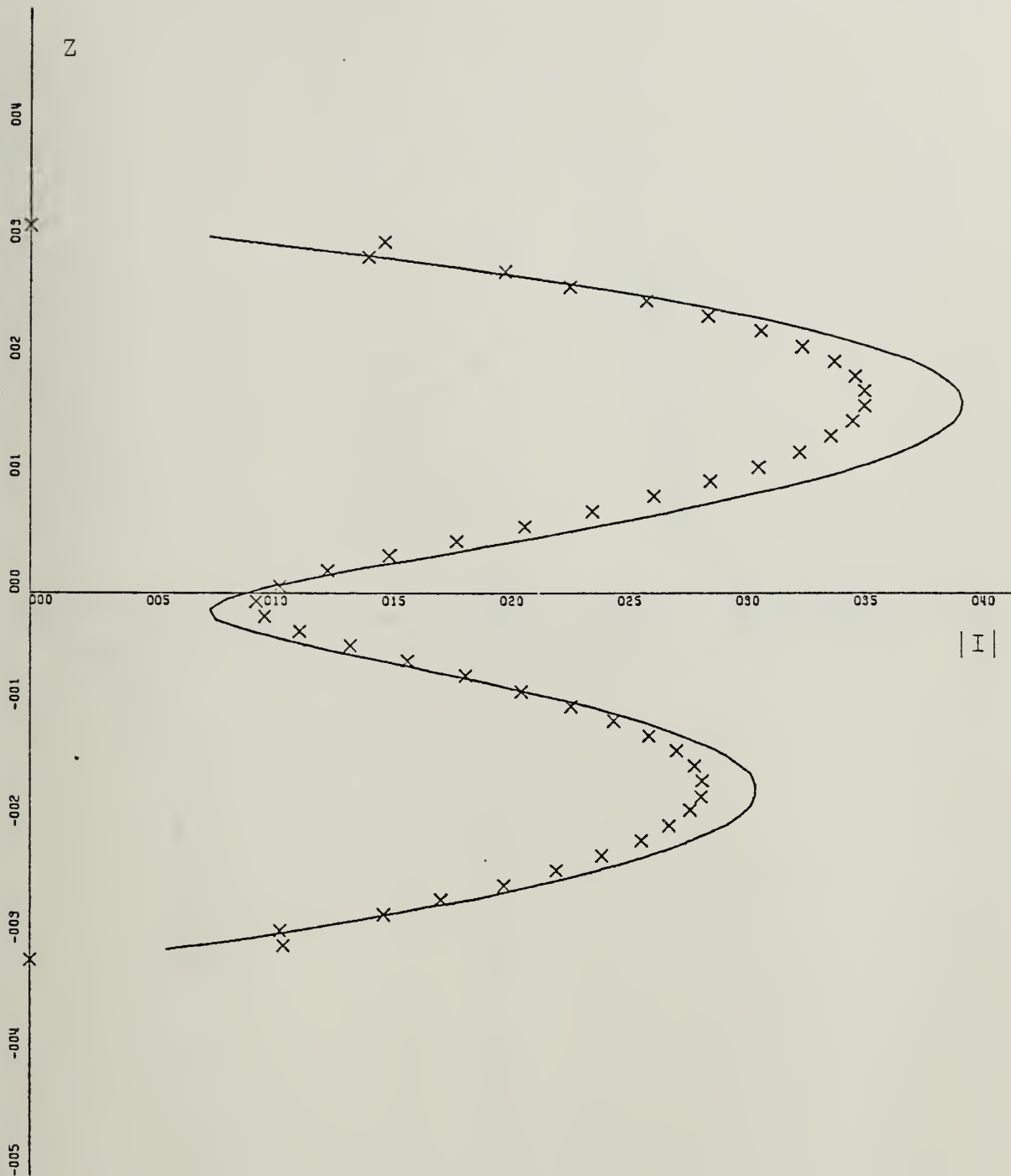


X-SCALE=5.00E+01 UNITS INCH.

Y-SCALE=1.00E+00 UNITS INCH.

CURRENT PHASE : FEM/T=SOLID : INT.EQ=PLUS

ZL=1.0:AL=0.02:BL=0.001:ALFA=90:NW=70

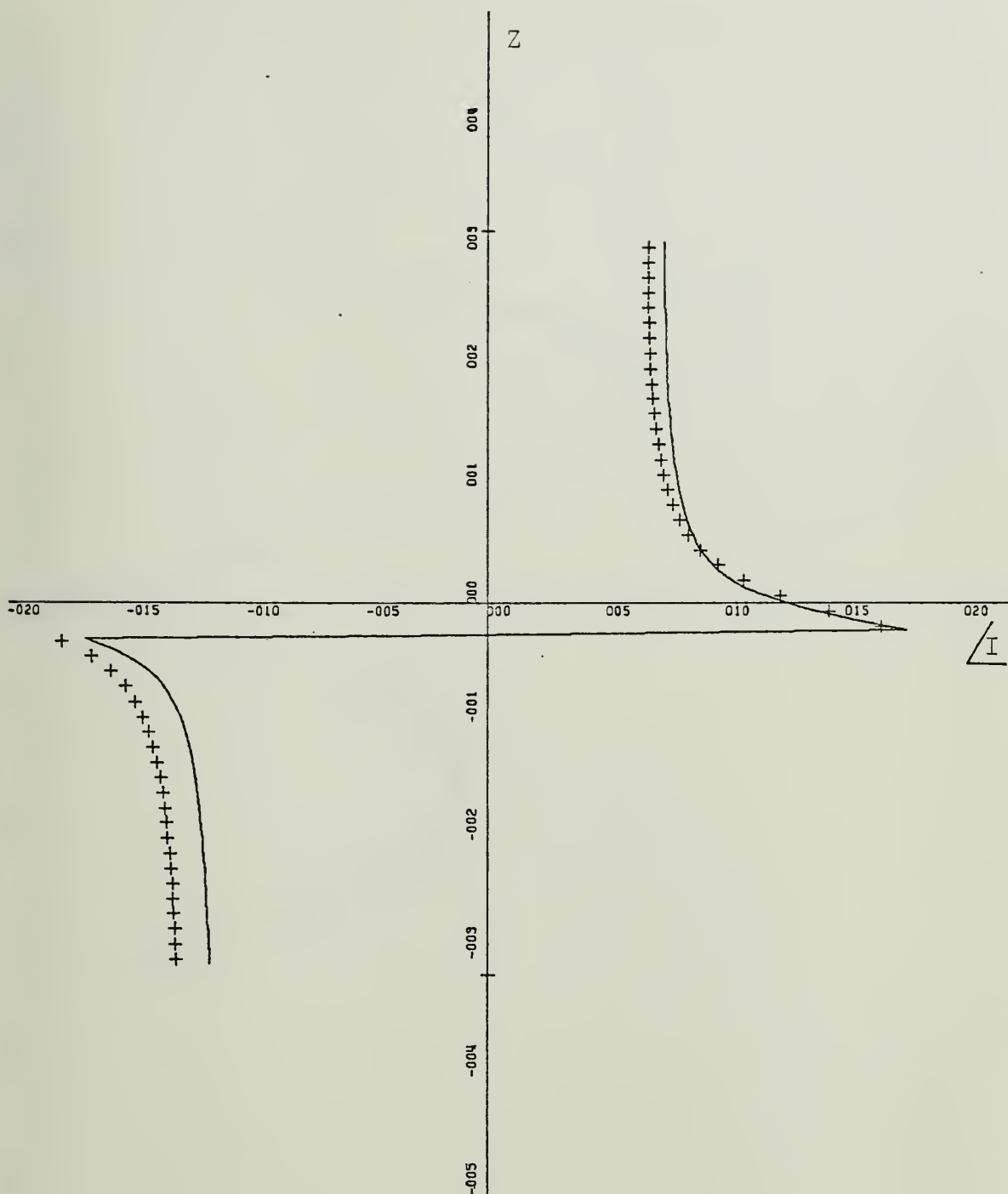


X-SCALE=5.00E-04 UNITS INCH.

Y-SCALE=1.00E+00 UNITS INCH.

CURRENT MAGNITUDE : FEM/T=SOLID : INT.EQ=X

ZL=1.0:AL=0.02:BL=0.001:ALFA=60:NW=70

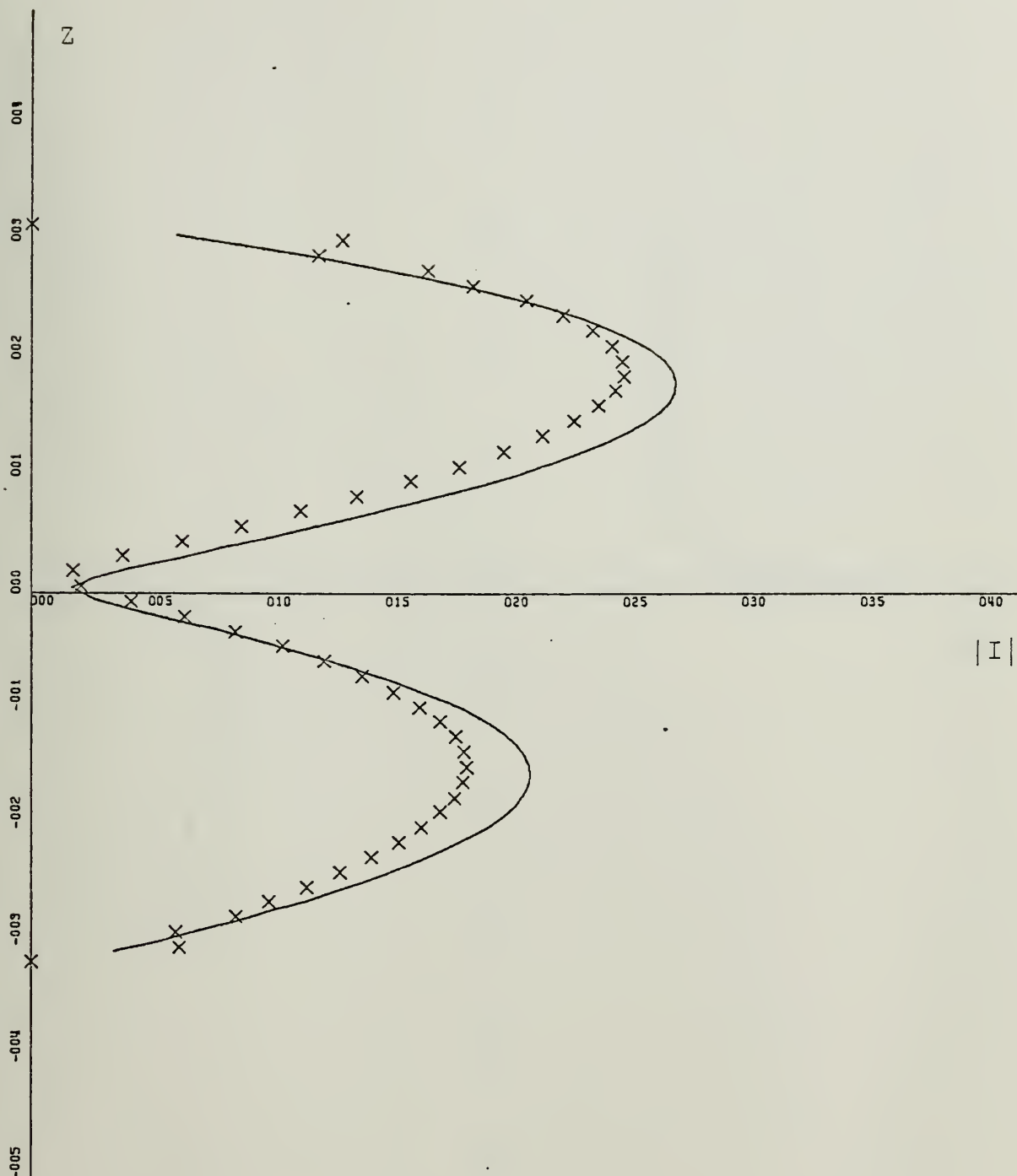


X-SCALE=5.00E+01 UNITS INCH.

Y-SCALE=1.00E+00 UNITS INCH.

CURRENT PHASE : FEM/T=SOLID : INT.EQ=PLUS

ZL=1.0:AL=0.02:BL=0.001:ALFA=60:NW=70

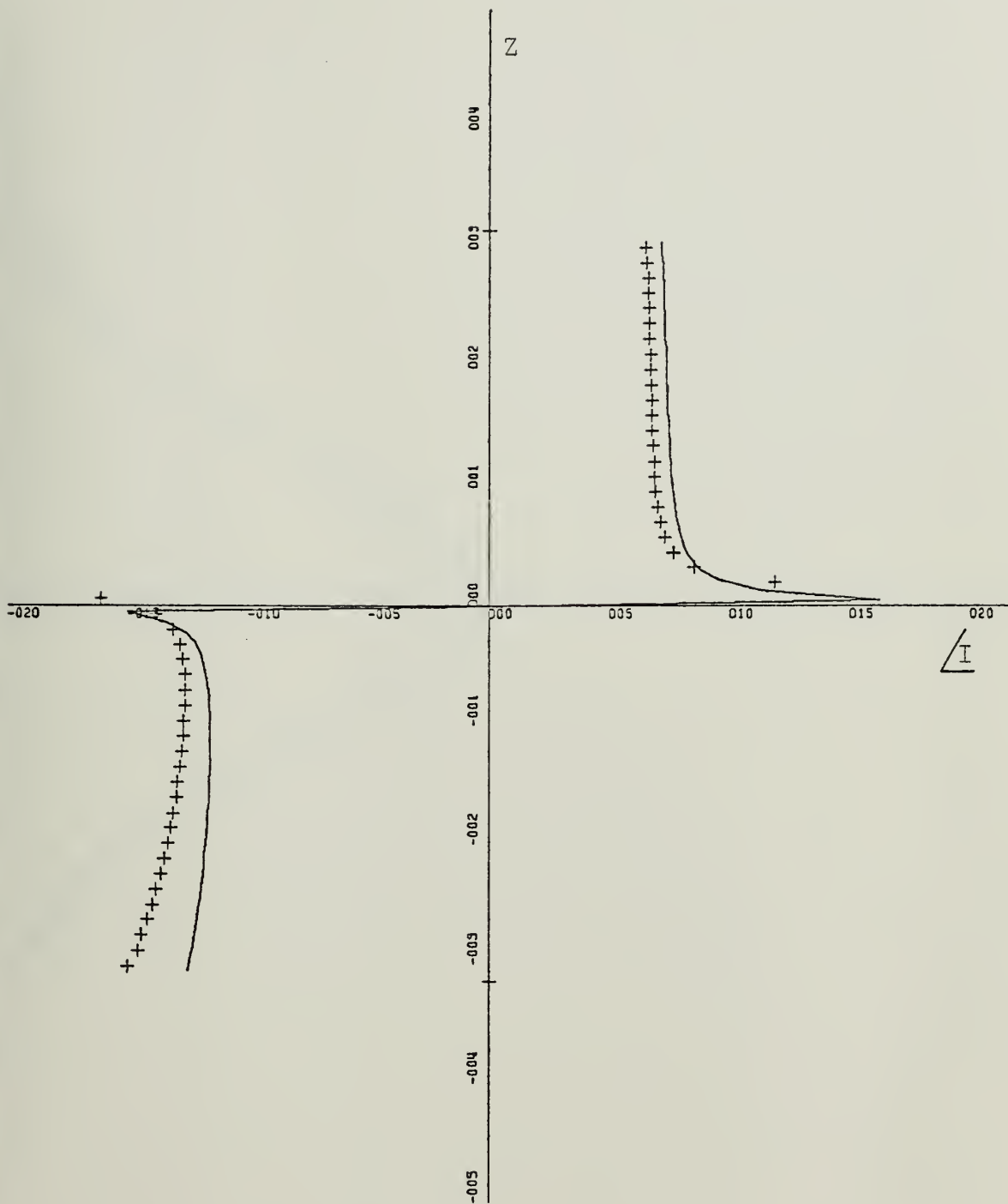


X-SCALE=5.00E-04 UNITS INCH.

Y-SCALE=1.00E+00 UNITS INCH.

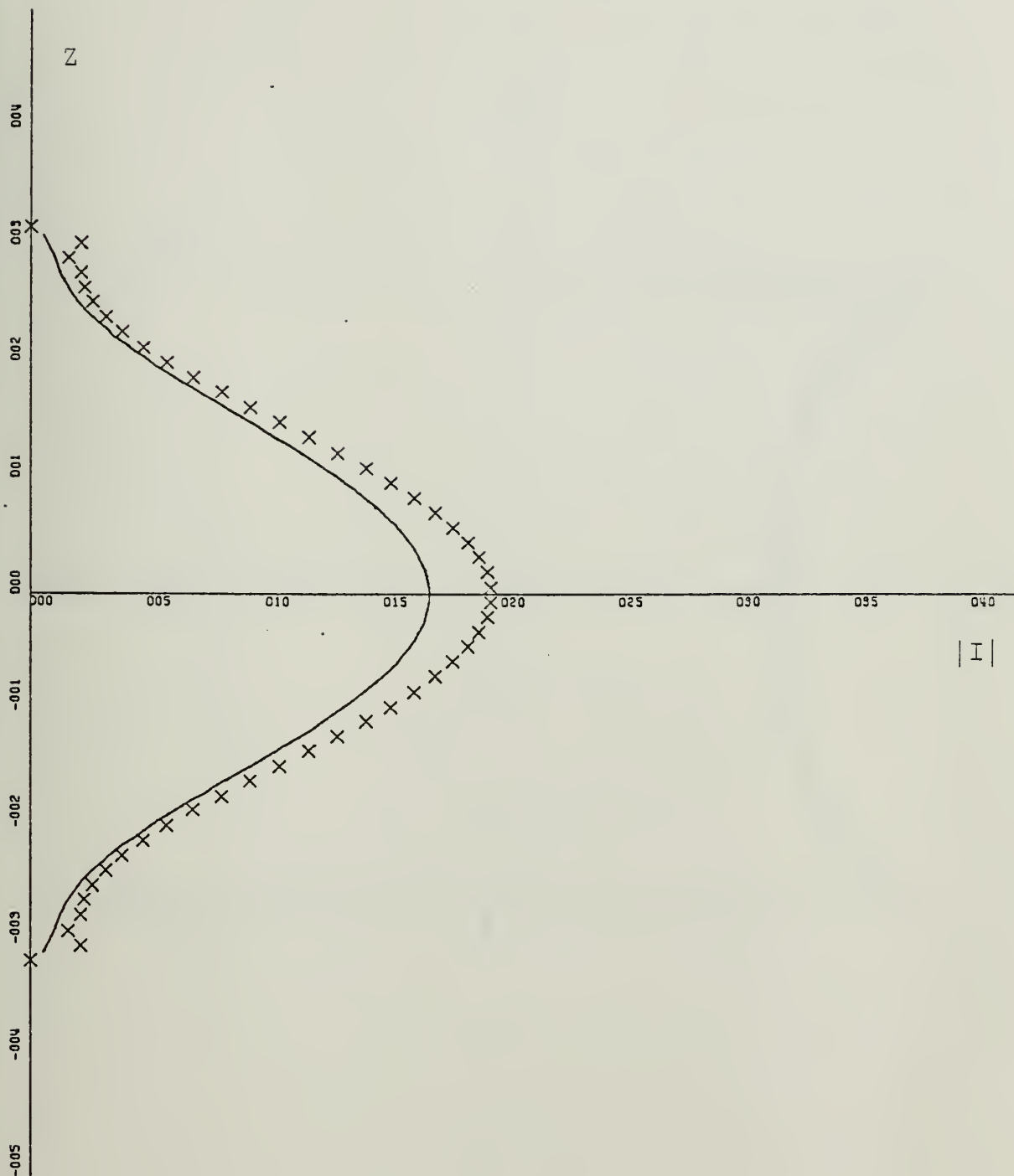
CURRENT MAGNITUDE : FEM/T=SOLID : INT.EQ=X

ZL=1.0:AL=0.02:BL=0.001:ALFA=30:NW=70



X-SCALE=5.00E+01 UNITS INCH.
Y-SCALE=1.00E+00 UNITS INCH.

CURRENT PHASE : FEM/T=SOLID : INT.EQ=PLUS
ZL=1.0:AL=0.02:BL=0.001:ALFA=30:NW=70

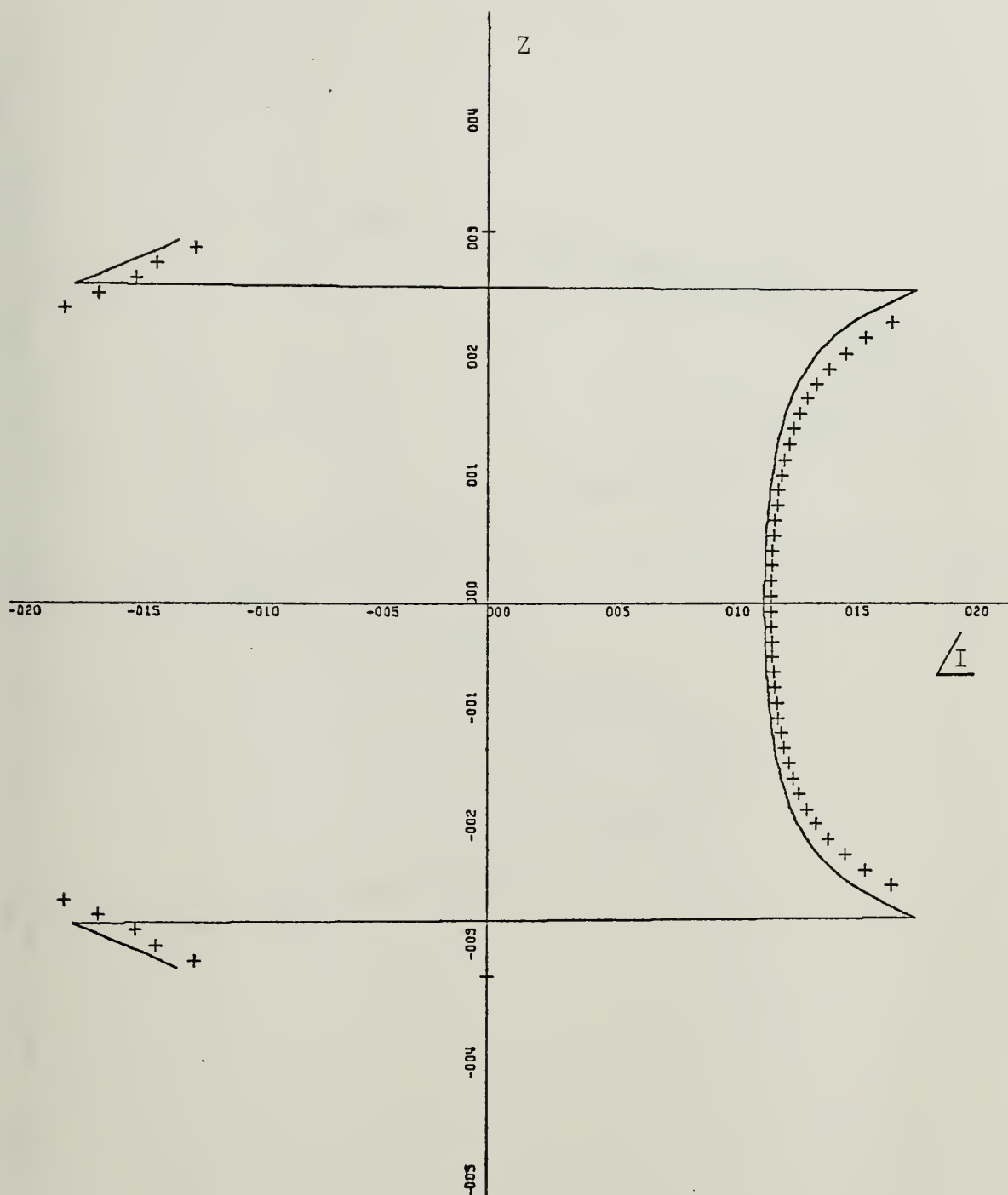


X-SCALE=5.00E-04 UNITS INCH.

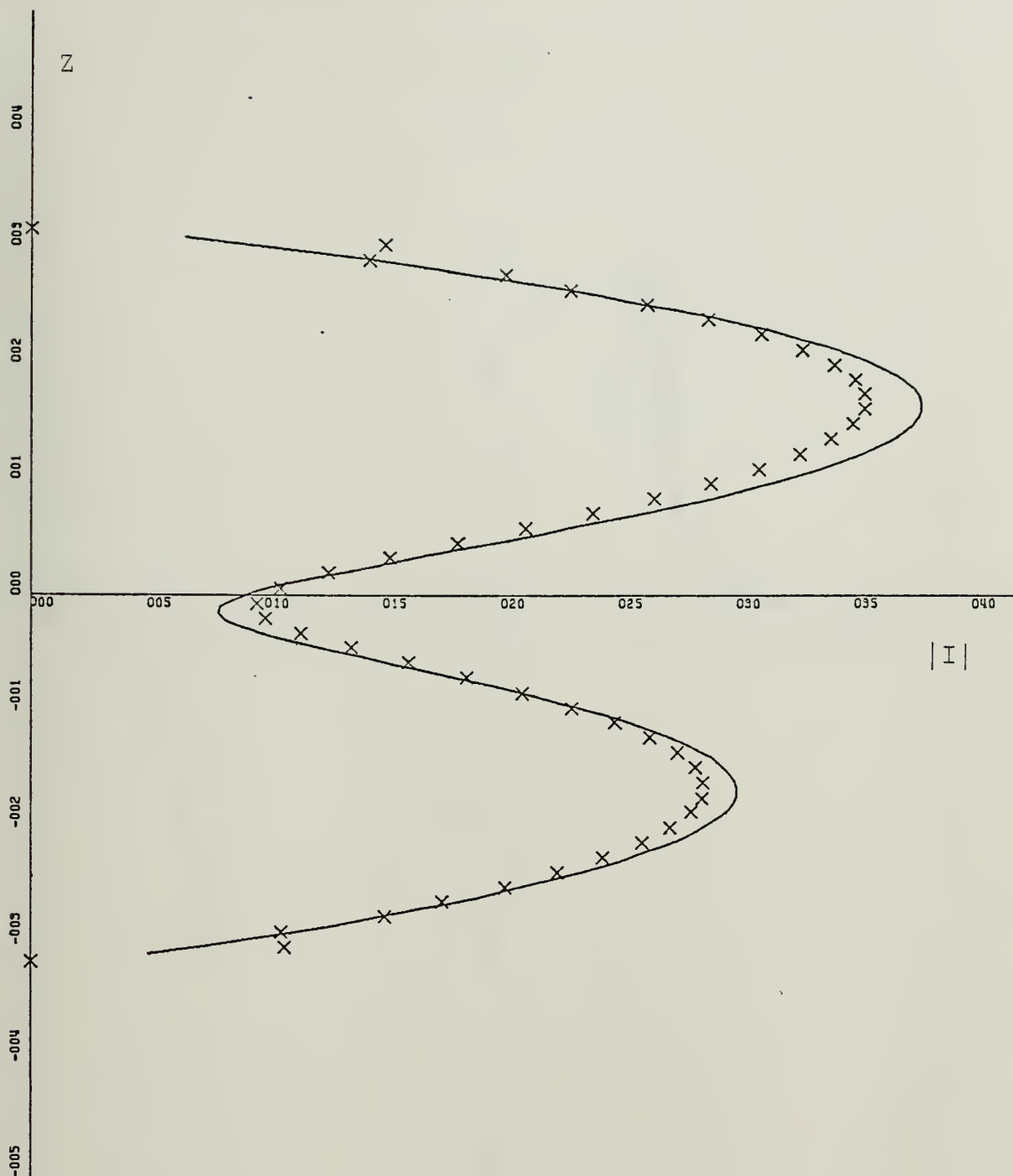
Y-SCALE=1.00E+00 UNITS INCH.

CURRENT MAGNITUDE : FEM/T=SOLID : INT.EQ=X

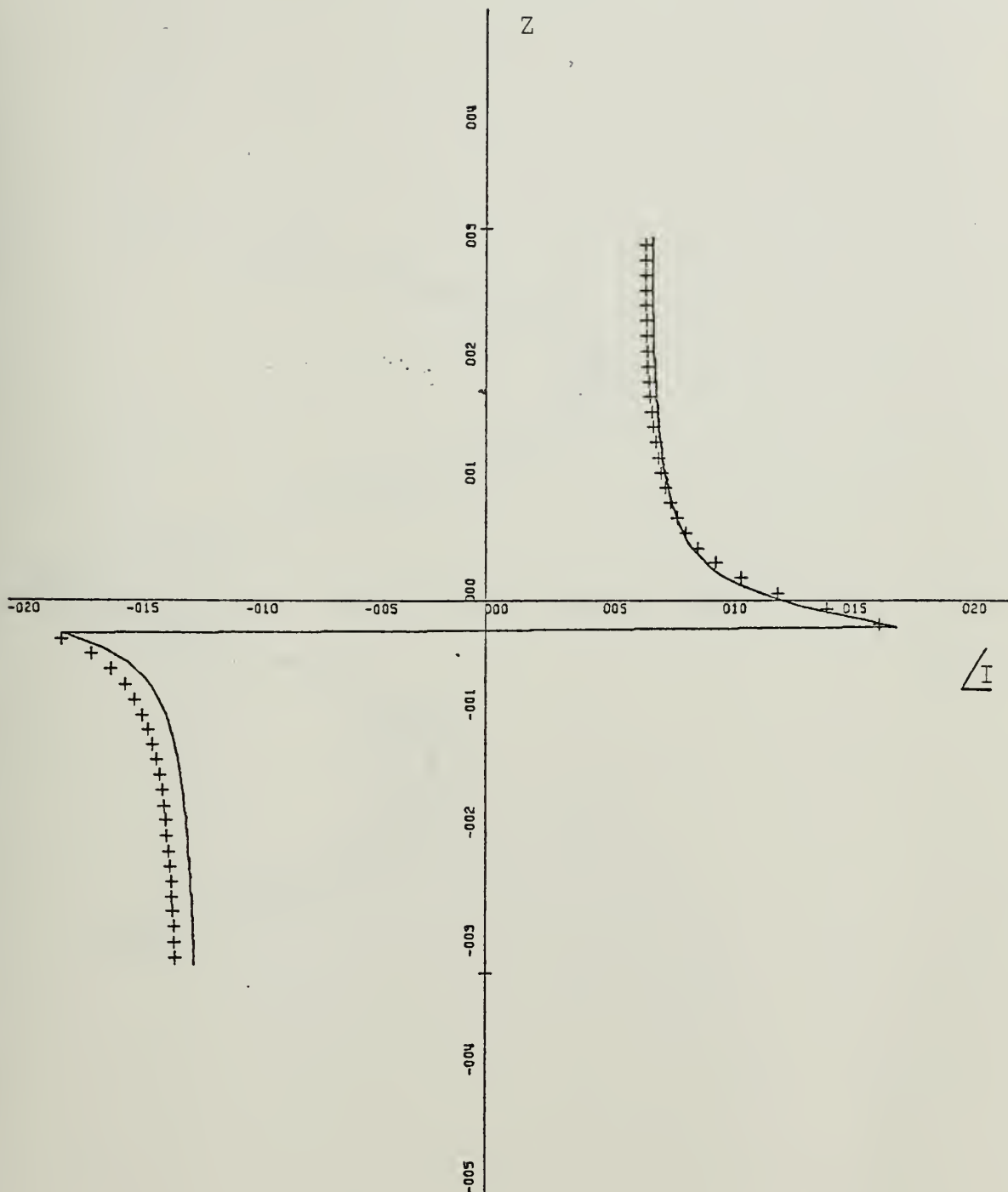
ZL=1.0:AL=0.02:BL=0.001:ALFA=90:NW=100



X-SCALE=5.00E+01 UNITS INCH.
 Y-SCALE=1.00E+00 UNITS INCH.
 CURRENT PHASE : FEM/T=SOLID : INT.EQ=PLUS
 ZL=1.0:AL=0.02:BL=0.001:ALFA=90:NW=100



X-SCALE=5.00E-04 UNITS INCH.
 Y-SCALE=1.00E+00 UNITS INCH.
 CURRENT MAGNITUDE : FEM/T=SOLID : INT.EQ=X
 ZL=1.0:AL=0.02:BL=0.001:ALFA=60:NW=100

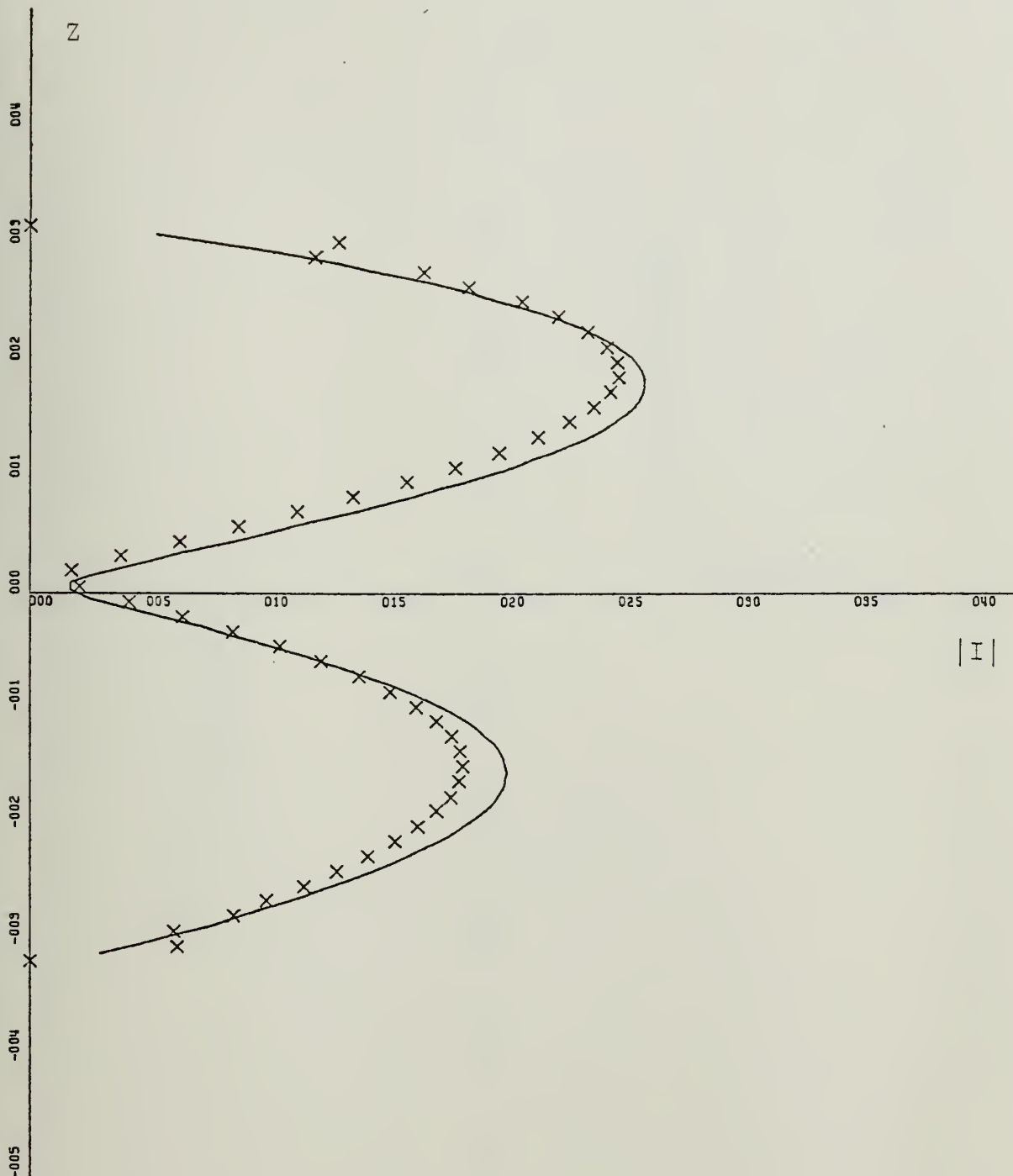


X-SCALE=5.00E+01 UNITS INCH.

Y-SCALE=1.00E+00 UNITS INCH.

CURRENT PHASE : FEM/T=SOLID : INT.EQ=PLUS

ZL=1.0:AL=0.02:BL=0.001:ALFA=60:NW=100

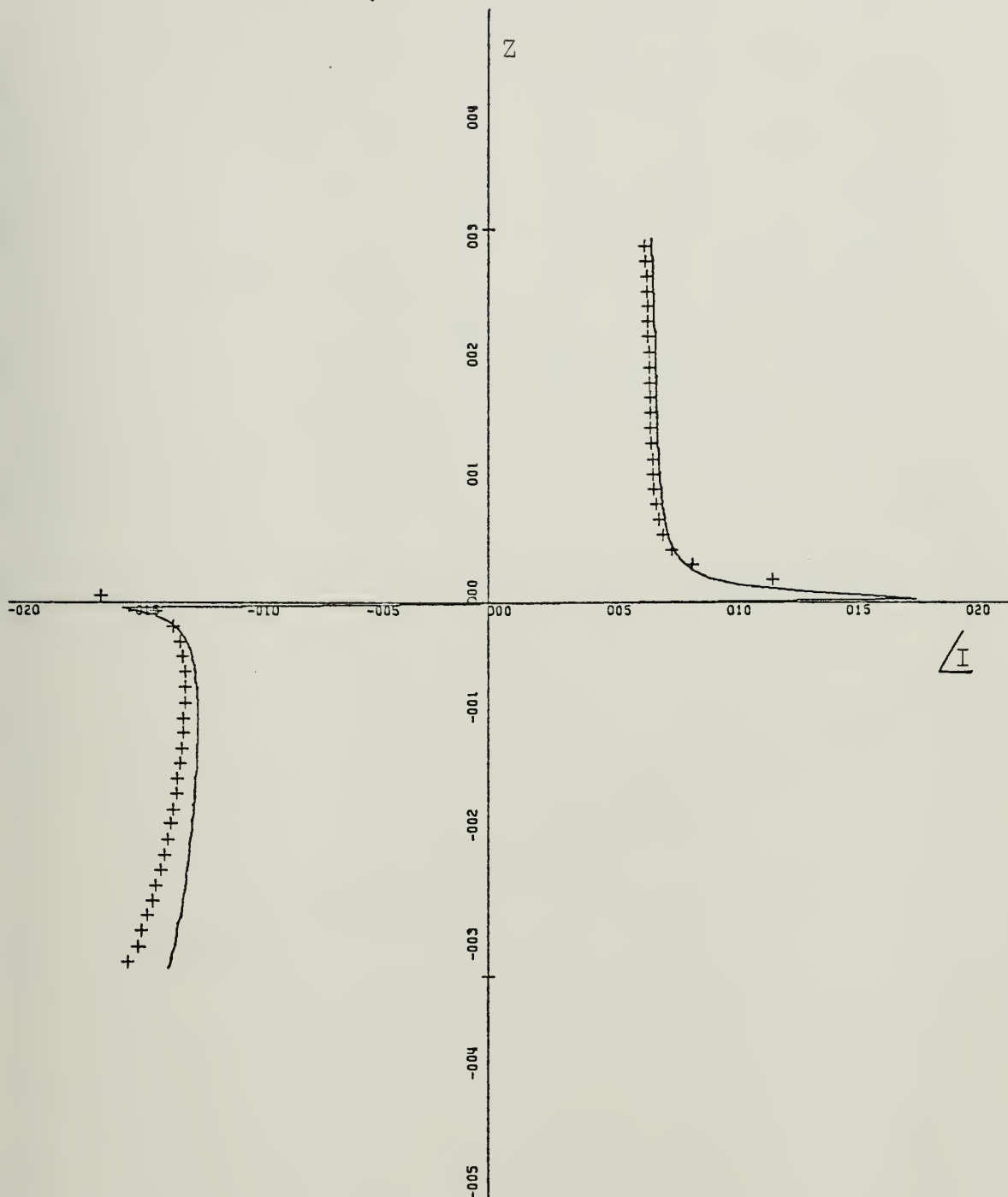


X-SCALE=5.00E-04 UNITS INCH.

Y-SCALE=1.00E+00 UNITS INCH.

CURRENT MAGNITUDE : FEM/T=SOLID : INT.EQ=X

ZL=1.0:AL=0.02:BL=0.001:ALFA=30:NW=100



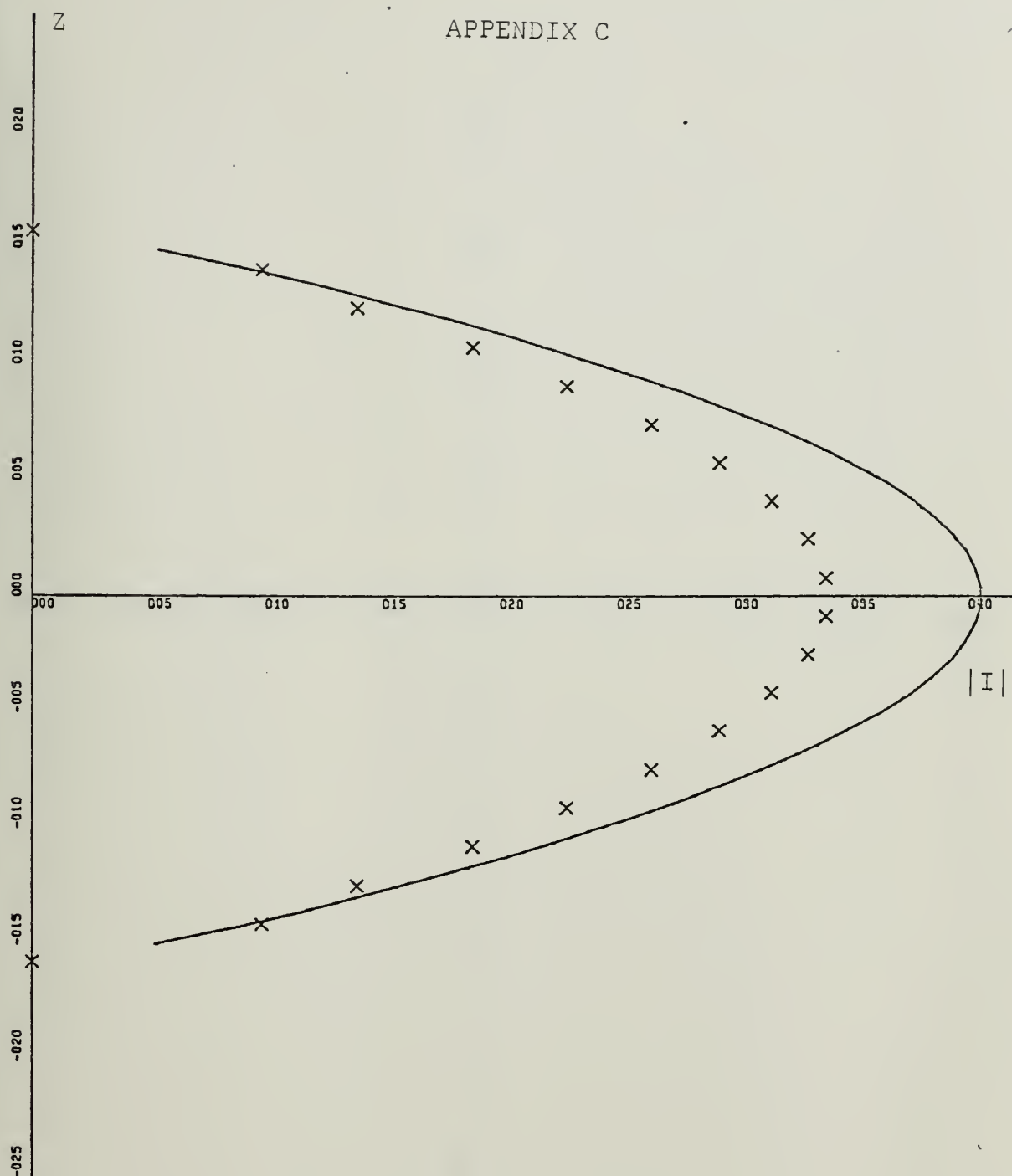
X-SCALE=5.00E+01 UNITS INCH.

Y-SCALE=1.00E+00 UNITS INCH.

CURRENT PHASE : FEM/T=SOLID : INT.EQ=PLUS

ZL=1.0:AL=0.02:BL=0.001:ALFA=30:NW=100

APPENDIX C

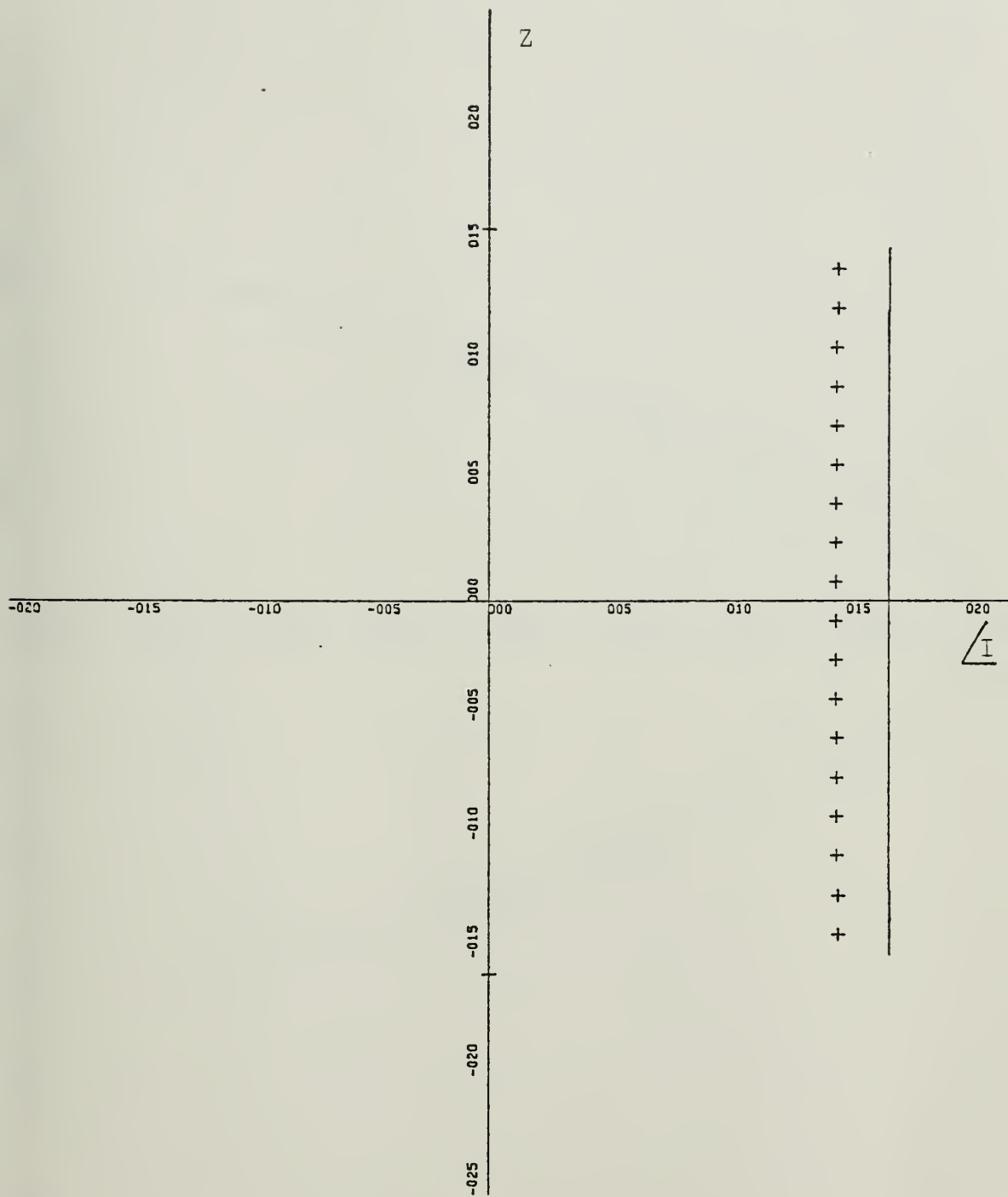


X-SCALE=5.00E-04 UNITS INCH.

Y-SCALE=5.00E-01 UNITS INCH.

CURRENT MAGNITUDE : FEM/T=SOLID : INT.EQ=X

ZL=.5:AL=0.01:BL=0.001:ALFA=90:NW=40

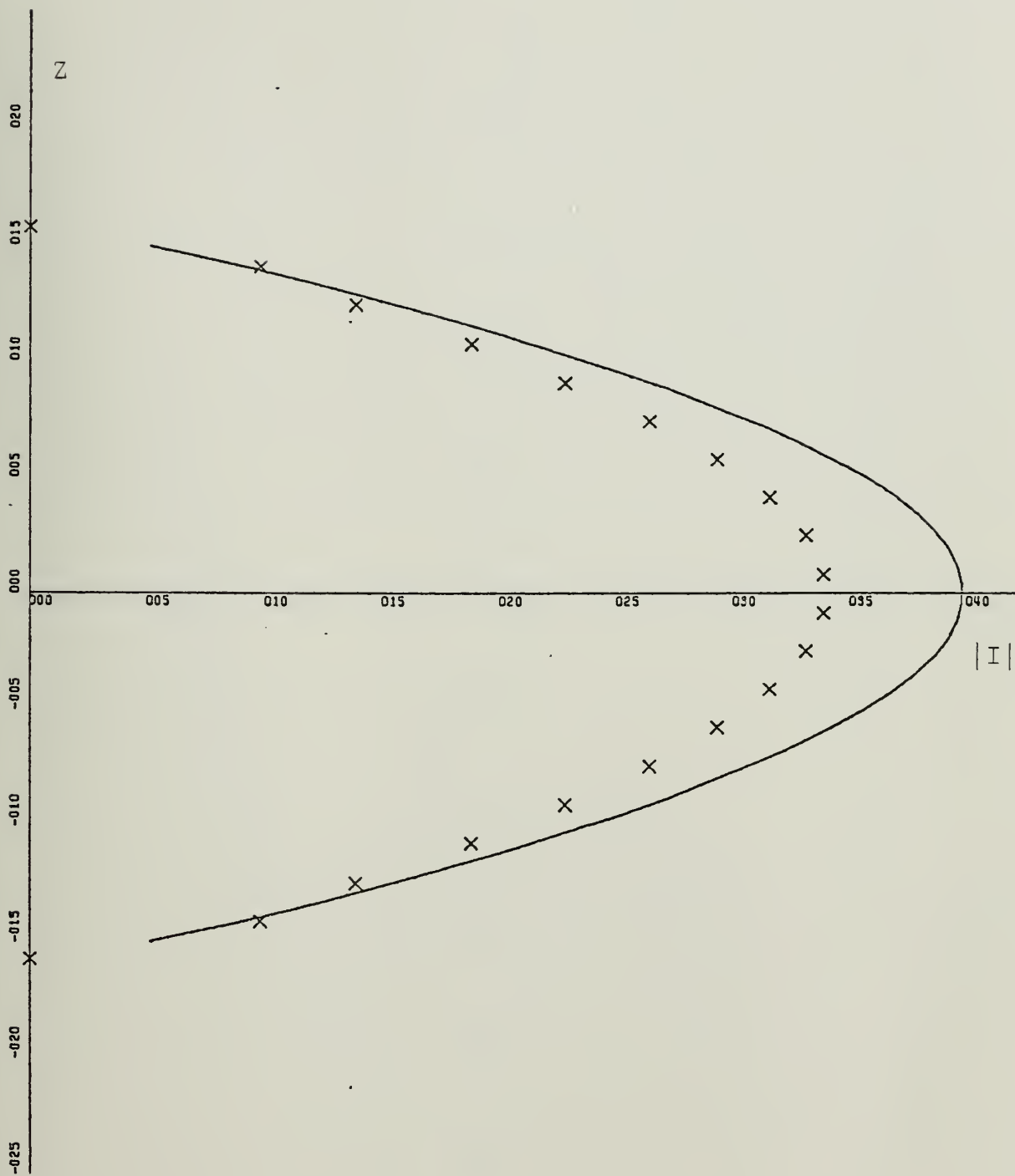


X-SCALE=5.00E+01 UNITS INCH.

Y-SCALE=5.00E-01 UNITS INCH.

CURRENT PHASE : FEM/T=SOLID : INT.EQ=PLUS

ZL=.5:AL=0.01:BL=0.001:ALFA=90:NW=40

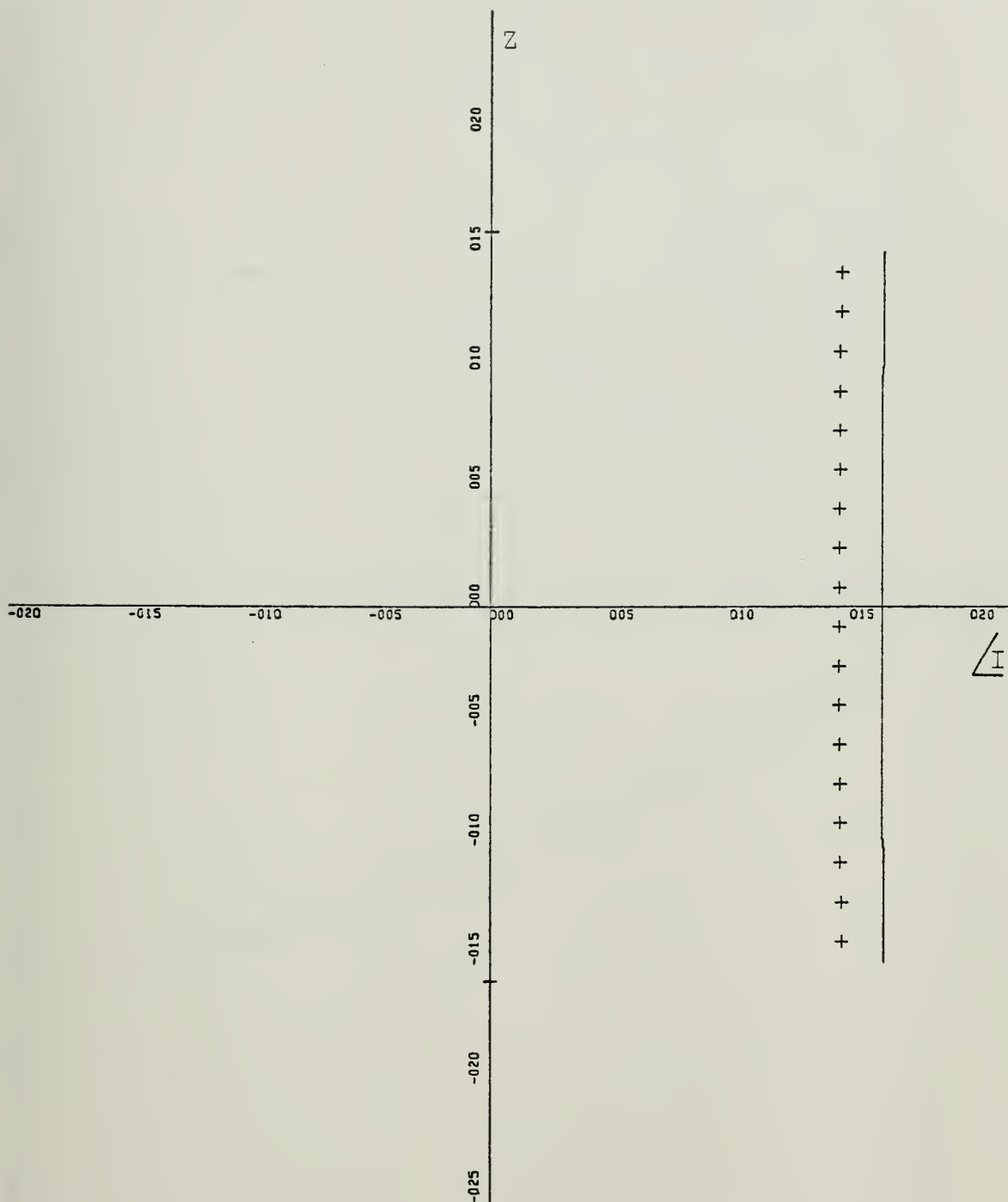


X-SCALE=5.00E-04 UNITS INCH.

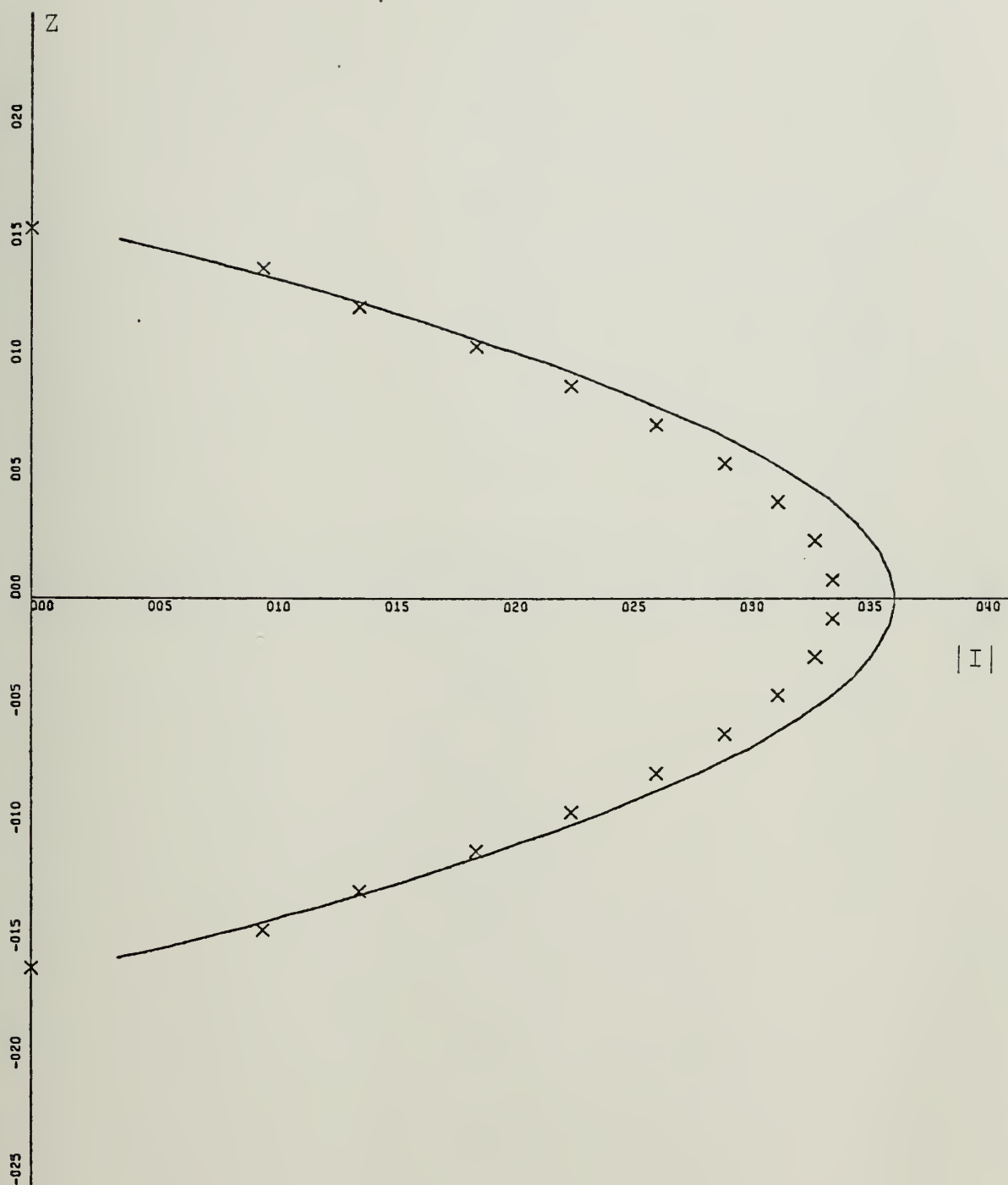
Y-SCALE=5.00E-01 UNITS INCH.

CURRENT MAGNITUDE : FEM/T=SOLID : INT.EQ=X

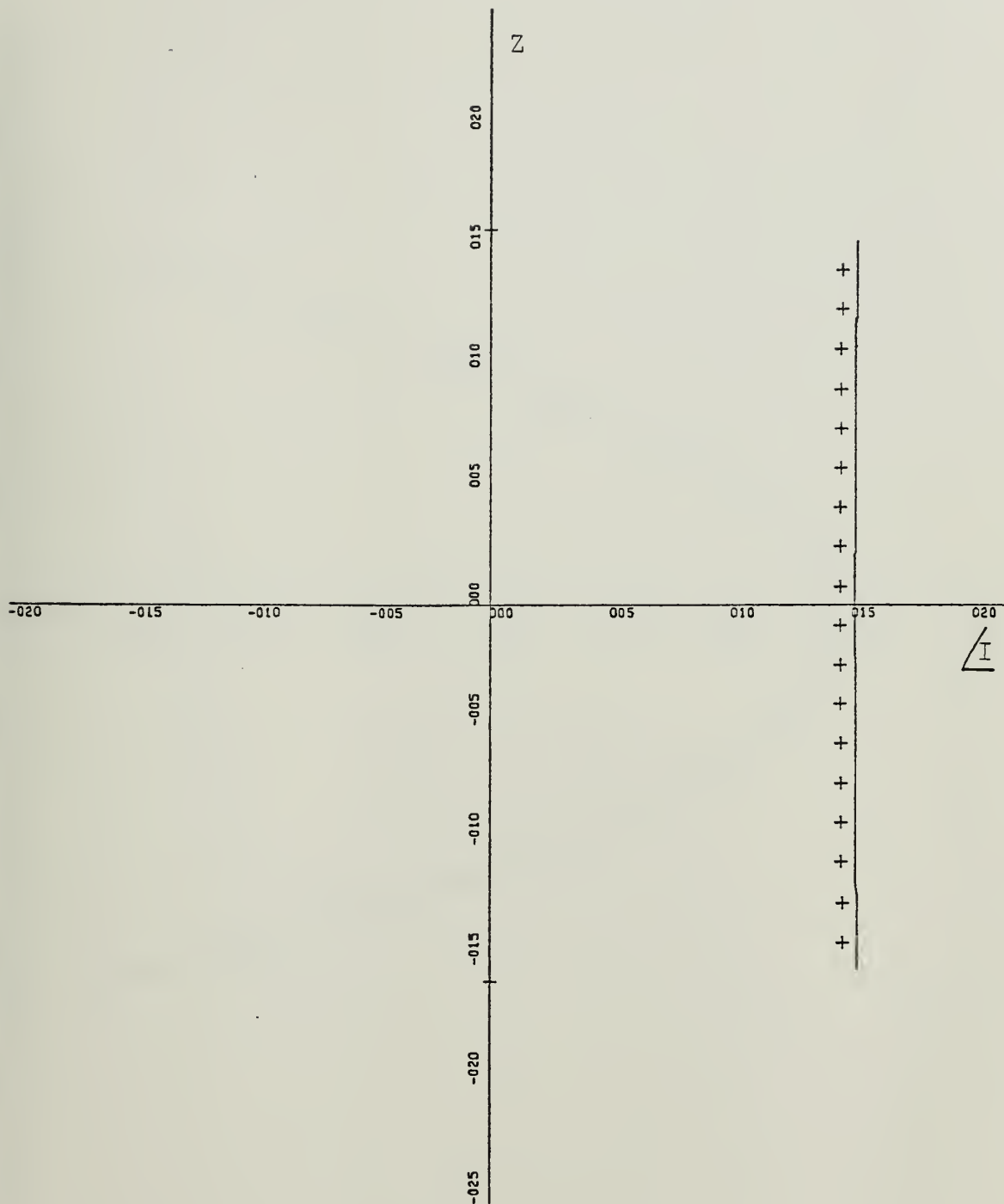
ZL=.5:AL=0.01:BL=0.0005:ALFA=90:NW=40



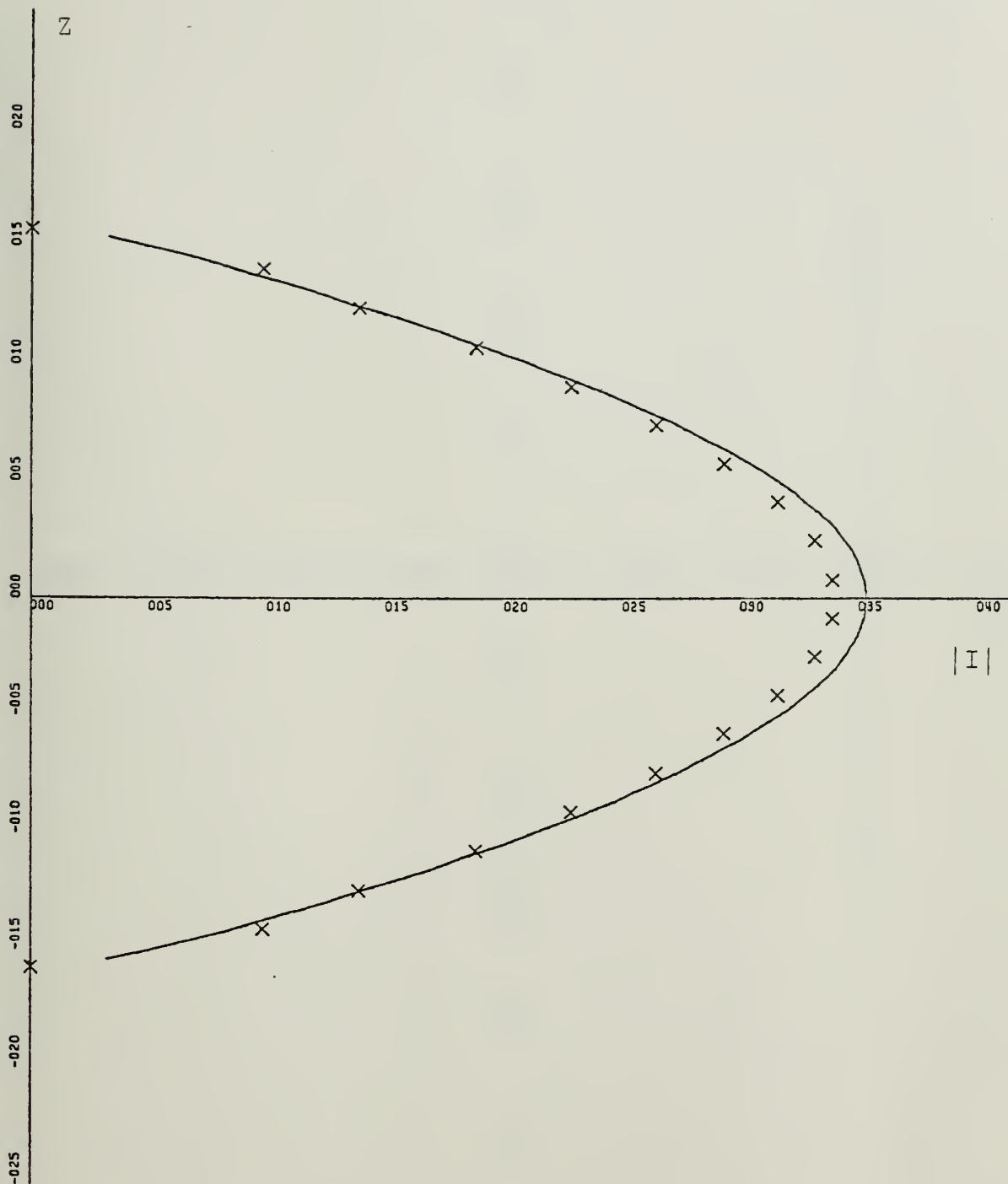
X-SCALE=5.00E+01 UNITS INCH.
 Y-SCALE=5.00E-01 UNITS INCH.
 CURRENT PHASE : FEM/T=SOLID : INT.EQ=PLUS
 ZL=.5:AL=0.01:BL=0.0005:ALFA=90:NW=40



X-SCALE=5.00E-04 UNITS INCH.
 Y-SCALE=5.00E-01 UNITS INCH.
 CURRENT MAGNITUDE : FEM/T=SOLID : INT.EQ=X
 ZL=.5:AL=0.01:BL=0.0005:ALFA=90:NW=70



X-SCALE=5.00E+01 UNITS INCH.
 Y-SCALE=5.00E-01 UNITS INCH.
 CURRENT PHASE : FEM/T=SOLID : INT.EQ=PLUS
 ZL=.5:AL=0.01:BL=0.0005:ALFA=90:NW=70

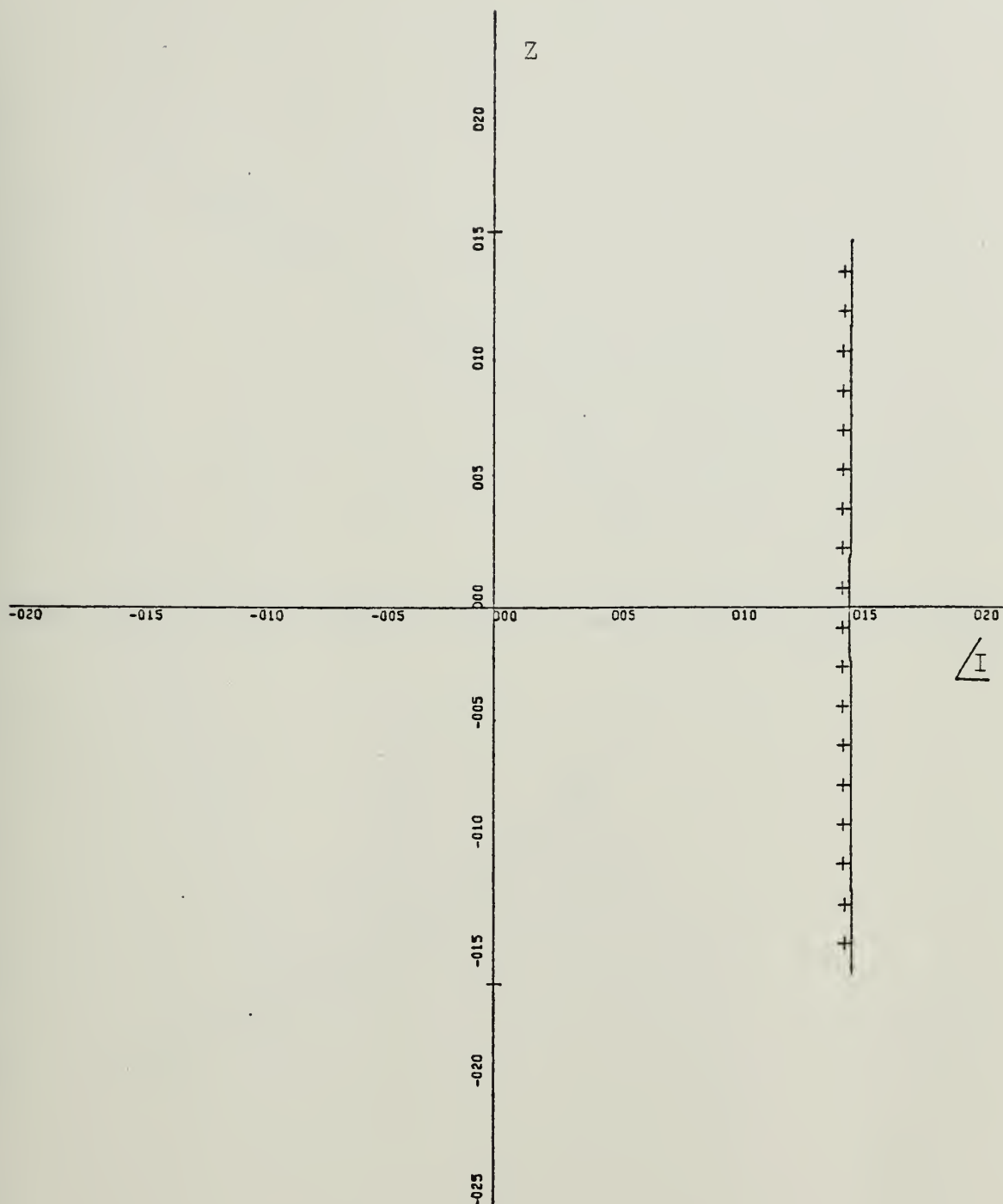


X-SCALE=5.00E-04 UNITS INCH.

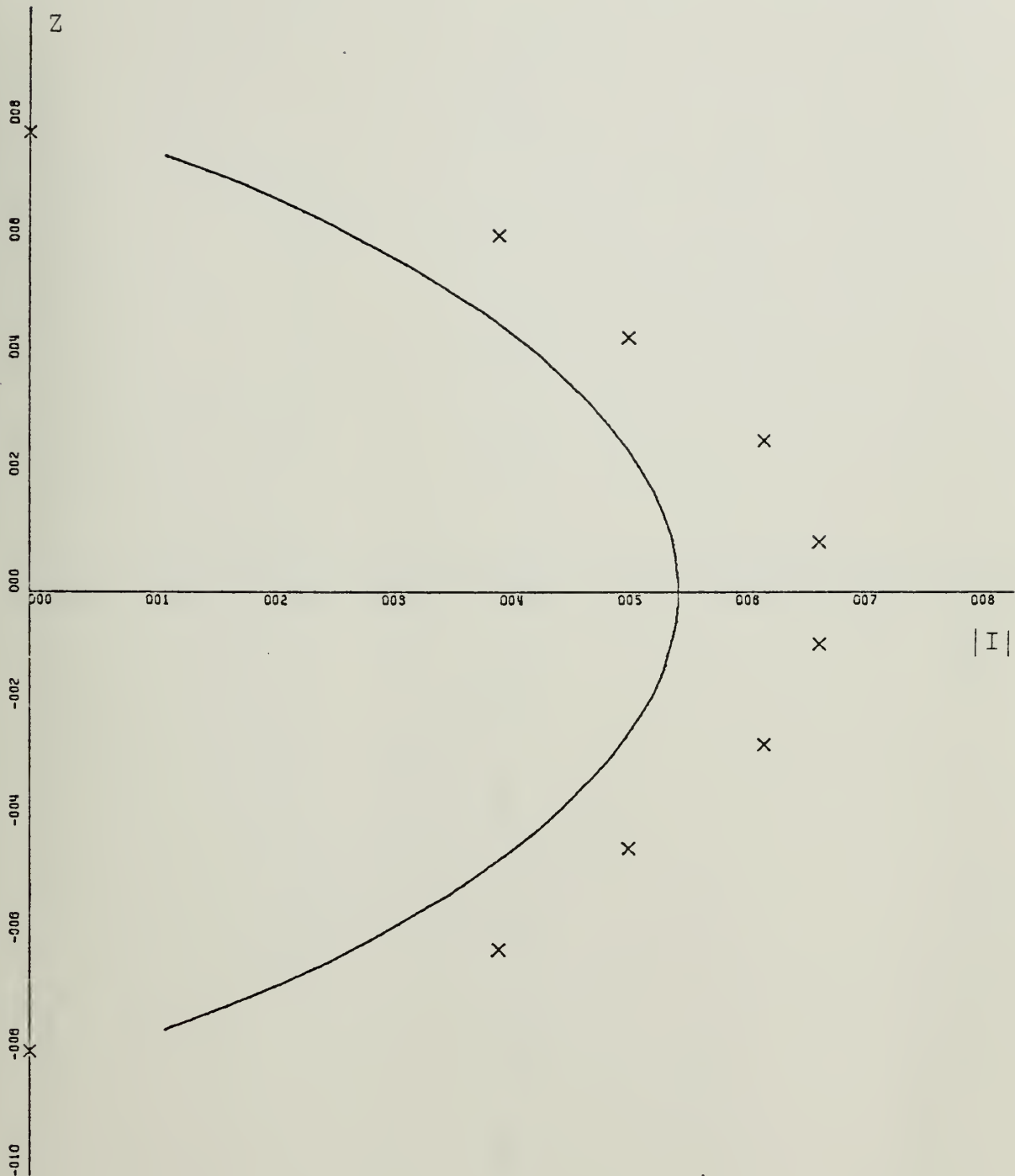
Y-SCALE=5.00E-01 UNITS INCH.

CURRENT MAGNITUDE : FEM/T=SOLID : INT.EQ=X

ZL=.5:AL=0.01:BL=0.0005:ALFA=90:NW=100



X-SCALE=5.00E+01 UNITS INCH.
 Y-SCALE=5.00E-01 UNITS INCH.
 CURRENT PHASE : FEM/T=SOLID : INT.EQ=PLUS
 ZL=.5:AL=0.01:BL=0.0005:ALFA=90:NW=100

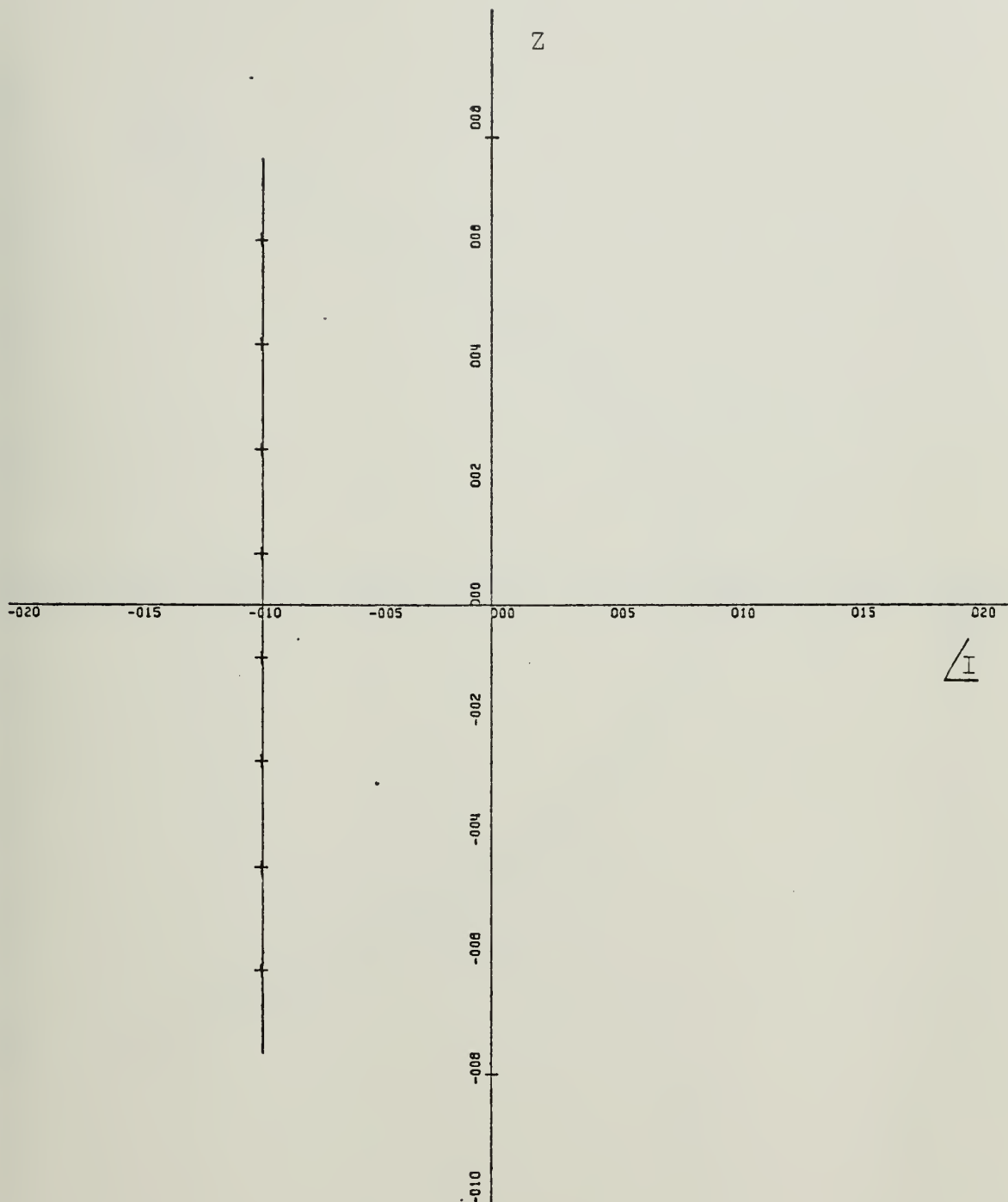


X-SCALE=1.00E-04 UNITS INCH.

Y-SCALE=2.00E-01 UNITS INCH.

CURRENT MAGNITUDE : FEM/T=SOLID : INT.EQ=X

ZL=.25:AL=0.01:BL=0.001:ALFA=90:NW=40

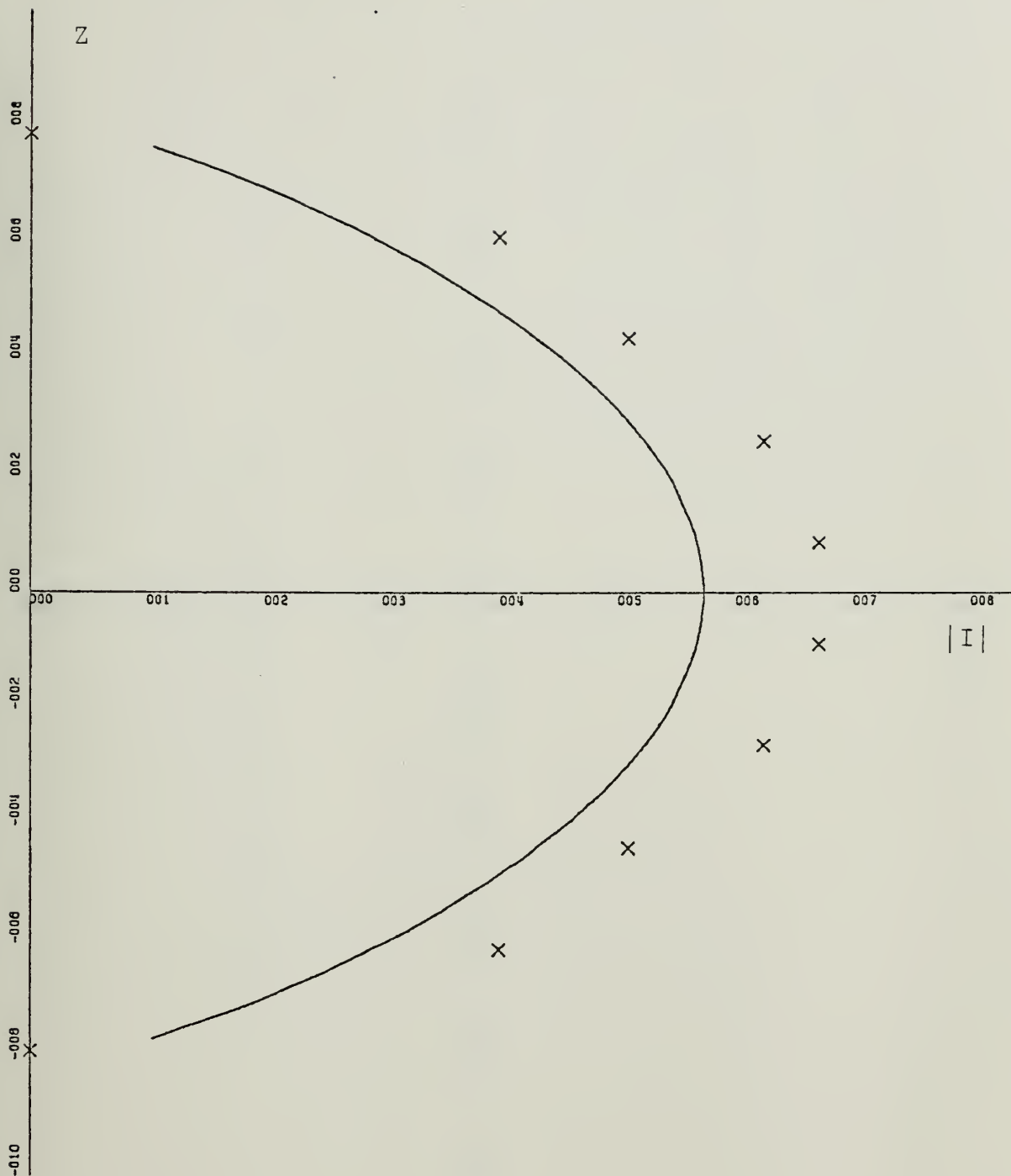


X-SCALE=5.00E+01 UNITS INCH.

Y-SCALE=2.00E-01 UNITS INCH.

CURRENT PHASE : FEM/T=SOLID : INT.EQ=PLUS

ZL=.25:AL=0.01:BL=0.001:ALFA=90:NW=40

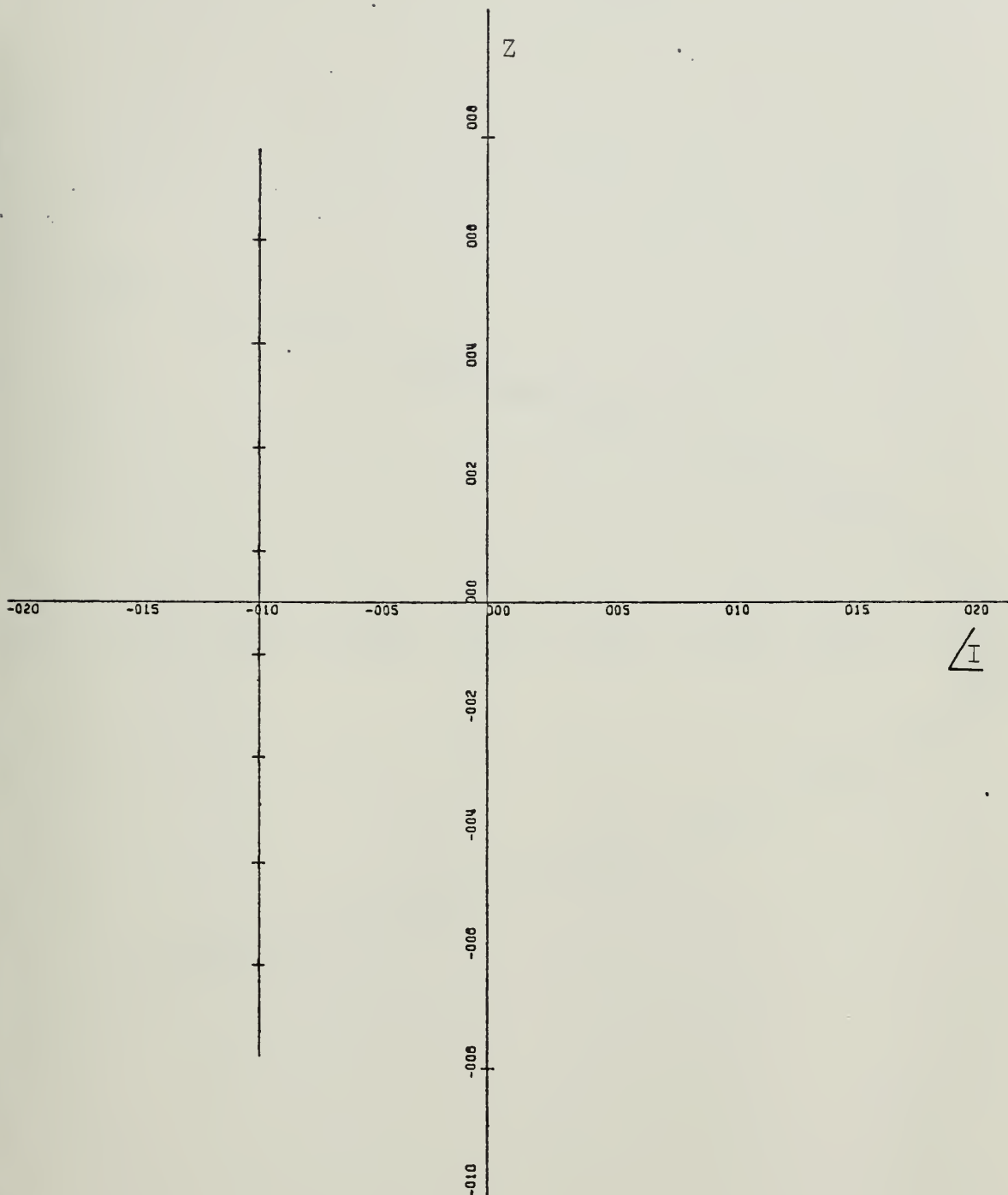


X-SCALE=1.00E-04 UNITS INCH.

Y-SCALE=2.00E-01 UNITS INCH.

CURRENT MAGNITUDE : FEM/T=SOLID : INT.EQ=X

ZL=.25:AL=0.01:BL=0.0005:ALFA=90:NW=70

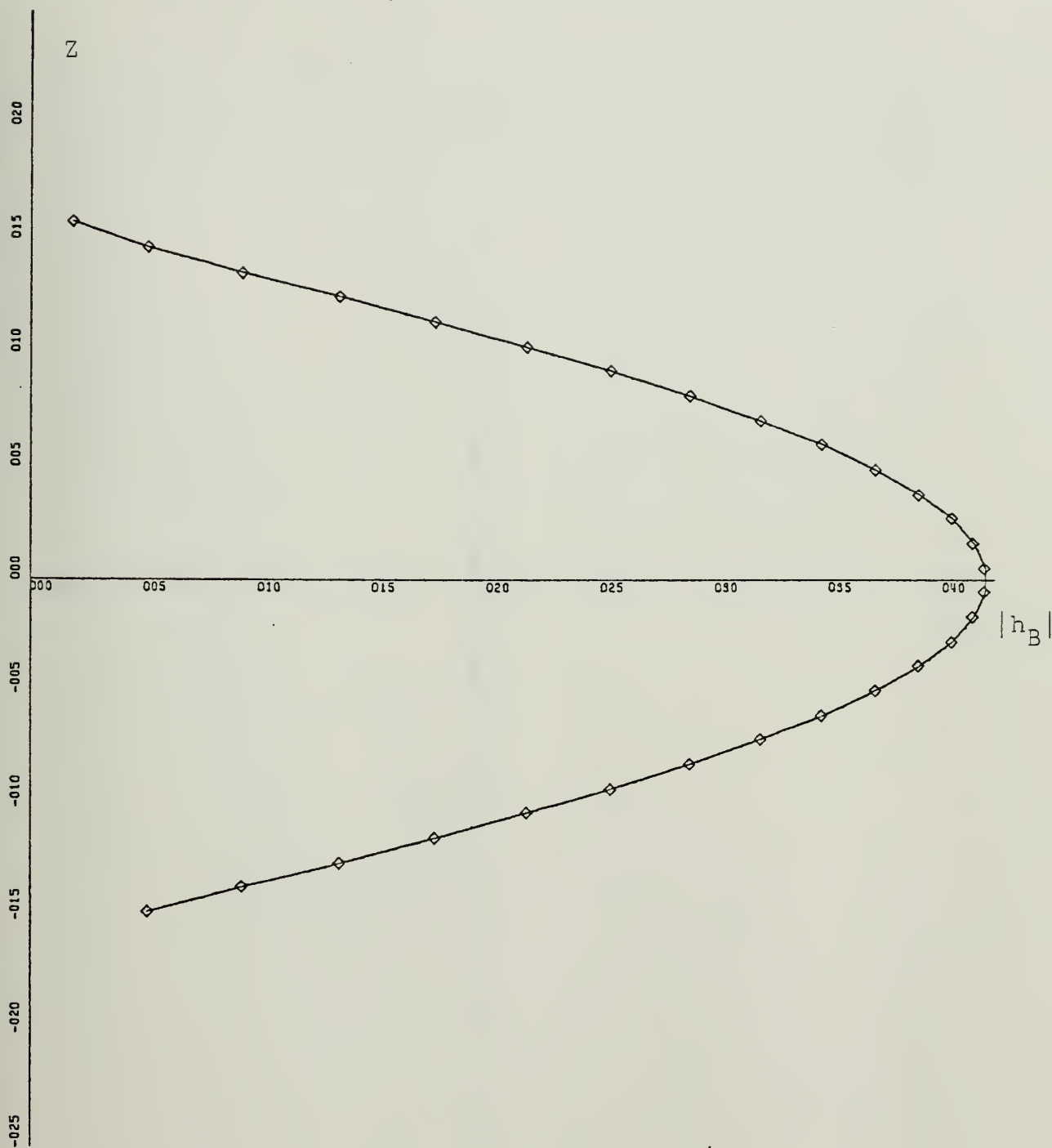


X-SCALE=5.00E+01 UNITS INCH.

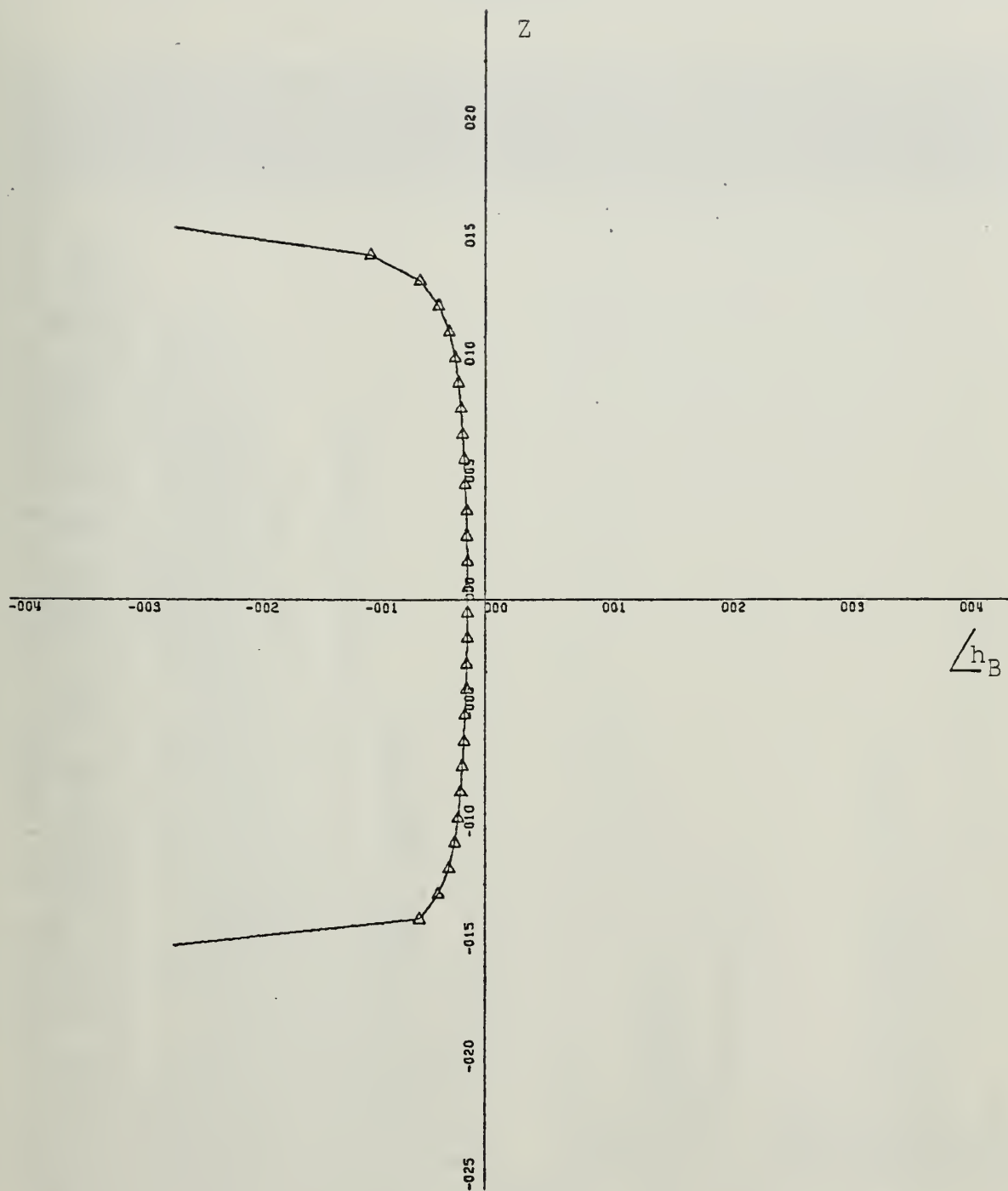
Y-SCALE=2.00E-01 UNITS INCH.

CURRENT PHASE : FEM/T=SOLID : INT.EQ=PLUS

ZL=.25:AL=0.01:BL=0.0005:ALFA=90:NW=70



X-SCALE=5.00E+02 UNITS INCH.
 Y-SCALE=5.00E-01 UNITS INCH.
 BOUNDARY FIELD MAG. : ZL=.5 : DR=DZ/4
 SOLID=EXACT : DIAMONDS=T : AL=1/100



X-SCALE=1.00E+00 UNITS INCH.

Y-SCALE=5.00E-01 UNITS INCH.

BOUNDARY FIELD PHASE : $ZL=.5$: $DR=DZ/4$

SOLID=EXACT : TRIANGLES=T : $AL=1/100$

APPENDIX D

```

CCCCCCCCCCCC
THIS PROGRAM CALCULATES THE INDUCED CURRENT ON A THIN WIRE IN FREE
SPACE DUE TO AN INCIDENT PLANE WAVE. IT USES THE FEM AND THE INTEGRAL
VECTORS POTENTIAL A. IT ALSO FINDS THE CURRENT BY HALLENS INTEGRAL
EQUATION, AND BOTH ARE PLOTTED BY DRAWP (VERSATEC). A ROUTINE TO
CHECK THE T MATRIX (VECTOR POT.) IS INCLUDED BUT MAY BE DELETED
WITH NO HARM.
TO USE, SPECIFY: NO. OF NODES=NW; DIMENSIONS OF ARRAYS:
T(NB,NB), HW(NW), HI(NB), C(NB), A(NW,NW), B(NW,NB), HB(NB), HS(NB),
RP(NW), THETA(NW), ZP(NW), IEX(NW), RPT(NB), ANGLE(NB), RPT(NB),
ANGLE(NB), ZPB(NB), CMAG(NB), CFAT(NB), CMAG(NB) (NB=NW+1)
COMPLEX F30,F21,F12,F20,F11,F10
COMMON/TEN/F30,F21,F12,F20,F11,F10,P30,P21,P12,P20,P11,P10
COMPLEX T(41,41), HW(40), HI(41), C(41), HB(41), HS(41)
REAL RP(40), THETA(40), ZP(40),
1A(40,40), B(40,41), ANGLE1(41), RPT(41), ANGLE(41), ZPB(41),
1IEX(40), RPT(41), ZC(20)
1CMAG(20), CFAT(20), ZC(20)
COMPLEX UINT(3,3), LINT(3,3), DETERM
REAL RTB(28)/23*0.0, R(3), Z(3)
REAL*8 TITLE(12)
INTEGER ITB(12)/12*0/
EQUIVALENCE (TITLE,RTB(5))
MOR = 1
NW = 40
NB = 20
NB = VW+1
ALAM = 1.0/50.0
BLAM = 0.001
ZLAM = 0.5
DR = 5.283185*BLAM
DZ = ZLAM*6.283185/NB
RA = ALAM*6.283185
DO 10 J = 1,NW
ZP(J) = DZ*(2.0*J-NB)/2.0
CONTINUE
R(1) = RA+DR
R(2) = R(1)
R(3) = R(1)
Z(1) = DZ
Z(2) = 2.*DZ
Z(3) = Z(2)
VARELA = FINDS THE ELEMENT INTEGRALS
CALL VARELA (MOR,R,Z,UINT)
R(1) = RA+DR
R(2) = R(1)
R(3) = R(1)
Z(1) = 2.*DZ
Z(2) = DZ

```

10

C


```

C      Z(3) = Z(2)
C      CALL VARELA (MOR,R,Z,LINT)
C      ABLOAD FILLS THE A AND B MATRICES WITH THE ELEMENT INTEGRALS
C      CALL ABLOAD (JINT,LINT,NW,NB,A,B)
C      GFINTE FINDS THE T MATRIX BY GAUSSIAN INTEGRATION OF THE VECTOR
C      POTENTIAL A
C      CALL GFINTE (NW,NB,DR,DZ,RA,T)
C      RM = RA+DR
C      ZL = NB+DZ/2.0
C      THIS ROUTINE FINDS A RADIATED MAGNETIC FIELD (DUE TO A GIVEN
C      SINUSOIDAL CURRENT) THIS FIELD IS TO BE COMPARED TO THE FIELD
C      PRODUCED BY HS=T*IEX
C      CALL HIGEN (RM,DZ,NW,IEX,H3,NB,ZL)
C      HS IS THE SCATTERED FIELD. (T MATRIX TEST)
C      DO 17 I=1,NB
C      HS(I) = (0.0,0.0)
C      DO 25 I = 1,N3
C      DO 30 J = 1,NW
C      HS(I) = HS(I)+T(I,J)*IEX(J)*60.0/ALAM
C      CONTINUE
C      CFORW YIELDS C=-(A+B*T)INV*B
C      CALL CFORM (NW,NB,A,B,T,C,DETERM,COND)
C      DETMAG = CABS(DETERM)
C      DO 77 I = 6,5
C      ALFA = (1.570798/6.0)*I
C      ZCURR CALCULATES THE INCIDENT PLANE WAVE HI AND GIVES HW=C*HI
C      CALL ZCURR (HW,HI,RA,DR,DZ,ALFA,NW,NB,RP,THETA,T)
C      INTEQ IS THE INTEGRAL EQUATION FORMULATION USED FOR COMPARISON
C      CALL INTEQ (ZC,CMAG,CFAZ)
C      DO 20 J = 1,NI
C      ZC(J) = 6.283185*ZC(J)
C      ITB(1) = 1
C      ITB(2) = 1
C      ITB(3) = 9
C      ITB(8) = 2
C      ITB(9) = 5
C      ITB(10) = 0
C      ITB(11) = 0.0
C      READ (5,51) TITLE
C      CALL DRAWP (NI,CMAG,ZC,ITB,RTB)
C      ITB(1) = 3
C      ITB(2) = 0
C      CALL DRAWP (NW,RP,ZP,ITB,RTB)
C      ITB(1) = 1
C      ITB(2) = 2
C      ITB(10) = 2
C      ITB(11) = 4

```

```

FFM00490
FFM00500
FFM00510
FFM00520
FFM00530
FFM00540
FFM00550
FFM00560
FFM00570
FFM00580
FFM00590
FFM00600
FFM00610
FFM00620
FFM00630
FFM00640
FFM00650
FFM00660
FFM00670
FFM00680
FFM00690
FFM00700
FFM00710
FFM00720
FFM00730
FFM00740
FFM00750
FFM00760
FFM00770
FFM00780
FFM00790
FFM00800
FFM00810
FFM00820
FFM00830
FFM00840
FFM00850
FFM00860
FFM00870
FFM00880
FFM00890
FFM00900
FFM00910
FFM00920
FFM00930
FFM00940
FFM00950
FFM00960

```



```

FFM000970
FFM000980
FFM000990
FFM010000
FFM010100
FFM010200
FFM010300
FFM010400
FFM010500
FFM010600
FFM010700
FFM010800
FFM010900
FFM011000
FFM011100
FFM011200
FFM011300
FFM011400
FFM011500
FFM011600
FFM011700
FFM011800
FFM011900
FFM012000
FFM012100
FFM012200
FFM012300
FFM012400
FFM012500
FFM012600
FFM012700
FFM012800
FFM012900
FFM013000
FFM013100
FFM013200
FFM013300
FFM013400
FFM013500
FFM013600
FFM013700
FFM013800
FFM013900
FFM014000
FFM014100
FFM014200
FFM014300
FFM014400

```

```

RTB(1) = 5.00E+01
READ (5,51) TITLE
CALL DRAWP (NI,CF, AZ,ZC,ITB,RTB)
ITB(1) = 3
ITB(2) = 0
CALL DRAWP (NW,THETA,ZP,ITB,RTB)
FORMAT (6A8)
WRITE (6,300) (HI(I),I = 1,NB)
WRITE (6,400) (RP(I),THETA(I),I = 1,NW)
WRITE (6,100) ALAM,NW,DR,DZ,ZLAM,ALFA
FORMAT (10F12.6)
100 1, DZ = ,E12.6, ZLAM = ,E12.6, DR = ,E12.6/
ALFA = ,F7.2)
200 1, WRITE(6,200) DETMAG,COND
FORMAT(10F12.6)
300 1, DETMAG = ,E12.6, COND = ,E12.6)
FORMAT(10F12.6)
400 1, THE INCIDENT FIELD VECTOR IS ,//100( , (E12.6,1X,
1E12.6)/)
400 1, THE POLAR FORM (RP,THETA) OF THE WIRE CURRENT IS
1//100( , (E12.6,2X,E12.6)/)
77 1, CONTINUE
DO 40 I = 1,N3
RP1T(I) = CABS(HB(I))
ANGLE1(I) = ATAN2(AIMAG(HB(I)),REAL(HB(I)))*180.0/3.1415927
CONTINUE
40 1, WRITE (6,500) (RP1T(I),ANGLE1(I),I = 1,N3)
FORMAT (10F12.6)
500 1, THE EXACT BOUNDARY FIELD IS ,//100( , (E12.6,
12X,E12.6)/)
DO 50 I = 1,N3
RP1T(I) = CABS(HS(I))
ANGLE1(I) = ATAN2(AIMAG(HS(I)),REAL(HS(I)))*180.0/3.1415927
CONTINUE
50 1, WRITE (6,600) (RP1T(I),ANGLE1(I),I = 1,N3)
FORMAT (10F12.6)
600 1, THE T MATRIX FIELD IS (RP,ANGLE) //100( , (E12.6,2X,
1E12.6)/)
DO 60 I = 1,N3
ZPB(I) = DZ*(2.0*I-NB)/2.0
ITB(1) = 1
ITB(2) = 0
ITB(8) = 2
ITB(9) = 5
ITB(10) = 0
60 1, READ (5,51) TITLE
CALL DRAWP (NB,RP1T,ZPB,ITB,RTB)
ITB(1) = 3
ITB(2) = 4
CALL DRAWP(NB,RP1T,ZPB,ITB,RTB)
ITB(1) = 1
ITB(2) = 0
ITB(8) = 2

```



```

DO 7 L = 1, NW
T(K,L) = (0.0, 0.0)
CONTINUE
RM = RA + DR

```

7 5

```

W(1) = 0.36268378
W(2) = 0.31370665
W(3) = 0.22238103
W(4) = 0.10122854
X(1) = 0.18343464
X(2) = 0.52553241
X(3) = 0.79666648
X(4) = 0.96023986

```

```

DO 10 I = 1, NB
DO 20 V = 1, NW
F10 = (0.0, 0.0)
F20 = (0.0, 0.0)

```

```

DO 30 VG = 1, 4
LF11 = F1 (X(NG), N, M, NW, DR, DZ, RA)
LF12 = F1 (-X(NG), N, M, NW, DR, DZ, RA)
LF21 = F2 (X(NG), N, M, NW, DR, DZ, RA)
LF22 = F2 (-X(NG), N, M, NW, DR, DZ, RA)
F10 = F10 + W(NG) * (LF11 + LF12)
F20 = F20 + W(NG) * (LF21 + LF22)

```

30 20 10

```

CONTINUE
T(M,V) = 0.5 * RA * RM * (F10 + F20)
CONTINUE
CONTINUE
RETURN
END

```

C

```

FUNCTION F1(X, V, M, NW, DR, DZ, RA)
COMPLEX F1, EJR, GMZ
WZ = (X + 1.) / 2. * V - NW - 3. / 2.
ZNM1 = DZ * (2. * M - NW - 1.) / 2.
ZM = ZNM1 + DZ * WZ
ZX = ZNM1 + DR
RM = RA + DR
RMZ = SQRT((ZX - ZM) * 2 + RM * RM)
EJR = CMPLX(COS(RMZ), -SIN(RMZ))
GMZ = EJR * CMPLX(1. / RMZ, 1.) / (RMZ * RMZ)
F1 = DZ * WZ * GMZ / 2.
RETURN
END

```

C

```

FUNCTION F2(X, V, M, NW, DR, DZ, RA)
COMPLEX F2, EJR, GMZ
WZ = (1. - X) / 2.

```

FFM01920
FFM01930
FFM01940
FFM01950
FFM01960
FFM01970
FFM01980
FFM01990
FFM02000
FFM02010
FFM02020
FFM02030
FFM02040
FFM02050
FFM02060
FFM02070
FFM02080
FFM02090
FFM02100
FFM02110
FFM02120
FFM02130
FFM02140
FFM02150
FFM02160
FFM02170
FFM02180
FFM02190
FFM02200
FFM02210
FFM02220
FFM02230
FFM02240
FFM02250
FFM02260
FFM02270
FFM02280
FFM02290
FFM02300
FFM02310
FFM02320
FFM02330
FFM02340
FFM02350
FFM02360
FFM02370
FFM02380
FFM02390


```

ZN = DZ*(2.*N-NW-1.)/2.
ZM = DZ*(2.*M-NW-1.)/2.
RM = ZN+DR
ZX = ZN+DZ*(X+1.)/2.
RMZ = SQRT((ZX-ZM)**2+RM*RM)
EJR = CMPLX(CJS(RMZ),-SIN(RMZ))
GMZ = EJR*CMPLX(1./RMZ,1.)/(RMZ*RMZ)
F2 = DZ*WZ*GMZ/2.
RETURN
END

```

CC

```

SUBROUTINE CF3RM (NW,NB,A,B,T,C,DETERM,COND)
TO SAVE CORE,T IS USED AS A WORKING SPACE. MATRIX MULTIPLICATION
IS DONE USING ONE ROW (COLJMN) OF T AT A TIME. RESULTS ARE STORED
IN C, THEN PUT IN THE NO LONGER NEEDED ROW (COLUMN) OF T
COMPLEX T(NB,V3),C(NB),DETERM
REAL A(NW,NW),B(NW,NB)
DO 50 J = 1,NW
DO 1 K = 1,NW
C(K) = (0.0,0.0)
DO 30 I = 1,NW
DO 30 L = 1,N3
C(I) = C(I)+B(I,L)*T(L,J)
DO 40 K = 1,NW
T(K,J) = C(K)
CONTINUE
DO 60 I = 1,NW
DO 70 J = 1,NW
T(I,J) = A(I,J)+T(I,J)
CONTINUE
CALL CSMINV (T,NB,NW,DETERM,COND,0)
T IS NOW THE INVERSE OF T IN LINE 14
DO 90 J = 1,NW
DO 2 K = 1,NB
C(K) = (0.0,0.0)
DO 80 I = 1,N3
C(I) = C(I)-T(J,L)*B(L,I)
DO 85 K = 1,N3
T(J,K) = C(K)
CONTINUE
RETURN
END

```

CC

1

30

40

50

70

60

C

2

80

85

90

CC

FFM02400
FFM02410
FFM02420
FFM02430
FFM02440
FFM02450
FFM02460
FFM02470
FFM02480
FFM02490
FFM02500
FFM02510
FFM02520
FFM02530
FFM02540
FFM02550
FFM02560
FFM02570
FFM02575
FFM02580
FFM02590
FFM02600
FFM02610
FFM02620
FFM02630
FFM02640
FFM02650
FFM02660
FFM02670
FFM02680
FFM02690
FFM02700
FFM02710
FFM02720
FFM02730
FFM02740
FFM02750
FFM02760
FFM02770
FFM02780
FFM02790
FFM02800
FFM02810
FFM02820
FFM02830
FFM02840
FFM02850
FFM02860

C

```

SUBROUTINE ZCURR (HW,HI,RA,DR,DZ,ALFA,VW,NB,RP,THETA,T)
COMPLEX T(VB,V3),HW(NW),HI(NB),ALFDEP
REAL RP(NW),THETA(NW)
DO 10 I = 1,NW
  HW(I) = (0.0,0.0)
CONTINUE

```

10

```

RM = RA+DR
X = RM*SIN(ALFA)
ADJO = -0.5*X*(1./16.)*X**3-(1./384.)*X**5
DO 20 I = 1,N3
  ZNB = DZ*(2.*I-NB)/2.0
  ZC = ZNB*COS(ALFA)
  ALFDEP = CMPLX(SIN(ZC),COS(ZC))
  HI(I) = ALFDEP*ADJO
CONTINUE

```

20

```

DO 30 I = 1,NW
  DO 40 J = 1,N3
    HW(I)+T(I,J)*HI(J)
CONTINUE

```

40
30

```

DO 50 I = 1,NW
  RP(I) = CABS(HW(I))*RA/(120.0*3.1415927)
  THETA(I) = ATAN2(AIMAG(HW(I)),REAL(HW(I)))*180.0/3.1415927
CONTINUE
RETURN
END

```

50

C

C

C

C

C

```

SUBROUTINE CS1INV (A,NDIM,N,DETERM,CJND,INORM)
  INORM = FLAG TO NORMALIZE COLUMNS AND ROWS OF MATRIX A
  MATRIX NORMALIZATION BY M.A. MORGAN
COMPLEX A(NDIM,NDIM),PIVOT(100),AMAX,T,SWAP,DETERM,U
INTEGER IPIVOT(100),INDEX(100,2)
REAL TEMP,ALPHA(100),COL(100),ROW(100)
IF (INORM.NE.1) GO TO 7
DO 3 K=1,N
  COL(K)=0.0
DO 1 J=1,N
  A(J,K)=A(J,K) COL(K)=AJK
IF(AJK.GT.COL(K)) COL(K)=AJK
CONTINUE
DO 2 J=1,N
  A(J,<)=A(J,<)/COL(K)
CONTINUE
ROW VORMALIZING
DO 6 J=1,N

```

1

2
3

C

```

FFM02870
FFM02880
FFM02890
FFM02900
FFM02910
FFM02920
FFM02930
FFM02940
FFM02950
FFM02960
FFM02970
FFM02980
FFM02990
FFM03000
FFM03010
FFM03020
FFM03030
FFM03040
FFM03050
FFM03060
FFM03070
FFM03080
FFM03090
FFM03100
FFM03110
FFM03120
FFM03130
FFM03140
FFM03150
FFM03160
FFM03170
FFM03180
FFM03190
FFM03200
FFM03210
FFM03220
FFM03230
FFM03240
FFM03250
FFM03260
FFM03270
FFM03280
FFM03290
FFM03300
FFM03310
FFM03320
FFM03330
FFM03340

```



```

FFM03350
FFM03360
FFM03370
FFM03380
FFM03390
FFM03400
FFM03410
FFM03420
FFM03430
FFM03440
FFM03450
FFM03460
FFM03470
FFM03480
FFM03490
FFM03500
FFM03510
FFM03520
FFM03530
FFM03540
FFM03550
FFM03560
FFM03570
FFM03580
FFM03590
FFM03600
FFM03610
FFM03620
FFM03630
FFM03640
FFM03650
FFM03660
FFM03670
FFM03680
FFM03690
FFM03700
FFM03710
FFM03720
FFM03730
FFM03740
FFM03750
FFM03760
FFM03770
FFM03780
FFM03790
FFM03800
FFM03810
FFM03820

```

```

      ROW(J)=0.0
      DO 4 K=1,N
        AJK=CABS(A(J,K))
        IF(AJK.GT.ROW(J)) ROW(J)=AJK
      CONTINUE
      DO 5 K=1,N
        A(J,K)=A(J,K)/ROW(J)
      CONTINUE
      DETERM = CMP_X(1.0,0.0)
      SUMAXA=0.
      DO 20 J=1,N
        ALPHA(J)=0.0
        SUMR3W=0.
        DO 10 I=1,N
          ALPHA(J)=ALPHA(J)+A(J,I)* CONJG(A(J,I))
          SUMR3W=SUMR3W + CABS(A(J,I))
        ALPH3W=SUMR3W
        IF(SUMR3W.GT.SJMAXA) SUMAXA=SUMR3W
        IPIVOT(J)=0
        DO 60 I=1,N
          AMAX=CPLX(0.0,0.0)
          DO 105 J=1,N
            IF (IPIVOT(J)-1) 60, 105, 60
            IF (IPIVOT(K)-1) 80, 100, 740
            TEMP=AMAX* CONJG(AMAX)-A(J,K)* CONJG(A(J,K))
            IF(TEMP) 85, 85, 100
            IROW=J
            ICOL=K
            AMAX=A(J,K)
          CONTINUE
          IPIVOT(ICOL)=IPIVOT(ICOL)+1
          IF (IROW-ICOL) 140, 260, 140
          DETERM=-DETERM
          DO 200 L=1,N
            SWAP=A(IROW,L)
            A(IROW,L)=A(ICOL,L)
            A(ICOL,L)=SWAP
            SWAP=ALPHA(IROW)
            ALPHA(IROW)=ALPHA(ICOL)
            ALPHA(ICOL)=SWAP
            INDEX(I,1)=IROW
            INDEX(I,2)=ICOL
            IPIVOT(I)=A(ICOL,I)
            U = IPIVOT(I)
            DETERM = DETERM*U

```



```

DETERM=DETERM/ALPHA(ICOLUMN)
TEMP=PIVOT(I)*CONJG(PIVOT(I))
IF(TEMP)330,720,330
330 A(ICOLUMN,ICOLUMN)=CMPLX(1.0,0.0)
DO 350 L=1,N
U=PIVOT(I)
350 A(ICOLUMN,L)=A(ICOLUMN,L)/J
380 DO 550 LI=1,N
IF(LI-ICOLUMN)400,550,400
400 T=A(LI,ICOLUMN)
A(LI,ICOLUMN)=CMPLX(0.0,0.0)
DO 450 L=1,N
U=A(ICOLUMN,-)
450 A(LI,L)=A(LI,L)-U*T
550 CONTINUE
600 CONTINUE
620 DO 710 I=1,N
L=N+1-INDEX(L,1)-INDEX(L,2) 630, 710, 630
IF (INDEX(L,1))
630 JROW=INDEX(L,1)
JCOLUMN=INDEX(-,2)
DO 705 K=1,N
SWAP=A(K,JROW)
A(K,JROW)=A(K,JCOLUMN)
A(K,JCOLUMN)=SWAP
705 CONTINUE
710 CONTINUE
SUMAXI=0.
DO 910 I=1,N
SUMROW=0.
DO 900 J=1,N
SUMROW=SUMROW+CABS(A(I,J))
900 SUMROW=SUMROW.GT.SUMAXI SUMAXI=SUMROW
910 CONTINUE
COND=SUMAXA*SUMAXI
IF(INORM.NE.1) GO TO 955
DO 950 K=1,N
DO 950 J=1,N
950 A(J,K)=A(J,K)/(ROW(K)*COL(J))
955 CONTINUE
WRITE(6,730)
720 FORMAT('0',10('*****'),'0',10('*****'))
730 RETURN
740 RETURN
END
C
C
C

```



```

SUBROUTINE VARELA (MOR,X,Y,H2)
COMPL=X/F30,F21,F12,F20,F11,F10
COMMON/TEN/F30,F21,F12,F20,F11,F10,P30,P21,P12,P20,P11,P10
COMPLEX H2(3,3),A(3,3),C2
REAL T(3,3),X(3),Y(3)
C2=(1.0,0.0)
RM=0.0
Q=((X(3)*Y(3)+X(3)*Y(1)+X(1)*Y(2))
1  -((X(3)*Y(2)+X(1)*Y(3)+X(2)*Y(1)))/2.0
T(1,1)=Y(2)-Y(3)
T(1,2)=Y(3)-Y(1)
T(1,3)=Y(1)-Y(2)
T(2,1)=X(3)-X(2)
T(2,2)=X(1)-X(3)
T(2,3)=X(2)-X(1)
T(3,1)=X(2)*Y(3)-X(3)*Y(2)
T(3,2)=X(3)*Y(1)-X(1)*Y(3)
T(3,3)=X(1)*Y(2)-X(2)*Y(1)
DO 1 J=1,3
DO 1 K=1,3
1  T(J,K)=T(J,K)/(2.0*Q)
CALL ARINT (RM,C2,X,Y,MOR)
A(1,1)=4.*F30-P30
A(2,2)=F30+F12-P12
A(3,3)=F10-P10
A(2,1)=2.*F21-P21
A(1,2)=A(2,1)
A(3,1)=2.*F20-P20
A(1,3)=A(3,1)
A(3,2)=F11-P11
A(2,3)=A(3,2)
DO 5 KND=1,3
DO 3 K=1,3
H2(KND,K)=(0.,0.)
DO 2 L=1,3
DO 2 J=1,3
H2(KND,K)=H2(KND,K)+T(J,KND)*A(J,L)*T(L,K)
2  CONTINUE
3  CONTINUE
5  RETURN
END
C
SUBROUTINE ARINT (RM,C2,X,Y,MOR)
COMPLEX F30,F21,F12,F20,F11,F10
COMMON/TEN/F30,F21,F12,F20,F11,F10,P30,P21,P12,P20,P11,P10
COMPLEX F(4),C2,CSR
REAL X(3),Y(3),X1(3),X2(3),Y1(3),Y2(3),P(4)

```

```

FFM04310
FFM04320
FFM04330
FFM04340
FFM04350
FFM04360
FFM04370
FFM04380
FFM04390
FFM04400
FFM04410
FFM04420
FFM04430
FFM04440
FFM04450
FFM04460
FFM04470
FFM04480
FFM04490
FFM04500
FFM04510
FFM04520
FFM04530
FFM04540
FFM04550
FFM04560
FFM04570
FFM04580
FFM04590
FFM04600
FFM04610
FFM04620
FFM04630
FFM04640
FFM04650
FFM04660
FFM04670
FFM04680
FFM04690
FFM04700
FFM04710
FFM04720
FFM04730
FFM04740
FFM04750
FFM04760
FFM04770
FFM04780

```



```

RM2=RM#RM
C=CS2(C2)
X1(3)=X(1)
X2(2)=X(1)
Y1(3)=Y(1)
Y2(2)=Y(1)
X1(1)=X(2)
X2(3)=X(2)
Y1(1)=Y(2)
Y2(3)=Y(2)
X1(2)=X(3)
X2(1)=X(3)
Y1(2)=Y(3)
Y2(1)=Y(3)
DI=1.0-2.*MOR
P30=0.0
P21=0.
P12=0.
P20=0.
P11=0.
P10=0.
F30=(0.,0.)
F21=(0.,0.)
F12=(0.,0.)
F20=(0.,0.)
F11=(0.,0.)
F10=(0.,0.)
DO 33 L=1,3
CHANGES 8/15/78 TO HANDLE DEC 10 ROUND OFF
XS=X2(L)+X1(L)
IF(XS.LT.1.0E-4) GO TO 22
DX=X2(L)-X1(L)
DY=Y2(L)-Y1(L)
IF(ABS(DX/XS).LT.1.0E-5) GO TO 22
A=DY/DX
B=Y1(L)-A*X1(L)
A2=A*A
A3=A*A2
B2=B*B
B3=B*B2
CALL LININT (RM, RM2, C, C2, X1(L), X2(L), F, P)
P30=P30+DI*(A*(4)+B*(3))
P30=P30+DI*(A*(4)+B*(3))
P21=P21+DI*(A2*(4)+2*A*B*(3)+B2*(2))/2.
P21=P21+DI*(A2*(4)+2*A*B*(3)+B2*(2))/2.
P12=P12+DI*(A3*(4)+3*A2*B*(3)+3*A*B2*(2)+B3*(1))/3.
P12=P12+DI*(A3*(4)+3*A2*B*(3)+3*A*B2*(2)+B3*(1))/3.
P20=P20+DI*(A*(3)+B*(2))

```

C

```

FFM04790
FFM04800
FFM04810
FFM04820
FFM04830
FFM04840
FFM04850
FFM04860
FFM04870
FFM04880
FFM04890
FFM04900
FFM04910
FFM04920
FFM04930
FFM04940
FFM04950
FFM04960
FFM04970
FFM04980
FFM04990
FFM05000
FFM05010
FFM05020
FFM05030
FFM05040
FFM05050
FFM05060
FFM05070
FFM05080
FFM05090
FFM05100
FFM05110
FFM05120
FFM05130
FFM05140
FFM05150
FFM05160
FFM05170
FFM05180
FFM05190
FFM05200
FFM05210
FFM05220
FFM05230
FFM05240
FFM05250
FFM05260

```



```

F20=F20+DI*(A*(3)+B*F(2))
P11=P11+DI*(A2*P(3)+2*A*B*P(2)+B2*P(1))/2.
F11=F11+DI*(A2*F(3)+2*A*B*F(2)+B2*F(1))/2.
P10=P10+DI*(A*P(2)+B*P(1))
F10=F10+DI*(A*F(2)+B*F(1))
22 CONTINUE
33 RETURN
END

```

C

```

SUBROUTINE LININT (RM,RM2,C,C2,XS,XF,F,P)
REAL P(4)
COMPLEX C,C2,Z1,Z2,W1,W2,CLN,F0,F(4),D1,D2,CM,CM2
CM=CMPLX(RM,0.0)
CM2=CMPLX(RM2,0.0)
XSK=XS
XFK=XF

```

```

11 DO 11,4
   AK=FLDAT(K+1)
   XSK=XS*XSK
   XFK=XF*XFK
   P(K)=(XFK-XSK)/AK

```

11

```

   W1=C*XS+CM
   W2=C*XF+CM
   Z1=C*XS-CM
   Z2=C*XF-CM
   IF(RM.GT.0.1)G3 TO 22
   IF(CABS(Z1).GT.1.0E-5) G3 TO 13
   Z1=(1.0,0.0)
   W1=(1.0,0.0)
   IF(CABS(Z2).GT.1.0E-5) G3 TO 22
   Z2=(1.0,0.0)

```

13

```

22 CONTINUE
   D1=CLN(Z2)-CLN(Z1)
   D2=CLN(W2)-CLN(W1)
   F0=0.5*(D1-D2)/C
   F(1)=0.5*(D1+D2)/C2
   F(2)=(XF-XS)+i*W*F0/C2
   F(3)=(P(1)+CM2*F(1))/C2
   F(4)=(P(2)+CM2*F(2))/C2
RETURN
END

```

```

FUNCTION CSR(Z)

```

C

```

COMPLEX CSR,Z
R=CABS(Z)
P=0.5*ATAN2(AIMAG(Z),REAL(Z))

```

```

FFM05270
FFM05280
FFM05290
FFM05300
FFM05310
FFM05320
FFM05330
FFM05340
FFM05350
FFM05360
FFM05370
FFM05380
FFM05390
FFM05400
FFM05410
FFM05420
FFM05430
FFM05440
FFM05450
FFM05460
FFM05470
FFM05480
FFM05490
FFM05500
FFM05510
FFM05520
FFM05530
FFM05540
FFM05550
FFM05560
FFM05570
FFM05580
FFM05590
FFM05600
FFM05610
FFM05620
FFM05630
FFM05640
FFM05650
FFM05660
FFM05670
FFM05680
FFM05690
FFM05700
FFM05710
FFM05720
FFM05730
FFM05740

```



```

CSR=SQRT(R)*CMPLX(COS(P),SIN(P))
RETURN
END
C
FUNCTION CLN(Z)
COMPLEX CLN,Z
ZR=REAL(Z)
ZI=AIMAG(Z)
ZABS=SQRT(ZR*ZR+ZI*ZI)
R=ALOG(ZABS)
FI=-1.0*ARCCOS(ZR/ZABS)
CLN=CMPLX(R,FI)
RETURN
END
C
SUBROUTINE INTEQ (Z,CMAG,CFAZ)
HALLENS I.E. SOLN OF THIN-WIRE SCATTERING
ASSUMING INCEZ=1 V/M
NWIRE=NO WIRE PTS WITH ENDS
FREQ=MHZ
ZLEN=WIRE LENGTH (M)
RAD=WIRE RADIUS (M)
ZBOT=Z AT WIRE BOTTOM (M)
NINC=NO INC FLDS
DALPHA=ARRAY OF INC ANGLES (DEG) WITH EZ=EO SIN(ALPHA)
COMPLEX A(20),U(20),Z(20),C,D,E
REAL DALPHA(1),Z(20),CMAG(20),CFAZ(20)
FORMAT(2I5)
READ(5,100) NWIRE,NINC
READ(5,101) FREQ,ZLEN,RAD,ZBOT
READ(5,101) (DALPHA(I),I=1,NINC)
FORMAT(5F10.3)
PI=3.1415927
DTR=PI/180.
RTD=180./PI
DZ=ZLEN/(NWIRE-1.)
WL=300./FREQ
WN=2.*PI/WL
WRITE(6,102) NWIRE,NINC,FREQ,ZLEN,RAD,ZBOT,WL
FORMAT(1INWIRE,NINC,FREQ,ZLEN,RAD,ZBOT,WL:.,/,.,2I6,5F9.3)
CALL TWMAT(NWIRE,RAD,ZBOT,ZLEN,WL,A)
INC FLD LOOP
DO 44 I=1,NINC
DALPHA(I)
WRITE(6,103) DALPHA(I)
FORMAT(10INC ALPHA (DEG):.,F10.3,/)
CHANGE ALPHA TO CORRESPOND TO MAIN PROGRAM
C
100
101
102
C
103

```

```

FFM05750
FFM05760
FFM05770
FFM05780
FFM05790
FFM05800
FFM05810
FFM05820
FFM05830
FFM05840
FFM05850
FFM05860
FFM05870
FFM05880
FFM05890
FFM05900
FFM05910
FFM05920
FFM05930
FFM05940
FFM05950
FFM05960
FFM05970
FFM05980
FFM05990
FFM06000
FFM06010
FFM06020
FFM06030
FFM06040
FFM06050
FFM06060
FFM06070
FFM06080
FFM06090
FFM06100
FFM06110
FFM06120
FFM06130
FFM06140
FFM06150
FFM06160
FFM06170
FFM06180
FFM06190
FFM06200
FFM06210
FFM06220

```



```

11      ALPHA(I) = 180.0-DALPHA(I)
      ALPHA=DTX*ALPHA(I)
      CA=CCS(ALPHA)
      SA=SV(ALPHA)
      DO 11 N=1,NWIRE
      Z(N)=ZBOT+(N-1)*DZ
      ERE=CCS(WN*CA*Z(N))
      EIM=SV(WN*CA*Z(N))
      U(N)=CMPLX(-EIM,ERE)/(377.*WN*SA)
      DO 22 N=1,NWIRE
      ZI(N)=(0.,0.)
      DO 22 M=1,NWIRE
      ZI(N)=ZI(N)+A(N,M)*U(M)
      WRITE(6,104) ZI(1),ZI(NWIRE)
104      FORMAT(10C AND D: ',4E14.6,/' ON,Z,RE(I),IM(I),MAG(I),DEG(I):',/)
      ZI(1)=(0.,0.)
      ZI(NWIRE)=(0.,0.)
      DO 33 N=1,NWIRE
      CMAG(N)=ABS(ZI(N))
      CFZ(N)=0.0
      IF(CMAG(N).LT.1.E-15) GO TO 32
      CFZ(N)=RTD*ATAN2(AIMAG(ZI(N)),REAL(ZI(N)))
      CONTINUE
      WRITE(5,105) N,Z(N),ZI(N),CMAG(N),CFZ(N)
105      FORMAT(' ',I7,=10.3,3E14.6,F10.3)
33      CONTINUE
44      RETURN
      DEBUG SUBCHK
      END

C      SUBROUTINE TWMAT(NX,RA,Z1,XL,XWAVE,TW)
      COMPLEX TW(20,20),G(20),DET
      REAL X(20)
      NMX = 20
      N1=NX-1
      GENERATE N+2 NODES ON WIRE WITH Z1 AS FIRST NODE
      AND INCREMENTS OF 1/(N+1)
      DO 1 I=1,NX
      X(I)=Z1+(I-1)*XL/(NX-1)
      P=XL/(NX-1)/3.
      Q=P/2.
      XKO=2*3.141593/XWAVE
      LOAD T=EC,D CJEFFICIENT TERMS
      DO 2 I=1,NX
      THETA=XKO*X(I)
      TW(I,1)=SIN(THETA)
      TW(I,NX)=COS(THETA)

```

```

FFM06230
FFM06240
FFM06250
FFM06260
FFM06270
FFM06280
FFM06290
FFM06300
FFM06310
FFM06320
FFM06330
FFM06340
FFM06350
FFM06360
FFM06370
FFM06380
FFM06390
FFM06400
FFM06410
FFM06420
FFM06430
FFM06440
FFM06450
FFM06460
FFM06470
FFM06480
FFM06490
FFM06500
FFM06510
FFM06520
FFM06530
FFM06540
FFM06550
FFM06560
FFM06570
FFM06580
FFM06590
FFM06600
FFM06610
FFM06620
FFM06630
FFM06640
FFM06650
FFM06660
FFM06670
FFM06680
FFM06690
FFM06700

```



```

2      C
CONTINUE
LOAD REST OF COEFFICIENTS
DO 3 I=1,NX
CALL GKRL(G,X,XKO,RA,NX,I)
DO 4 I=2,N1
TW(I,I)=QG(I1-1)+2*P*G(I1)+2*G(I1+1)
CONTINUE
CONTINUE
INVERT THE IMP MATRIX
INORM=1
CALL CSINV(TW,NMX,NX,DET,COND,INORM)
DMAG=CABS(DET)
WRITE(6,110) DMAG,COND
110  FORMAT('OZWMAT DET AND COND:',2E11.3,/)
RETURN
DEBUG SUBCHK
END

C
SUBROUTINE GKRL(G,X,XKO,RA,NX,M)
REAL X(NX)
COMPLEX G(NX)
PI=3.1415927
XM=X(M)
DO 11 N=1,NX
XN=X(N)
R=SQRT((XV-XM)*(XN-XM)+RA*RA)
FORMAT(10X,E12.4)
C=CJS(XKO*R)
S=-1.*SIN(XKO*R)
G(N)=CMPLX(C,S)/(4.0*PI*R)
CONTINUE
RETURN
END

11
C
C
C
SUBROUTINE HISEV (RM,DZ,NW,IEX,HB,NB,ZL)
COMPLEX HR(NB)
REAL IEX(NW)
DO 10 I=1,NW
ZNW = DZ*(2.0*I-NB)/2.0
IEX(I) = SIN(ZL+ZNW)
IF(ZNW.GT.0.0) IEX(I) = SIN(ZL-ZNW)
CONTINUE
DO 20 I=1,N3
ZNB = DZ*(2.0*I-NB)/2.0
RK = SQRT(ZNB*ZNB+RM*RM)
RK = SQRT((ZNB-ZL)**2+RM*RM)

```

```

FFM06710
FFM06720
FFM06730
FFM06740
FFM06750
FFM06760
FFM06770
FFM06780
FFM06790
FFM06800
FFM06810
FFM06820
FFM06830
FFM06840
FFM06850
FFM06860
FFM06870
FFM06880
FFM06890
FFM06900
FFM06910
FFM06920
FFM06930
FFM06940
FFM06950
FFM06960
FFM06970
FFM06980
FFM06990
FFM07000
FFM07010
FFM07020
FFM07030
FFM07040
FFM07050
FFM07060
FFM07070
FFM07080
FFM07090
FFM07100
FFM07110
FFM07120
FFM07130
FFM07140
FFM07150
FFM07160
FFM07170
FFM07180

```



```

R2K = SQRT((ZNB+ZL)**2+RM*RM)
APART = SIN(R1K)+SIN(R2K)-2.*SIN(RK)*CJS(ZL)
BPART = COS(R1K)+COS(R2K)-2.*COS(RK)*CJS(ZL)
HB(I) = ((30.0*5.283185/RM)*CMPLX(APART, BPART)
20 CONTINUE
    RETURN
    END
/*
C //GO.PLOT PARM DD *
  &PLOT SCALE = 0.7, YSTART = 2.0, STRIPO=2.0 $END
C //GO.SV SIN DD *
  20 I 0.5 0.02 -.25
  300.0
  90.0
  CURRENT MAGNITUDE : FEM/T=SOLID : INT.EQ=X
  ZL=.5:AL=0.02:BL=0.001:ALFA=90:NW=40
  CURRENT PHASE : FEM/T=SOLID : INT.EQ=PLUS
  ZL=.5:AL=0.02:BL=0.001:ALFA=90:NW=40
  WIRE CURRENT MAGNITUDE:AL=.02:BL=.001
  SOLID = EXACT PHASE : DIAMONDS = FEM : NW=40
  WIRE CURRENT PHASE : ZL=.5 : RL=0.001
  CROSSES = EXACT PHASE : TRIANGLES = FEM : NW=40
  BOUNDARY FIELD MAG. : ZL=.5 : DR=DZ/9.8
  SOLID=EXACT : DIAMONDS=T : AL=1/100
  BOUNDARY FIELD PHASE : ZL=.5 : DR=DZ/9.8
  SOLID=EXACT : TRIANGLES=T : AL=1/100

```

```

FFM07190
FFM07200
FFM07210
FFM07220
FFM07230
FFM07240
FFM07250
FFM07260
FFM07270
FFM07280
FFM07290
FFM07300
FFM07310
FFM07320
FFM07330
FFM07340
FFM07350
FFM07360
FFM07370
FFM07380
FFM07390
FFM07400
FFM07410
FFM07420
FFM07430
FFM07440
FFM07450

```


LIST OF REFERENCES

1. R. F. Harrington, Time-Harmonic Electromagnetic Fields, McGraw-Hill, 1961.
2. A. R. Mitchell and R. Wait, The Finite Element Method in Partial Differential Equations, Wiley, 1977.
3. M. A. Morgan, S. K. Chang, and K. K. Mei, "Coupled Azimuthal Potentials for Electromagnetic Field Problems in Inhomogeneous Axially Symmetric Media", IEEE Trans. Antennas Propagation, Vol. AP-25, pp. 413-417, May 1977.
4. M. A. Morgan, Finite Element Computation of Field Problems, paper presented at Sperry Research Center, 7 December 1978.
5. G. Strang and G. J. Fix, An Analysis of the Finite Element Method, Prentice-Hall, 1973.
6. M. Abramowitz and I. Stegun, Handbook of Mathematical Functions, Dover, New York, 1970.
7. R. F. Harrington, Field Computation by Moment Methods, McGraw-Hill, 1968, Chap. 4.
8. E. C. Jordan and K. G. Balmain, Electromagnetic Waves and Radiating Systems, Prentice-Hall, 1968, pp. 333-338.

INITIAL DISTRIBUTION LIST

	No. Copies
1. Defense Documentation Technical Center Cameron Station Alexandria, Virginia 22314	2
2. Library, Code 0142 Naval Postgraduate School Monterey, California 93940	2
3. Department Chairman, Code 62 Department of Electrical Engineering Naval Postgraduate School Monterey, California 93940	1
4. Professor M. A. Morgan, Code 62Mw Department of Electrical Engineering Naval Postgraduate School Monterey, California 93940	2
5. Professor K. G. Gray, Code 62Gy Department of Electrical Engineering Naval Postgraduate School Monterey, California 93940	1
6. Lieuteuant Bryant Welch, USN 1404 Hester Drive Lakeland, Florida 39301	1

Thesis

189513

W3877 Welch

c.1

Concept evaluation:
field feedback computa-
tion of electromagnetic
scattering.

18 NOV 87

32079

Thesis

189513

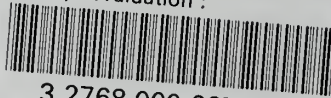
W3877 Welch

c.1

Concept evaluation:
field feedback computa-
tion of electromagnetic
scattering.

thesW3877

Concept evaluation :



3 2768 000 99755 5
DUDLEY KNOX LIBRARY